

Washington University in St. Louis

## Washington University Open Scholarship

---

All Theses and Dissertations (ETDs)

---

January 2010

### Two-Direction Cracking Shear-Friction Membrane Model for Finite Element Analysis of Reinforced concrete

Jeffrey Mitchell

*Washington University in St. Louis*

Follow this and additional works at: <https://openscholarship.wustl.edu/etd>

---

#### Recommended Citation

Mitchell, Jeffrey, "Two-Direction Cracking Shear-Friction Membrane Model for Finite Element Analysis of Reinforced concrete" (2010). *All Theses and Dissertations (ETDs)*. 466.

<https://openscholarship.wustl.edu/etd/466>

This Thesis is brought to you for free and open access by Washington University Open Scholarship. It has been accepted for inclusion in All Theses and Dissertations (ETDs) by an authorized administrator of Washington University Open Scholarship. For more information, please contact [digital@wumail.wustl.edu](mailto:digital@wumail.wustl.edu).

WASHINGTON UNIVERSITY IN ST. LOUIS  
School of Engineering and Applied Science  
Department of Mechanical, Aerospace, and Structural Engineering

Thesis Examination Committee:

Dr. Thomas Harmon, Chair

Dr. Philip Gould

Dr. Srinivasan Sridharan

TWO-DIRECTIONAL CRACKING SHEAR-FRICTION MEMBRANE MODEL FOR  
FINITE ELEMENT ANALYSIS OF REINFORCED CONCRETE

by

Jeffrey P. Mitchell

A thesis presented to the School of Engineering  
of Washington University in partial fulfillment of the  
requirements for the degree of

MASTER OF SCIENCE

August 2010

Saint Louis, Missouri

## ABSTRACT OF THE THESIS

Two-Directional Cracking Shear-Friction Membrane Model for Finite Element Analysis of  
Reinforced Concrete

by

Jeffrey P. Mitchell

Master of Science in Civil Engineering (Structures)

Washington University in St. Louis, 2010

Research Advisor: Professor Thomas G. Harmon

There are a multitude of existing material models for the finite element analysis of cracked reinforced concrete that provide reduced shear stiffness but do not limit shear strength. In addition typical models are not based on the actual physical behavior of shear transfer across cracks by shear friction recognized in the ACI Building Code and present in previous experimental work. Recently a shear friction model was proposed that was able to capture the recognized cracked concrete behavior by limiting the shear strength as a function of yielding in the reinforcement across the crack. However, the proposed model was only formulated for the specific case of one-directional cracking parallel to the applied shear force. The goal of this research is to update and generalize this proposed shear friction model for finite element use. In order to generalize the theory, the shear friction model was expanded to two-directional cracking at any orientation. This expansion is necessary for

handling the analysis of complex structures and non-proportional loading cases present in real design and testing situations. This generalized model was formulated as a total strain based model using the approximation that crack strains are equal to total strains and later reformulated to separate crack strains from total strains to improve the overall model's accuracy. In addition, various loading programs and convergence methods were tested in an attempt to achieve full cyclical convergence. Finally this research provides comparative studies of the generalized shear friction model and other existing models for a loading case and crack orientation similar to that of a shear wall. Inconsistencies in predicted stresses, displacements and material interactions show the necessity for further testing and analysis to determine the actual behavior for this seemingly important case.

# Acknowledgments

A special thanks goes to Dr. Harmon for sharing his knowledge and experience in the area of reinforced concrete modeling and for providing guidance and encouragement throughout the research process. I would also like to thank the National Science Foundation for the GK-12 Fellowship that funded this research and provided me with invaluable experiences (grant number DGE-0538541). Lastly, I would like to thank my parents for their past and continued support that has allowed me to get where I am today.

Jeffrey P. Mitchell

*Washington University in St. Louis*

*August 2010*

# Contents

<b>Abstract</b> .....	ii
<b>Acknowledgments</b> .....	iv
<b>List of Tables</b> .....	vii
<b>List of Figures</b> .....	viii
<b>1 Introduction</b> .....	1
1.1 Problem Definition.....	1
1.2 Research Objectives.....	2
1.3 Research Approach.....	3
1.4 Thesis Organization.....	4
<b>2 Literature Review</b> .....	6
2.1 Review of ACI Building Code Shear-Friction Provisions.....	7
2.1.1 Basis for Shear-Friction Design Provisions.....	9
2.2 Finite Element Modeling of Reinforced Concrete Membrane Elements.....	10
2.2.1 Development of Membrane Elements.....	11
2.2.2 Reinforced Concrete Membrane Constitutive Relationships.....	12
2.2.3 Modeling Techniques.....	13
2.2.4 Accuracy and Range of Application of Models.....	13
2.3 Evaluation of Cracked Concrete Shear Strength Models.....	14
2.3.1 Accuracy of Models.....	14
2.3.2 Classes of Shear Stress-Strain Relationships.....	16
2.3.3 Shear Stress-Strain Relationships: Summary.....	21
2.4 Shear-Friction Membrane Model Development.....	23
2.4.1 Initial Concept Development.....	23
2.4.2 Finite-Element Formulation: Crack-Opening Path.....	27
2.4.3 Finite-Element Formulation: Effective Strain.....	28
2.4.4 Finite-Element Formulation: Shear Stresses.....	32
2.4.5 Finite-Element Formulation: Procedures.....	33
2.4.6 Model Results and Verification.....	34
2.5 Research Direction – Two Crack Directions.....	38
<b>3 Orthogonal Cracking Shear Friction Model Iterations</b> .....	39
3.1 Description of Developmental Procedures.....	40
3.2 Element & Simplified Structural Model.....	41
3.3 Orthogonal Cracking.....	43
3.4 The Orthogonal Shear Friction Theory.....	44

3.4.1	Review of Concepts .....	44
3.4.2	Stress/Strain Formulations .....	45
3.4.3	Secant Stiffness Matrix Formulation .....	49
3.4.4	Active Crack Criteria.....	54
3.5	Uniform State of Stress and Strain .....	57
3.6	Shear stress across the Crack Surface.....	57
3.7	Developmental Phases of the Finite Element Model.....	59
3.7.1	Phase One: Non-Linear Cyclical Model Framework .....	59
3.7.2	Phase Two: Initial Shear Friction Implementation.....	61
3.7.3	Phase Three: Proportional Load Vector (PLV) .....	61
3.7.4	Phase Four: Constant Vertical Load (CVL) .....	74
3.7.5	Phase Five: Modified Newton-Raphson Method (MNRM) .....	81
<b>4</b>	<b>Orthogonal Shear Friction Theory: Crack Strain Separated (CSS)</b> .....	<b>87</b>
4.1	Model Definitions .....	88
4.2	Crack Strain Separated Stress-Strain Formulations .....	89
4.2.1	Crack Strains.....	89
4.2.2	Effective Strain .....	91
4.2.3	Normal Concrete Stress.....	91
4.2.4	Shearing Stresses.....	92
4.2.5	Secant Stiffness Matrix Formulations: Net Shearing Strain .....	98
4.2.6	Active Crack Criteria.....	102
4.3	Analysis of the Orthogonal Shear Friction Model: Crack Strain Separated.....	103
4.3.1	Results and Discussions.....	103
4.4	Study of CSS Results.....	107
<b>5</b>	<b>Conclusions and Future Work</b> .....	<b>115</b>
5.1	Objectives.....	116
5.2	Conclusions.....	118
5.3	Future Work.....	119
<b>Appendix A</b>	<b>Derivations</b> .....	<b>122</b>
<b>Appendix B</b>	<b>MATLAB Source Codes</b> .....	<b>126</b>
<b>References</b>	.....	<b>170</b>
<b>Vita</b>	.....	<b>173</b>

# List of Tables

Table 1.1: Summary of Shear Stress-Strain Relationship Classes ..... 22  
Table 3.1: Summary of Active Crack Criteria..... 56



# List of Figures

Figure 2.1:	Shear-friction concept, behavior and schematic .....	8
Figure 2.2:	Push-off test specimen configuration in previous tests .....	10
Figure 2.3:	Membrane element testers at the University of Toronto (a) and the University of Houston (b) .....	12
Figure 2.4:	Contact mechanism at shear displacement .....	19
Figure 2.5:	Aggregate interlock model, showing reinforcement modeled as springs.....	20
Figure 2.6:	Diagram of a stage in the crack opening damaging process and Shear Stress vs. Slip .....	21
Figure 2.7:	Experimentally determined relationship between slip and separation (a) Stresses developed on a crack surface (b) .....	24
Figure 2.8:	Crack opening path .....	25
Figure 2.9:	Friction Coefficients vs. Slip .....	25
Figure 2.10:	Crack Strain vs. Total Strain .....	28
Figure 2.11:	Effective crack strain .....	29
Figure 2.12:	Crack direction definition and separation.....	29
Figure 2.13:	Concrete Normal Stress vs. Effective strain .....	30
Figure 2.14:	Example non-linear Separation vs. Slip relationship.....	31
Figure 2.15:	Non-linear crack opening path in strain space .....	32
Figure 2.16:	Four-node element, loading and boundary conditions.....	33
Figure 2.17:	Experimental test set-up .....	35
Figure 2.18:	Shear Stress vs. Shear Slip .....	35
Figure 2.19:	Crack Opening vs. Shear Slip .....	36
Figure 2.20:	Shear Stress vs. Shear Strain .....	37
Figure 2.21:	Normal Strain vs. Shear Strain (crack-opening path).....	37
Figure 3.1:	Bilinear rectangular element, dimensions, DOF's and boundary conditions.....	42
Figure 3.2:	Element coordinate system .....	42
Figure 3.3:	Crack definitions and schematic of the slip-separation relationship Of the active crack.....	45
Figure 3.4:	Example shear stress limits on a one-dimensional plot .....	56
Figure 3.5:	Element subjected to pure shear .....	58
Figure 3.6:	Non-linear steel stress-strain relationship .....	60
Figure 3.7:	Partitioned DOF's for the PLV .....	63
Figure 3.8:	Shape vector applied to the element.....	64
Figure 3.9:	Shape vector and vertical load, $v$ , applied to element .....	65
Figure 3.10:	Flowchart of the PLV Algorithm .....	67
Figure 3.11:	Normal Strain (to Crack 1) vs. Shear Strain (PLV) .....	69
Figure 3.12:	Concrete Shear Stress (Crack 1) vs. Shear Strain (PLV).....	69
Figure 3.13:	Steel Stress vs. Total Strain (PLV) .....	71
Figure 3.14:	Concrete Normal Stress (Crack 1) vs. Normal Strain (PLV).....	72
Figure 3.15:	Concrete Normal Stress (Crack 1) vs. Effective Strain (PLV) .....	72

Figure 3.16: Shape Vector Multiplier vs. Prescribed Displacement (PLV) .....	73
Figure 3.17: Diagram of loading for the CVL formulation .....	75
Figure 3.18: Normal Strain (to Crack 1) vs. Shear Strain (CVL).....	77
Figure 3.19: Concrete Shear Stress (Crack 1) vs. Shear Strain (CVL) .....	77
Figure 3.20: Interaction between steel and concrete shearing stresses (CVL).....	78
Figure 3.21: Steel Stress vs. Total Strain (CVL).....	79
Figure 3.22: Normal Concrete Stress (Crack 1) vs. Normal Strain (CVL) .....	80
Figure 3.23: Concrete Normal Stress (Crack 1) vs. Effective Strain (CVL).....	80
Figure 3.24: Example procedure for the Modified Newton-Raphson Convergence Method.....	82
Figure 3.25: Flowchart of the Modified Newton-Raphson Algorithm.....	84
Figure 3.26: Concrete Shear Stress (Crack 1) vs. Shear Strain (MNRM).....	85
Figure 3.27: Interaction between concrete and steel shearing stresses (MNRM).....	85
Figure 4.1: Normal Strain vs. Crack Shear and Total Shear Strain .....	104
Figure 4.2: Crack Shear Strain and Concrete Shear Strain vs. Total Shear Strain.....	105
Figure 4.3: Comparison of Concrete Shear stress vs. Shear Strain for the CSS and MNRM analysis's.....	105
Figure 4.4: Concrete Shear Stress vs. Total, Concrete and Crack Shear Strains .....	106
Figure 4.5: Deformed Shape for zero prescribed displacement, CSS model (in) .....	108
Figure 4.6: Deformed Shape for zero prescribed displacement, Vecchio model (in).....	108
Figure 4.7: Deformed Shape for zero prescribed displacement, $\beta G$ model (in).....	109
Figure 4.8: Concrete, Steel and Total Shear Stresses vs. Total Shear Strain, $\beta G$ model.....	110
Figure 4.9: Deformed Shape for a prescribed displacement of 0.06 (in), $\beta G$ model.....	111
Figure 4.10: Concrete, Steel and Total Shear Stresses vs. Total Shear Strain, Vecchio model.....	111
Figure 4.11: Deformed Shape for a prescribed displacement of 0.06 (in), Vecchio model .....	112
Figure 4.12: Concrete, Steel and Total Shear Stresses vs. Total Shear Strain, CSS model .....	112
Figure 4.13: Deformed Shape for a prescribed displacement of 0.06 (in), CSS model .....	113
Figure 4.14: Comparison of Global Shear Stress vs. Prescribed Displacement for $\beta G$ , Vecchio and CSS models .....	114
Figure A.1: Schematic of a block being pushed “up the hill”.....	122
Figure A.2: Schematic of a block being pushed “up the hill” at an inclination, $\theta$ .....	124

# Chapter 1

## Introduction

Recently a dissertation was written by So, proposing a shear friction model for the finite element analysis of reinforced concrete membranes [15]. The model sought to improve finite modeling techniques for shear transfer across cracked reinforced concrete. The proposed shear friction theory is a rational model based on the physical behaviors present in the ACI Building Code provisions for shear friction. The shear friction theory is the only existing model that is capable of capturing the actual physical behavior of shear transfer in cracked reinforced concrete, including limiting the shear strength due to steel yielding. The purpose of this research is to update and improve the shear friction theory for general finite element use. Additionally, this research aims to provide comparative studies of the shear friction model and other existing models for reduced shear stiffness of cracked concrete.

### 1.1 Problem Definition

Limited testing and a multitude of existing models for the reduced shear stiffness of cracked reinforced concrete that do not limit shear strength, leaves room for experimentation and model improvements. The shear friction theory proposed by So, is the only existing model that is formulated based on the provisions in the ACI Building Code, models reduced shear stiffness based on rational physical principles, and

limits the shear strength[15]. Typical models reduce the shear stiffness of cracked concrete by multiplying the shear modulus by a shear retention factor that in theory can vary from 0 to 1. This type of model does not limit the shear strength. It is important to have a design tool that can capture both the reduced shear stiffness and strength due to cracking.

Although the shear friction theory proposed by So accomplishes both reduced shear stiffness and strength, the model is formulated for one specific case. The current model is capable of handling only a pre-cracked element, with only one crack direction. In addition the crack direction is oriented in the direction of the applied shear. In general design situations, such as shear walls, cracks may tend to form at various orientations to the applied shear. That is cracks tend to form in the direction of the maximum principle tensile stress. In addition, for cases such as non-proportional or cyclical loading, cracks may form in multiple directions depending on the direction of the loading. In order to further generalize the shear friction theory, cracks must be allowed to form at any orientation and in at least two directions.

## **1.2 Research Objectives**

Based on the successful results of the shear friction theory proposed by So, the intent of this research was to further develop the model to include multi-directional cracking at any orientation. This generalization of the shear friction theory is necessary for handling the analysis of complex structures and non-proportional loading cases present in real design and testing situations. The final goal is to be able to analyze a large structure, such as a shear wall, with multiple elements under cyclical loading. The jump to this complex analysis cannot be made immediately, as various objectives and studies are necessary to accurately develop the model. Presented here is a list of research objectives and steps necessary for the generalization of the shear friction theory.

1. Create a working finite element model for the analysis of a single reinforced concrete element that includes the shear friction theory. The model should also include cracking criteria, tension stiffening curve and cyclical material models.
2. Implement multi-direction cracking into the shear friction theory. This initial formulation will be for orthogonal cracking, where the two crack directions must be orthogonal to one another requiring only one crack coordinate system.
3. The finite element model will be a displacement controlled analysis subjecting the element to a uniform state of stress and strain in order to simplify the interpretation of the results.
4. Cyclical loading of the element in order for more than one crack direction to be active throughout the analysis.
5. Analysis of a larger structure requiring multiple elements with an orthogonal cracking shear friction model, such as a shear wall.

The research objectives listed here were changed and modified through the course of the model development as new understandings and difficulties presented themselves. These changes are reflected in the main body of the thesis and are summarized in the concluding chapter.

## **1.3 Research Approach**

This research was conducted in two parts:

1. Review and evaluation of shear friction behavior in cracked reinforced concrete, existing reduced shear stiffness models for cracked concrete present in literature, and the shear friction theory proposed by So.

2. Development and evaluation of a new finite element model, implementing the shear friction theory including multi-directional orthogonal cracking.

The first part of the research included an in depth literature review and study of available research for finite element modeling of reinforced concrete membrane elements. In addition the provisions for shear friction presented in the ACI Building Code as well as the original research that led to the development of the provisions were reviewed. Finally a study of the shear friction theory proposed by So, and the verification of that model were reviewed.

The second part of the research began with the development of a new finite element framework for the implementation of a new multi-directional orthogonal cracking model. This framework included the desired parameters present in the objectives. Next, the Orthogonal Shear Friction Theory was developed and inserted into the new finite element framework. The model was developed in five phases as new understandings and convergence issues required changes. The Orthogonal Shear Friction Theory was then reformulated to allow the separation of crack strains from total strains, improving the overall models accuracy. Finally, comparative studies were performed with the Crack Strain Separated model and other existing models.

## **1.4 Thesis Organization**

Chapter 2 includes the literature review, which was the first part of the research. Chapter 3 presents the formulation of the Orthogonal Shear Friction Theory and the necessary changes to the finite element framework to handle the theory. In addition the chapter includes five phases of the models development. These phases are highlighted by various convergence and loading methods necessary to meet the research objectives. Chapter 4 includes the formulation of the Crack Strain Separated shear friction model. Furthermore, the chapter includes a comparative study of the results of the Crack Strain

Separated model with other existing models providing useful information toward future work. Chapter 5 summarizes the thesis, findings and suggests future work.

# Chapter 2

## Literature Review

Loading conditions and structural configurations in reinforced concrete can sometimes produce situations where direct shear transfer through shear friction should be considered. These conditions have been studied in some detail by a number of individuals (Mattock, Birkeland et al.) and have produced the basic design methods present in Chapter 11 of the ACI Building Code and Commentary [1]. This chapter will discuss and review the following:

1. The shear-friction design provisions present in the ACI Building Code and the research and basic physical behavior of reinforced concrete that the code provisions are based on.
2. The importance and effectiveness of non-linear finite element modeling of reinforced concrete structures.
3. The methodology and effectiveness of previous research and models for shear strength of cracked reinforced concrete.
4. Development, rational and verification of the shear-friction membrane model.
5. Generalizing the shear-friction membrane for two-directional cracking.



## 2.1 Review of ACI Building Code Shear-Friction Provisions

Section 11.7 of ACI 318 specifies that the conditions for considering the transfer of shear by shear friction are: an interface between concretes cast at different times, an interface between concrete and steel reinforcement for precast concrete applications, an existing or potential crack or an interface between dissimilar materials [1]. For the purposes of this research, focus will be placed upon the conditions where an existing or potential crack location needs to be considered for direct transfer through shear friction. This is because the model presented in this research is intended for capturing the fundamental shear-friction behavior in the context of large structures, such as shear walls, not for the design of shear transfer across specific interfaces, such as precast concrete connections or concrete cast against existing concrete.

To understand the design provisions in the code it is important to first understand the basic physical principles that produced the equations. The Code states that a crack shall be assumed to occur along the shear plane that is in consideration and shear reinforcement shall be placed across the crack plane to resist the separation of the crack surfaces [1]. What causes this separation is the fact that when a crack surface forms in concrete the crack surface is irregular and rough. When the crack surfaces slip relative to one another due to applied shear forces, the irregular rough crack surface produces separation as well. That is, crack slip and crack separation are coupled together. Shear failure occurs when the separation of the crack is large enough to yield the reinforcement across it. It can then be recognized that the shear strength across a crack surface is due to the friction between the crack surfaces and is proportional to the normal compressive force provided by equal and opposite tension in the reinforcement. Dowel action can also contribute to shear strength. This strength may also be limited by the shearing off of protrusions in the crack surface. The physical behavior of slip

and separations as well as a schematic of the forces involved is well diagramed in Figure 2.1 [15].

The ACI Code provides a simple and easily applied design equation for the design of shear-friction reinforcement that states that the shear strength,  $V_n$ , is equal to  $A_{vf} f_y \mu$  [1]. Where  $A_{vf}$  is equal to the area of shear-friction reinforcement across the crack surface,  $f_y$  is the yield strength of the shear-friction reinforcement, and  $\mu$  is the coefficient of friction. Different coefficients of friction are recommended for different types of conditions of interfaces and concrete densities. The Code also specifies upper limits on the shear strength. More importantly the Code recognizes that permanent net tension or compression should be taken into design consideration, compression being additive to the clamping force,  $A_{vf} f_y$ , and tension needing to be taken solely by reinforcement not included in shear strength calculation.

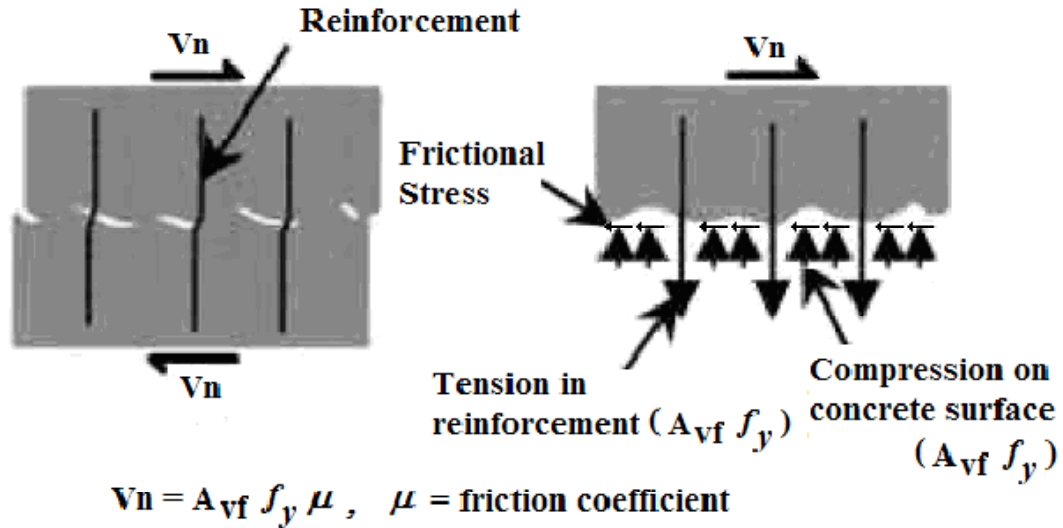


Figure 2.1 Shear-friction concept, behavior and schematic [18].

### **2.1.1 Basis for Shear-Friction Design Provisions**

The shear-friction provisions in the design code were originally developed in a paper by Philip W. Birkeland and Howard W. Birkeland in 1966. The paper was written to address design issues in precast concrete connections, specifically shear interfaces associated with corbels, and beam bearing situations where shear failure as slippage along maximum shear planes is the main concern [3]. The hypothesis recognized that shear-friction resistance to slippage was a function of an external clamping force across the crack plane provided by either permanent external loading or reinforcing steel. Birkeland also hypothesized that slipping across a crack surface would produce separation due to irregular inclined planes in the cracked concrete interface. It was also recognized that the ultimate shear capacity would be reached at the yield point of reinforcement. Birkeland proposed that his shear friction hypothesis be thoroughly verified through testing.

Thorough testing was performed primarily by researchers at the University of Washington. Many papers were published discussing tests performed to expand the understanding of shear-friction and transfer of forces across a crack. The basic properties investigated were: characteristics of the crack plane, characteristics and ratios of the reinforcement, the concrete strength, and direct stresses acting parallel and transverse to the shear plane [12]. In addition pre-cracked and initially un-cracked specimens were tested. All of the testing verified and improved the shear-friction provisions in the design code, most notably proving that the previous design provisions were overly conservative in many instances and expanding design equations to include many types of shear friction interfaces and external loading situations. Figure 2.2 shows the typical test set-up used in the experiments.

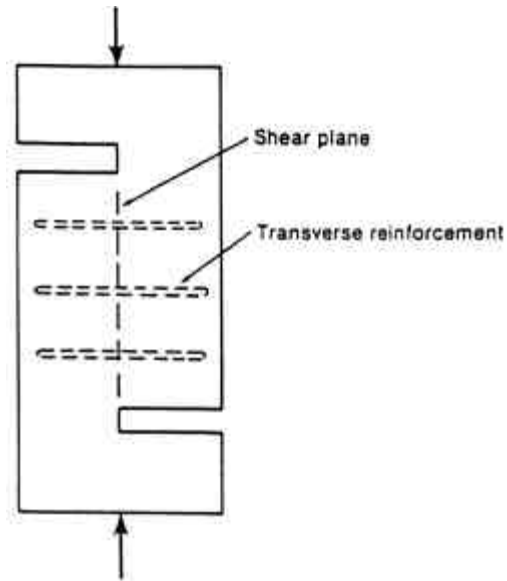


Figure 2.2 Push-off test specimen configuration in previous tests [18].

Most recently further testing was performed by Valluvan, Kreger and Jirsa [18] to evaluate the shear-friction provisions based on new information and testing. Again it was found that the current design provisions were conservative in many situations and suitable recommendations were made. The recommendations included more details on the upper bounds of strength calculations and a more accurate representation of contribution of shear-friction reinforcement and permanent net compression [18].

## 2.2 Finite Element Modeling of Reinforced Concrete Membrane Elements

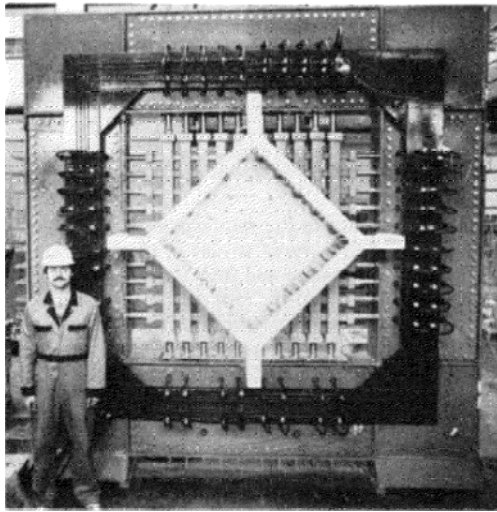
For many years the validity of the finite-element method has been widely accepted across many disciplines as an analysis tool for structures and many other applications such as heat transfer. It has and will be an important design and research method for

engineers and scientists to predict how structures and materials will respond to external loading.

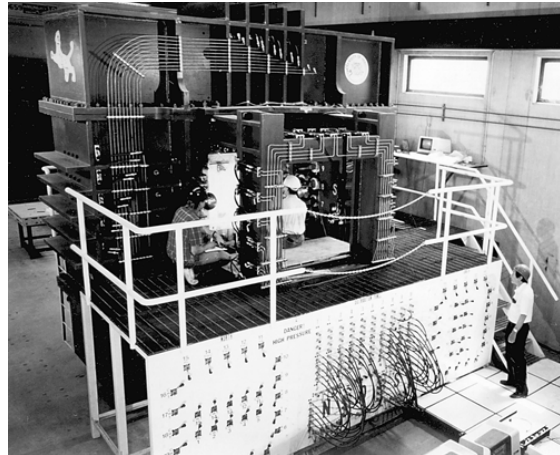
## **2.2.1 Development of Membrane Elements**

Over the past 30 years, an element based approach was developed to study reinforced concrete structures, the basis of which is the idea that the behavior of any whole structure can be predicted by integrating what can be learned from experiments about its parts or elements [11]. In many typical reinforced concrete structures, such as shear walls, applied loads are resisted primarily by in-plane stresses, often referred to as membrane stresses. Therefore, each membrane element can be visualized to resist two in-plane normal stresses and one in-plane shearing stress.

Testing reinforced concrete elements is essential to the success of implementing them in a finite-element analysis. The most successful method of testing this type of element is to perform full scale testing of concrete membrane structures, specifically individual square elements subjected to a uniform state of stress and strain. Only two such testing set-ups exist, one at the University of Toronto and one at the University of Houston. Figure 2.3(a) and 2.3(b) show the membrane testing machines. By integrating material behavior found from testing, finite-element analysis can predict how the load is shared by all of the elements in a global sense and how each element responds to its own applied loads [23].



(a)



(b)

Figure 2.3 Membrane element testers at the University of Toronto (a) and the University of Houston (b) [23, 14].

## 2.2.2 Reinforced Concrete Membrane Constitutive Relationships

Formulations of finite-element analysis of reinforced concrete depend primarily on the development of concrete and steel constitutive relationships that accurately model the behavior of cracked reinforced concrete. This is not a simple task as the stress-strain relationships of reinforcing steel, cracked concrete and their interaction are all non-linear. Some of these issues include but are not limited to: tension stiffening effect in cracked concrete to model the bond-slip behavior of reinforcement, unloading and reverse loading relationships for arbitrary loading, and shear transfer through shear-friction across a crack (the main focus of this research). These relationships have been studied and quantified in models with varying degrees of success. Discussions of these studies and models are in the literature [23, 19, 26 et al.]. The specific constitutive relationships chosen for this research are presented and discussed in a subsequent section of this chapter.

### **2.2.3 Modeling Techniques**

It is important to choose accurate and robust modeling techniques for finite element analysis that are able to capture the desired behavior. The ultimate goal of finite-element modeling is to provide easy to implement, computationally efficient and stable formulations that provide accurate and reasonable results. Again just as in selecting constitutive relationships there are differing methods and viewpoints for a finite model that accomplishes these goals. Some of these issues include: stiffness formulations (secant or tangent), and crack models (rotating or fixed). Some of the most robust models were developed by Vecchio and Hsu [23, 11]. A thorough review of modeling techniques and analysis methods are present in the literature, specifically [15].

Modeling techniques that are widely accepted and utilized are total-strain based models and “smeared” material properties. A total-strain based model expresses the elemental average stresses as a function of average strains using concrete and steel constitutive models. The smearing of strains and material properties also allows for principle transformations of stresses and strains which simplifies modeling of various orientations of cracks.

### **2.2.4 Accuracy and Range of Application of Models**

There are many issues in the finite-element analysis of reinforced concrete membrane structures that have not been fully developed. Good accuracy has been achieved by models that are applicable to monotonic loading of certain structures; however there are limited procedures that provide adequate simulations of behavior under arbitrary loading conditions, such as reverse-cyclical loading [13]. Also there are still critical parts of material models that do not accurately capture the behavior of cracked reinforced concrete. One problem is that many models are derived by fitting experimental data

rather than from basic physical principles. Two significant areas for improvement are a bond-slip relationship between reinforcement and concrete for cyclical loading and an appropriate model for the shear strength and stiffness in cracked concrete. A detailed review of current models for shear strength and stiffness is provided in the following section.

## **2.3 Evaluation of Cracked Concrete Shear Strength Models**

The specific area of improvement selected as the focus of this thesis is modeling shear strength and stiffness in cracked concrete. It is important to evaluate what has been done before in shear strength modeling to fully understand the rationale for improvement in modeling. The concentration of this section will be on evaluating and classifying previous methods of handling shear friction in finite-element analysis of reinforced concrete membranes.

### **2.3.1 Accuracy of Models**

Current models do not include strength and stiffness formulations for shear-friction that follows the actual material behavior presented in the ACI Building Code. Typical models reduce the shear stiffness by a shear retention factor,  $\beta$ , which ranges from 0 to 1 to account for the reduction in stiffness due to cracking. This does not attempt to limit the shear strength or allow the element to reach a maximum shear capacity. The shear-friction design method in ACI Building Code estimates the shear strength but not the shear stiffness. However, in some design situations, it is important to have a tool that covers stiffness properties for the shear design of reinforced concrete. Therefore, it is important to have a shear strength model that can handle both the strength and the



stiffness of shear transfer across a crack and that is based on the basic mechanical behavior of cracked concrete present in the Code.

In general current models handle some parts of the basic mechanical relationships of shear transfer across a cracked reinforced concrete, but do not enforce all the relationships. The list of basic mechanical relationships that should be enforced in a comprehensive and accurate shear-friction model are listed below.

- As a crack surface slips, it separates due to the rough, irregular surface of a concrete crack. This recognizes the importance of enforcing a crack opening path.
- As a crack separates tension forces are developed in the steel crossing the crack.
- Tension forces in the steel across a crack place equal and opposite compression forces on the crack surface allowing friction to develop. This recognizes the importance of the amount of steel provided across the crack.
- Accurate modeling and limitation of strength. When the separation is sufficient to yield the steel, the compression force can no longer increase with increased separation, limiting the shear strength.
- Accurate modeling of stiffness. Are shear forces sufficient to overcome the friction force developed on the crack surface and allow slip, or will the crack “lock-up” and develop the full shear stiffness of un-cracked concrete?
- Crack surfaces that are “open” can still be in contact due to slip.
- Crack surfaces not in contact will have limited resistance to shear provided by dowel action in the reinforcement.
- The presence of permanent net compressive forces on a crack is additive to the development of shear-friction.

## 2.3.2 Classes of Shear Stress-Strain Relationships

There are dozens of suggested methods for modeling shear stress-strain relationships in cracked concrete. However, for the sake of brevity, this section will highlight only certain classes of relationships that demonstrate the abilities, as a whole, of current models. In general there are five types of shear stress-strain relationships presented in the literature for use in finite-element analysis of reinforced concrete. They are as follows: (1) A constant shear modulus, (2) a smeared shear modulus as a function principal stresses and strains, (3) a local shear stress check at crack surfaces, (4) equivalent continuum behavior representing local crack slip, and (5) crack surface interlock and degradation [15].

### Constant Shear Modulus (1)

The constant shear modulus method is more commonly known as “beta-G” or the shear retention factor. It is obtained by multiplying the full, elastic shear modulus ( $G$ ) of un-cracked concrete by a shear retention factor ( $\beta$ ) that can range from 0 to 1. Typically this method is written as follows:

$$G = \beta \frac{E}{2(1+\nu)} \quad (2-1)$$

In equation (2-1),  $E$  is elastic modulus of concrete and  $\nu$  is Poisson's ratio. The use of the shear retention factor is inconsistent with all of the primary mechanical relationships presented in section 2.3.1 necessary for accurate shear models for cracked concrete. However, it is used in many commercial finite-element programs because it is easy to implement [15]. More important is the fact that there is no rational basis for selecting the value of  $\beta$ . In addition, it does not limit the shear strength.

### **Smearred Shear Modulus (2)**

A rational shear modulus was presented Zhu and Hsu that is provided on a smeared level as a function of principle stresses and strains [26]. This method assumes that the principle stress and strain directions coincide to simplify the shear modulus. This proposed secant shear modulus is presented in equation (2-2).

$$G = \frac{(\sigma_1^c - \sigma_2^c)}{2(\varepsilon_1 - \varepsilon_2)} \quad (2-2)$$

In equation (2-2),  $G$  is the secant shear modulus of concrete,  $\sigma_1^c$  &  $\sigma_2^c$  are the principle stresses in the concrete and  $\varepsilon_1$  &  $\varepsilon_2$  are the principle strains [26]. This method avoids the fundamental issue because it assumes that no shear stress can exist parallel to a crack surface. This smeared approach is also computationally efficient. However, the model does not enforce the slip-separation relationship of the crack surface or recognize the effect of steel yielding, which is what drives the fundament shear-friction behavior.

### **Local Shear Stress Check at Crack Locations (3)**

The Modified Compression-Field Theory (MCFT) provides a smeared secant shear modulus as a function of principle stresses and strains as well [23]. Equation (2-3) shows this relationship.

$$\bar{G} = \frac{\bar{E}_1 \cdot \bar{E}_2}{\bar{E}_1 + \bar{E}_2} \quad (2-3)$$

$$\text{where, } \bar{E}_1 = \frac{\sigma_1}{\varepsilon_1} \text{ and } \bar{E}_2 = \frac{\sigma_2}{\varepsilon_2}$$

In addition this method requires checking shear stress at crack locations. At crack locations the shear stress is a function of crack width, the interlock of aggregate in crack surfaces, and the concrete strength [23]. This is accurate in recognizing the locking of

rough crack surfaces to the shear strength of cracked concrete. However, the fundamental problem with the MCFT is that it does not allow shear slip or total shear stress along crack surfaces and it does not enforce the relationship of crack slip to crack separation. A full description and discussion of the MCFT is present in the literature [15].

#### **Equivalent Continuum Behavior Representing Local Crack Slip (4)**

Following the MCFT, the Disturbed Stress Field Model (DSFM) was developed to handle some of the issues not considered in the MCFT. The DSFM theory included rigid-body concrete shear slip by allowing deviations of the principal stress and strain directions [19, 20]. This method allowed the local shear stress check in the MCFT to be avoided. The DSFM adopted formulations for determining the shear slip as a function of local shear stress, crack width, crack spacing and cube strength. A full discussion of these formulations is present in the literature [15].

Even though the DSFM proved to be computationally advantageous to the MCFT, the shear stress and strain relationship in the DSFM did not show much difference in the ultimate shear strength capacity [15]. Even though the DSFM does take into account the crack width and crack slip it does not enforce the fundamental relationship of crack slip to crack separation. Therefore, crack slip can occur without stressing the reinforcement crossing the crack. This fact negates the fundamental relationship of stress in the reinforcement to the shear-friction developed across the crack, thus not allowing the amount of steel to have a relationship to both strength and stiffness.

#### **Crack Surface Interlock and Degradation (5)**

Walraven presented a paper on reinforced concrete crack surface subjected to seismic shear forces [24]. His shear-friction theory for cracked reinforced concrete is the only other theory that proposes a rational mechanistic model for a crack opening path. His theory is based on the locking of aggregate particles on a crack surface as a function of crack width and slip, and aggregate size and geometry. He then relates the shear-friction

force developed to the normal compressive force on the crack surface provided by tension in the reinforcement crossing the crack.

Figure 2.4 shows the contact mechanism proposed by Walraven. In this mechanism forces  $F_x$  and  $F_y$  are defined by the contact areas ( $a_x$  and  $a_y$ ), the crushing strength of the material matrix ( $\sigma_{pu}$ ), and the coefficient of friction ( $\mu$ ). Therefore the friction stress ( $\tau_{pu}$ ) is a function of  $\sigma_{pu}$  and  $\mu$ . Also the slip ( $\delta$ ) and the crack width ( $w$ ) are defined. Walraven then defines the internal stresses on the crack surface as functions of slip and separation of the crack as shown in equations (2-4) and (2-5).

$$\tau(w, \delta) = \tau(w_0 + \Delta w, \Delta \delta) = \sigma_{pu}(\sum a_y + \mu \sum a_x) \tag{2-4}$$

$$\sigma(w, \delta) = \sigma(w_0 + \Delta w, \Delta \delta) = \sigma_{pu}(\sum a_x - \mu \sum a_y) \tag{2-5}$$

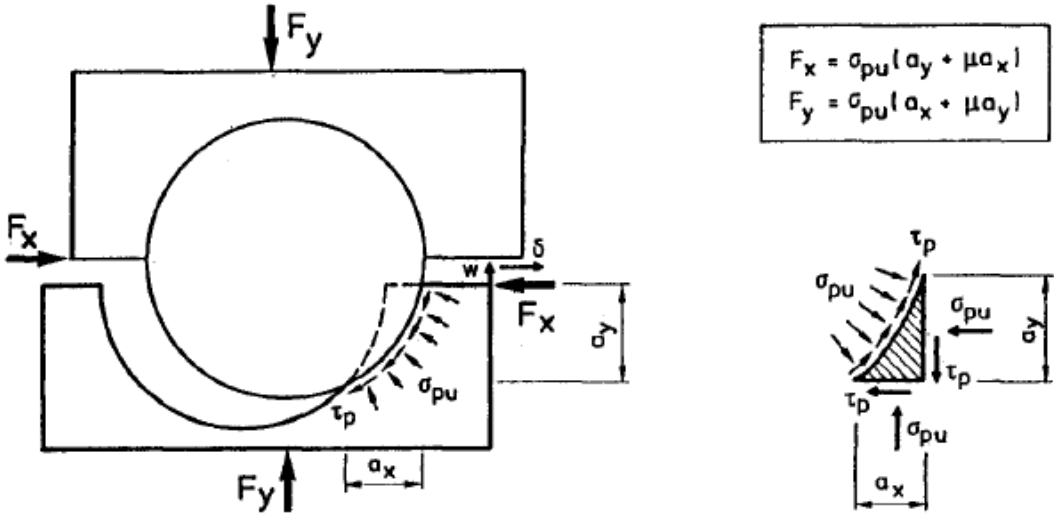


Figure 2.4 Contact mechanism at shear displacement [24].

The next important portion of Walraven’s theory is his aggregate interlock model shown in Figure 2.5. In addition to the above parameters, steel is now introduced and modeled as a spring. Tensile forces are developed in the springs based on crack

separation,  $w$ . These tensile forces are equated to a compressive stress ( $\sigma$ ) across the crack surface. Equilibrium of an iteration is achieved when this external compressive stress provided by the steel is equal to the required internal tension stress needed to develop the stress of friction to resist shear. If the external stress is greater than the internal stress then the shear displacement ( $\delta$ ) is not large enough and further displacement is necessary to gain equilibrium.

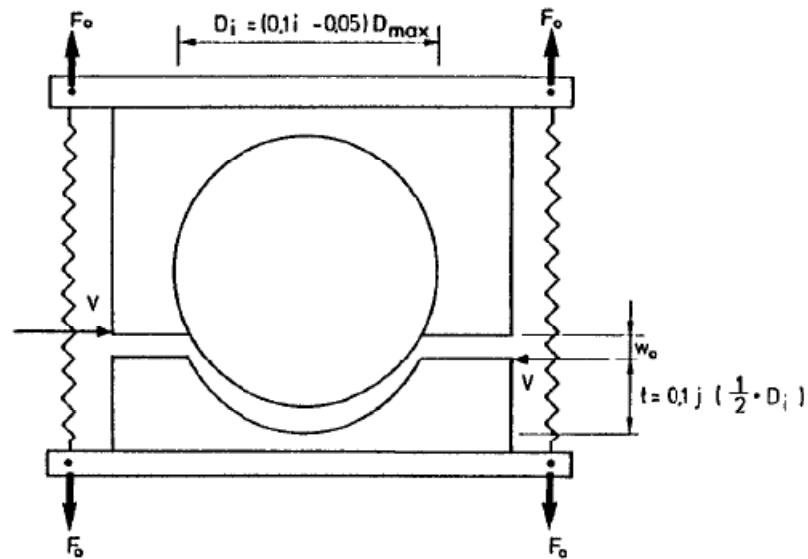


Figure 2.5 Aggregate interlock model, showing reinforcement modeled as springs [24].

Once this equilibrium point has been found, it is stored and forms the new boundary of the crack face and degrades that portion of the material which the particles have penetrated, representing crushing of the material. The material that has been penetrated is assumed to have moved into the open spaces of the crack and no longer provides interference on the crack surface. Figure 2.6 shows the degradation of the material interface and the shear stress versus slip relationship. In this way crack widths and crack slips are stored along the path as equilibrium is achieved, so that the natural crack opening mode and damage path is enforced.

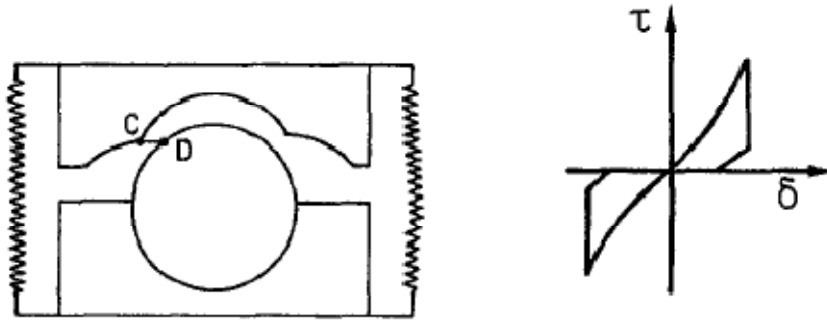


Figure 2.6 Diagram of a stage in the crack damaging process and Shear Stress vs. Slip [24].

This model does capture the fundamental behaviors of shear transfer across a crack and does so with a rational mechanistic model. The model enforces a relationship between slip and separation of a crack as well as relates the shear-friction across the crack to the reinforcement provided. Also the model takes into account the degradation of the crack surface during cyclical loading, which no other theory currently does. Nonetheless, there are a few issues not covered in this theory. The most obvious is that it is not proposed as a finite-element model. In addition, the model requires an input value for the maximum shear stress and does not have a steel yield model. This means that the model will not allow the shear strength to be limited; in other words it will reach its maximum value for each iteration.

### 2.3.3 Shear Stress-Strain Relationships: Summary

The various classes of shear stress-strain relationships present theories that vary in accuracy for capturing the fundamental mechanical behaviors of shear transfer in cracked concrete. The common missing thread in most classes is enforcing a relationship between slip and separation of crack surfaces. In general all classes also do not limit the shear strength based on the actual physical behavior present in the code, which is a function of yielding in the reinforcing steel. Table 1.1 summarizes the

various classes of shear stress-strain relationships and provides references to the literature for further review.

**Table 1.1 Summary of Shear Stress-Strain Relationship Classes**

Shear Stress/Strain Class	Summary	Sample Reference Literature
<b>Constant Shear Modulus (1)</b>	$\beta G$ , where $\beta$ is the shear retention factor varying from 0 to 1.	[8] [4] [5]
<b>Smearred Shear Modulus (2)</b>	Secant modulus based on principle stresses and strains.	[26]
<b>Local Shear Stress Check at Crack Locations (3)</b>	Secant modulus requiring shear checks as crack locations, known as the MCFT.	[23]
<b>Equivalent Continuum Behavior Representing Local Crack Slip (4)</b>	Accounts for shear slip as a function of local shear stress, crack width, and crack spacing. Also known as DSFM.	[19] [20]
<b>Crack Surface Interlock and Degradation (5)</b>	Shear stress developed by shear friction as a function of slip, crack width, and reinforcing steel. Also includes degradation of crack roughness. No limit on shear strength.	[24]



## **2.4 Shear-Friction Membrane Model Development**

A constitutive shear model was proposed in a dissertation by So, that accurately captured the fundamental behavior of shear transfer across cracked reinforced concrete [15]. This dissertation led to three papers that were accepted for publication and are listed at the end of the References section. The model enforced a functional relationship between crack slip and crack separation and predicts the shear strength of cracked concrete as a function of the amount of reinforcing steel across the crack surface. In order to further generalize the model for suitable modeling of broader situations it is important to review the modeling choices and concepts that were the basis for formulation.

### **2.4.1 Initial Concept Development**

The basic mechanical relationships of shear-friction behavior present in ACI 318 were the basis for formulating the initial concept. Previous testing and data was reviewed to develop a basic mechanical model of the behavior of slip across a crack. Figure 2.7(a) shows the experimentally determined relationship between slip and separation [25]. Figure 2.7(b) shows a mechanical model for this behavior [25]. Figure 2.7(a) clearly shows that increased slip across a crack plane produces increased separation and that increased normal stress flattens the slope of the slip/separation relationship. It is recognized that it is the rough surface of the crack plane that cause separation with slip.

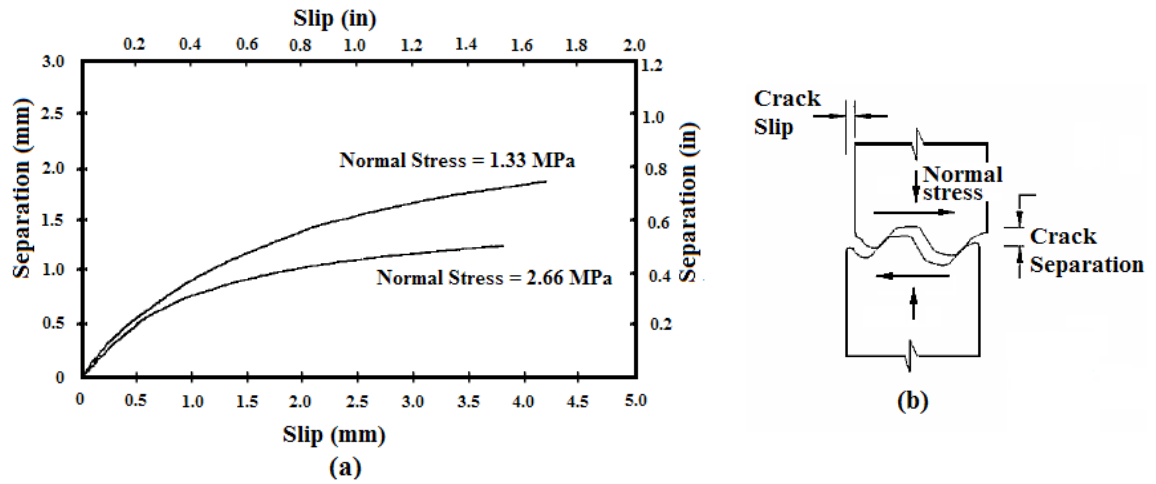


Figure 2.7 Experimentally determined relationship between slip and separation (a) Stresses developed on a crack surface (b) [25].

The separation of the crack causes tension stress in the steel across the crack which, in turn, causes an equal compressive stress normal to the crack surface. The compressive force on the crack surface allows friction to develop in the plane of the crack. Shear strength is then a function of the amount of steel crossing the crack and is limited when the separation is sufficient to yield the steel not allowing an increase in compressive force with increased separation. To enforce these relationships a simple mechanical model was created to represent the crack opening path (relationship between slip and separation) in terms of smeared crack normal ( $\epsilon_{cr}$ ) and shear ( $\gamma_{cr}$ ) strains divided by the crack spacing [15]. The crack opening path is defined by Figure 2.8.

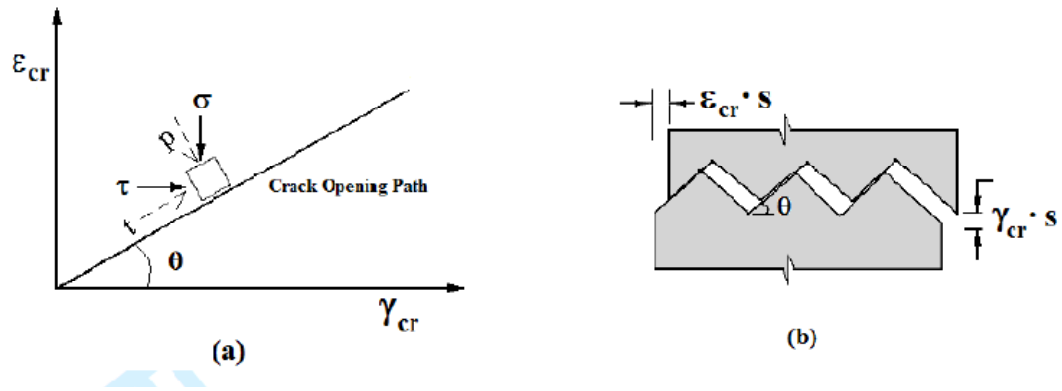


Figure 2.8 Crack opening path [15].

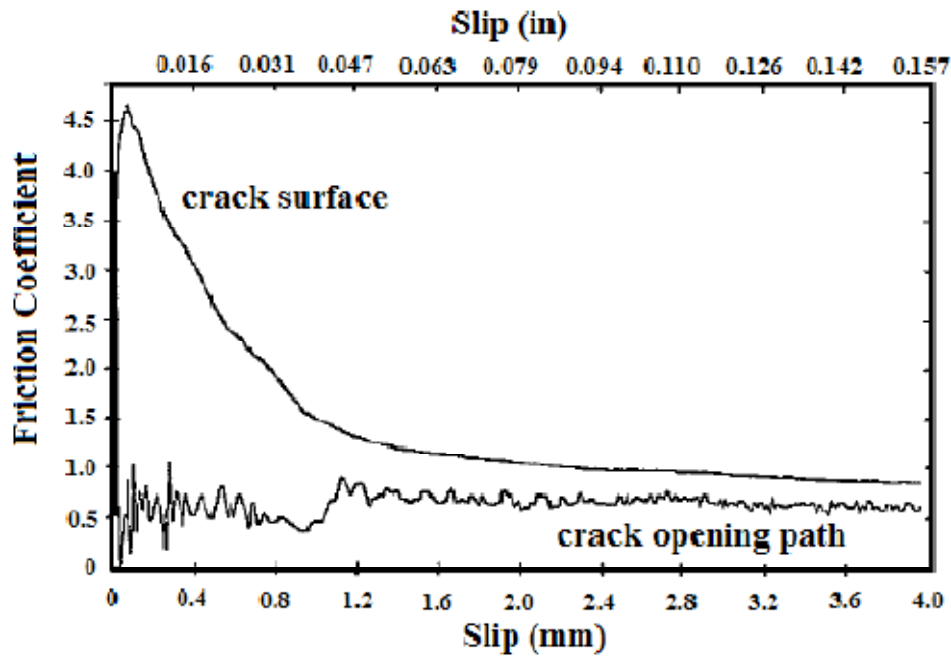


Figure 2.9 Friction Coefficients vs. Slip [25].

Friction developed on the surface of the crack can then be defined by the normal and shear forces acting on the crack surface ( $\tau$  and  $\sigma$  respectively) shown in Figure 2.8. That is, the friction coefficient,  $\mu$ , is equal to  $\tau/\sigma$ . However, further evaluation of previous testing showed that the coefficient of friction relative to the crack surface varied considerably with the amount of slip as is evident in Figure 2.9 [25]. Figure 2.9 shows

that it is more suitable to define the coefficient of friction in terms of the crack opening path.

Referring back to Figure 2.8(a), the crack opening path is simplified as a straight line. Again, in strain space the smeared crack strains,  $\epsilon_{cr}$  and  $\gamma_{cr}$ , are the crack separations and slips divided by the average crack spacing,  $S$ . This definition of smeared crack strains only works if the crack opening path is simplified to a linear relationship. Otherwise, the crack shear and normal stresses would not be uniquely determined by the crack strains. In other words, the stresses at the crack surface as a function of the smeared strains will only depend on the crack spacing,  $S$ , if the crack opening path is non-linear. In effect, simplifying the crack opening path as linear no longer necessitates keeping track of crack widths and slips. This important simplification is better understood once the concept of effective strain is established in Section 2.4.3.

Crack slip can now be thought of as pushing a block up a hill with a rough surface, and the coefficient of friction relative to the crack opening path can be defined. Referring to Figure 2.8(a), the friction coefficient relative to the surface of the hill is defined by equation (2-6) [15].

$$\mu' = \frac{t}{p} \tag{2-6}$$

Based on the test results presented in Figure 2.9, this definition of the friction coefficient gives values that vary little relative to slip. It also allows for a method for computing a friction coefficient for both directions of slip as pushing a block up a hill is harder than pushing it down a hill. The friction coefficients,  $\mu^{up}$  and  $\mu^{down}$ , are defined by Equations (2-7a) and (2-7b) for either the uphill or downhill direction as functions of the single crack path friction coefficient,  $\mu'$ , and the angle of the crack opening path,  $\theta$  (both should remain constant) [15]. A sample derivation of the friction coefficients,  $\mu^{up}$  and  $\mu^{down}$ , can be found in Appendix A.

$$\mu^{up} = \frac{[\sin \theta + \mu' \cos \theta]}{[\cos \theta - \mu' \sin \theta]} \quad (2-7a)$$

$$\mu^{down} = \frac{[\mu' \cos \theta - \sin \theta]}{[\cos \theta + \mu' \sin \theta]} \quad (2-7b)$$

## 2.4.2 Finite-Element Formulation: Crack-Opening Path

The proposed finite-element model uses a constant crack opening path friction coefficient,  $\mu'$ , and a linear crack opening path so that  $\gamma_{cr} = a\epsilon_{cr}$ , where  $a = \cot(\theta)$  and  $\theta$  is the angle of the crack opening path as shown in Figure 2.8 [15]. Again smeared crack strains are used as defined previously. The friction coefficient used to resist shear is defined based on whether slip is pushing the block up the hill or down the hill. Formulating the shear-friction model was done initially based on predicting stresses from total strains because it greatly simplifies the analysis. Total strains were shown to be almost exactly crack strains except for compressive strains and very low values of tensile strains as presented in Figure 2.10 [15]. Thus, the crack opening path can be approximately defined by the total strains rather than the crack strains such that,  $\gamma = a\epsilon$ . Where,  $\gamma$  and  $\epsilon$  are total strains relative to the direction of the crack.

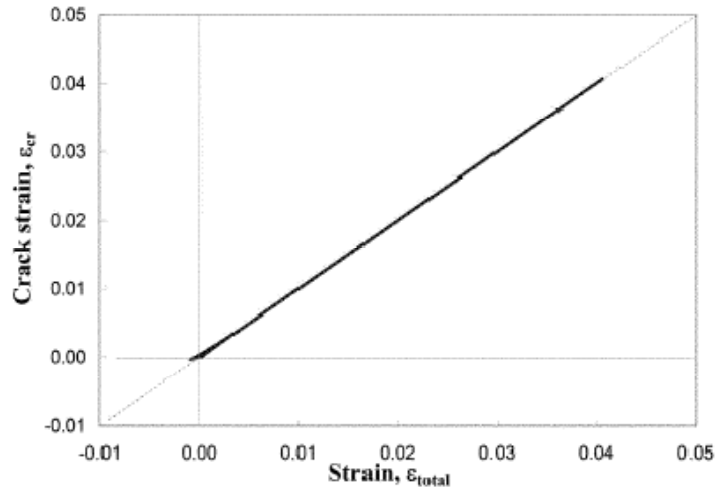


Figure 2.10 Crack Strain vs. Total Strain [15].

### 2.4.3 Finite Element Formulation: Effective Strain

Any set of displacements in a cracked reinforced concrete continuum can produce situations where the crack surfaces are either in contact with one another or not touching. This is because in theory the smeared strains that define the crack opening path,  $\gamma$  and  $\epsilon$ , are independent of one another. Therefore, there may be a portion of the strain normal to the crack that is independent of the separation effect due to the crack surface slip. This strain is defined as effective crack strain,  ${}^e\epsilon$  [15]. To illustrate this principle refer to point A in Figure 2.11, which for this state shown is a combination of  $\gamma$  and  $\epsilon$ . Also assume the crack is developed normal to the x-axis as shown in Figure 2.12. As presented previously, the total strains are used to define the crack opening path such that  $\gamma = a\epsilon$ . Now it can be seen that effective strain for this given crack orientation and set of strains represented by point A, can be defined by Equation (2-8). The absolute value of  $\gamma_{xy}$  is taken to account for slipping in either direction.

$${}^e\epsilon_y = \epsilon_y - \frac{|\gamma_{xy}|}{a} \quad (2-8)$$

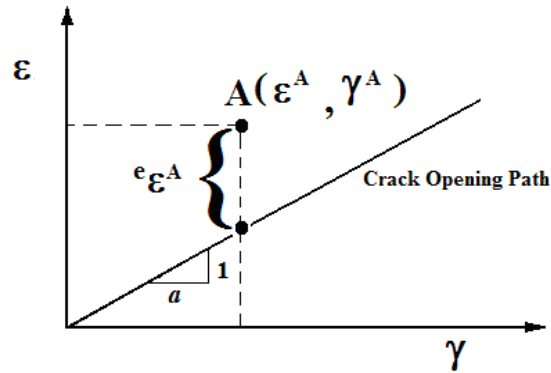


Figure 2.11 Effective crack strain [15].

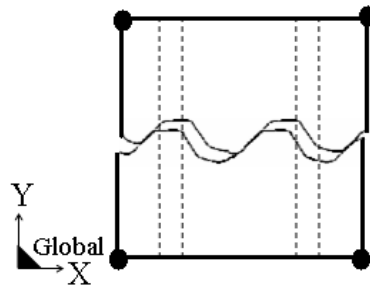


Figure 2.12 Crack direction definition and separation [15].

Effective strain is important because it is used to determine the concrete stress normal to the crack surface, defined as  $\sigma_y$  in Figure 2.13 [15]. Positive values for effective strain represent conditions where the crack surfaces are not in contact and no compression is developed across the crack, thus resistance to shear is taken solely by dowel action of the reinforcement. Negative values for effective strain represent conditions where the crack surfaces are in contact and compression is developed across the crack surface allowing shear-friction behavior. This definition of concrete stress normal to the crack surface includes a tension-stiffening curve, a reduced secant modulus,  $E_{cv}$ , for tensile strains and the full elastic modulus,  $E_c$ , to simplify the negative strain regime [15].

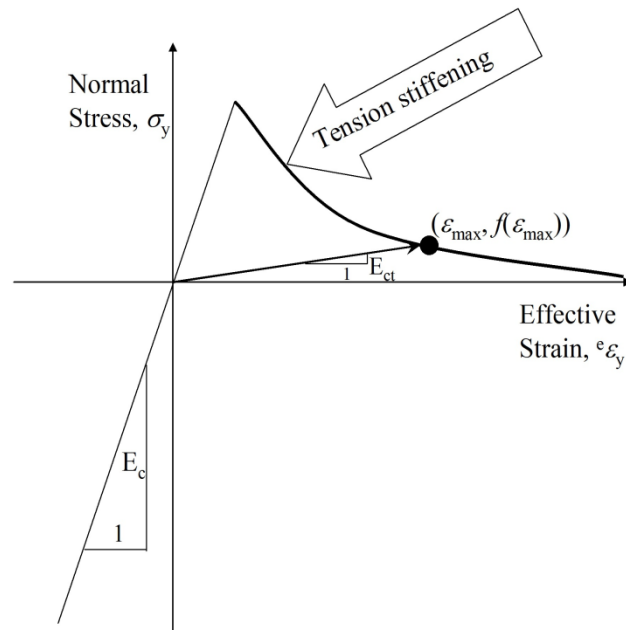


Figure 2.13 Concrete Normal Stress vs. Effective Strain [15].

The concept of effective strain is also important in understanding the need for a linear crack opening path. If the crack slip and separation path is non-linear, the crack spacing,  $S$ , cannot be disregarded and tracking individual crack widths and slips is necessary. This is because, in strain space, a non-linear slip-separation relationship will produce a variance in the zones that define if the crack surface is in contact or not. More importantly, this means that calculated concrete stresses relative to the crack will vary based on the average crack spacing which complicates the analysis considerably.

To better illustrate this point consider the simple non-linear crack opening path shown in Figure 2.14. Translating this path into strain space by dividing the separations and slips by the average crack spacing, creates a varying crack-opening relationship. Figure 2.15 shows this crack opening path in strain space for two different crack spacing's,  $S=10$  and  $S=20$ . Now consider point "B" in Figure 2.15 that represents the current strain condition. With respect to  $S=10$ , point "B" yields a negative value of effective strain which represents compression on the crack surface. However, with respect to  $S=20$ , point "B" yields a positive effective strain which represents the crack faces not in



contact. This difference is significant because effective strain is what defines the stress in the concrete normal to crack plane. With a non-linear relationship for the crack opening path this stress then becomes dependent on the average crack spacing. However, with a linear relationship the stress normal to the concrete is no longer dependent on the average crack spacing as long as the angle of the crack opening path remains constant.

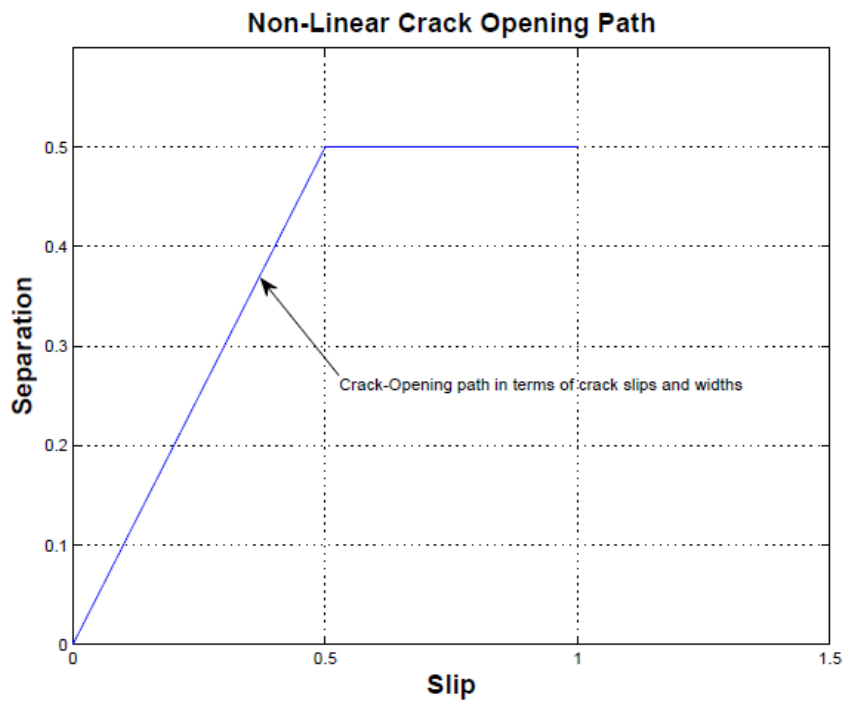


Figure 2.14 Example non-linear Separation vs. Slip relationship.

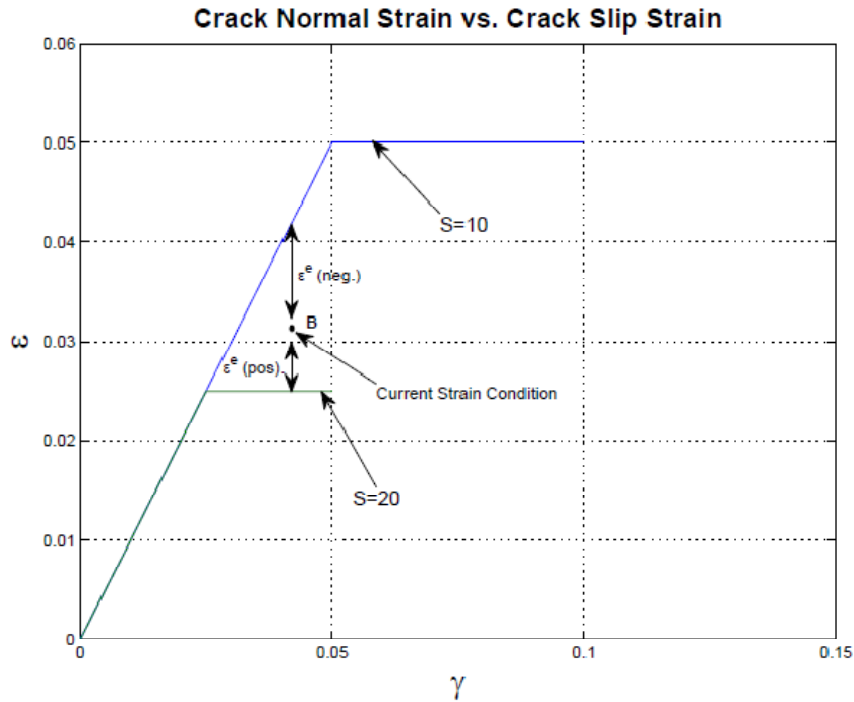


Figure 2.15 Non-linear crack opening path in strain space.

#### 2.4.4 Finite Element Formulation: Shear Stresses

Shear stresses are divided into two main categories and are defined by the effective strain. First, if the stress normal to the concrete crack surface,  $\sigma_y$ , is tensile the crack surfaces are not in contact and the shear is resisted only by dowel action of the reinforcement crossing the crack. Second, if the stress normal to the concrete crack surface,  $\sigma_y$ , is compressive the crack surfaces are in contact and shear can be resisted by shear-friction that is developed on the crack surface. When the normal stress is compressive the shear stress is then defined by either negative or positive total shearing strain. For negative and positive states of shearing strain, the shear stress is determined based on limiting values for slip along the surface. In other words, the crack surface could be slipping up the hill, down the hill or not slipping, depending on whether or not forces are sufficient to overcome the shear-frictional force. The equations for these

values of shear friction are left out here for the sake of brevity, but can be found in So, pp.141-143 [15]. These equations for shear stress were then formulated into secant stiffness matrices also present in the literature [15]. These basic equations are reformulated for two-directional cracking in a subsequent chapter of this thesis.

## 2.4.5 Finite Element Formulation: Procedures

The element geometry, boundary conditions, loading conditions and crack direction for the original formulation are established and defined in Figure 2.16 [15]. A low powered four-node quadrilateral element was chosen for the finite element analysis which has been shown to be adequate for the analysis of concrete membrane structures [15]. The single concrete membrane element analyzed was pre-cracked in the direction parallel to the loading. To ensure a state of pure shear the vertical or y-direction displacements of the top two nodes were slaved together. Horizontal displacements were then enforced cyclically subjecting it to a uniform state of stress and strain.

As stated before the model utilizes a secant stiffness formulation. A smeared approach was used for modeling material properties. In addition a total-strain based model was used as it simplifies the analysis and accurately captures the desired behavior as previously presented in Figure 2.10. For the convergence of non-linear material properties present in model, the iterative Newton-Raphson method was used.

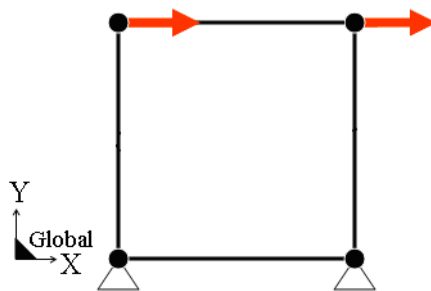


Figure 2.16 Four-node element, loading and boundary conditions [15].

## 2.4.6 Model Results and Verification

In a state of pure shear, by definition, shearing stress will be zero in the direction of the principal stresses. For a reinforced concrete membrane element subjected to pure shear with respect to the X-Y axes (Figure 2.16 where the displacements of the top two nodes are slaved together), this means that the principal maximum tensile stresses will act at an angle of 45 degrees from the applied shear forces. This forms a crack normal to the principal tensile stress. With a crack orientated in this direction there will be no shear stress. The vast majority of testing done on reinforced concrete membrane elements has been set-up this way. Without the presence of shear in the crack direction, the shear-friction concept becomes irrelevant. In other words, as the shear forces are applied cyclically to the element, cracks that form will simply open and close without slip, negating the applicability of the shear-friction provisions in ACI 318. With this in mind, only limited cyclical tests have been performed where shear was transferred across the crack surface. Such tests were performed by Gebreyouhannes et al. [6] and are presented as data for verification of the proposed shear friction finite element model.

The test set-up and dimensions for the experiments performed by Gebreyouhannes et al. are shown in Figure 2.17. As can be seen the specimen was subjected to cyclical shear forces across its pre-cracked surface, without inducing any moment. The results show that when the slip increased the shear stress also increased (Figure 2.18). However, the shear stress curve shown in Figure 2.18 does not show that shear strength across the crack is limited. This is because the steel restraining bars in the experiment did not yield. Figure 2.19 shows the crack slip versus the crack opening or separation, which clearly shows a linear crack opening path for both positive and negative slip. However, the trough of the crack opening path fills in with increased cycles. This is most likely due to the degradation of the crack faces and shearing off of protrusions which smoothes out the crack surface, decreasing the slope of the crack opening path.

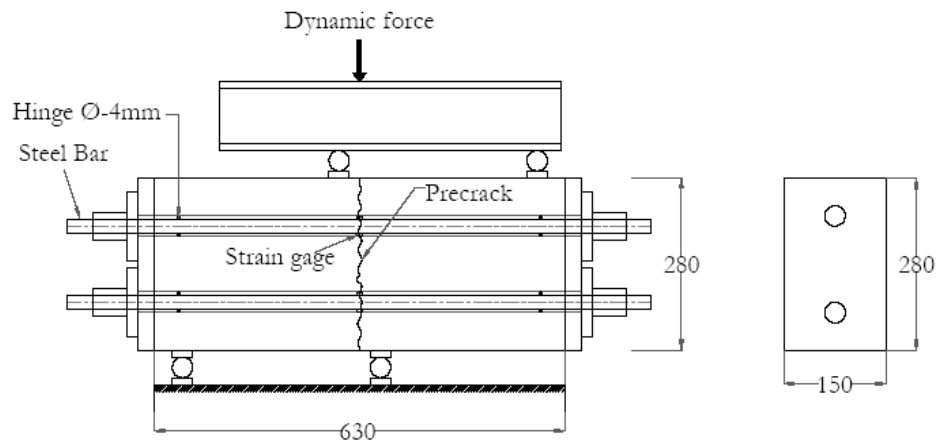


Figure 2.17 Experimental test set-up [6].

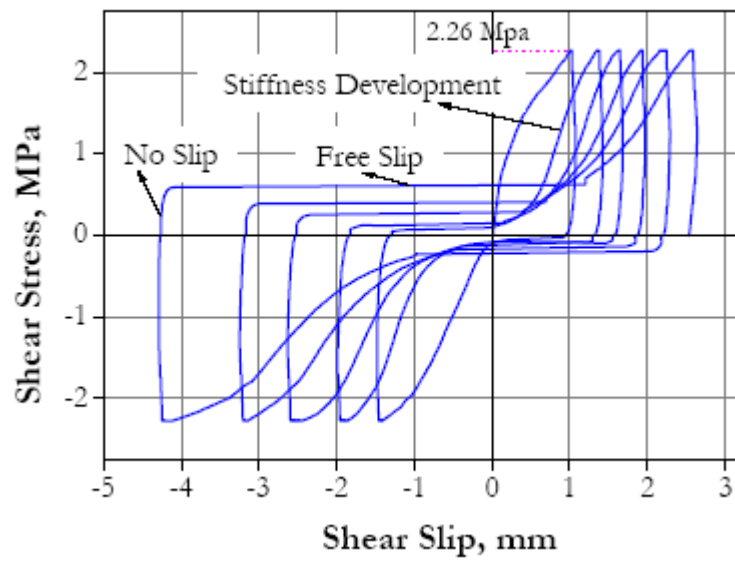


Figure 2.18 Shear Stress vs. Shear Slip [7].

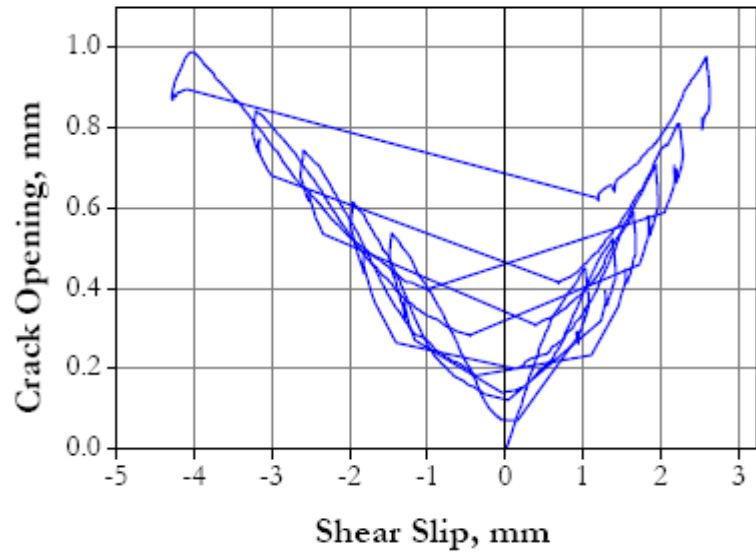


Figure 2.19 Crack Opening vs. Shear slip [7].

Comparative results of the analytical model to the experimental data are presented in Figures 2.20 and 2.21. Figure 2.20 shows crack slip versus shear stress. The clear difference between the experimental data in Figure 2.18, is the flattened portion of the shear stress which is due to yielding of the reinforcement crossing the crack. Figure 2.21 shows that the model enforces the relationship between crack slip and crack separation. When compared against Figure 2.19 the obvious difference is the filling in of the trough due to cyclical loading. This difference is because only one full cycle was run in the analytical model and more importantly the model currently has no way of capturing the degradation of the crack surfaces during cyclical loading. This specific point is a known behavior not captured by the analytical model and is a suggestion for future testing and development.

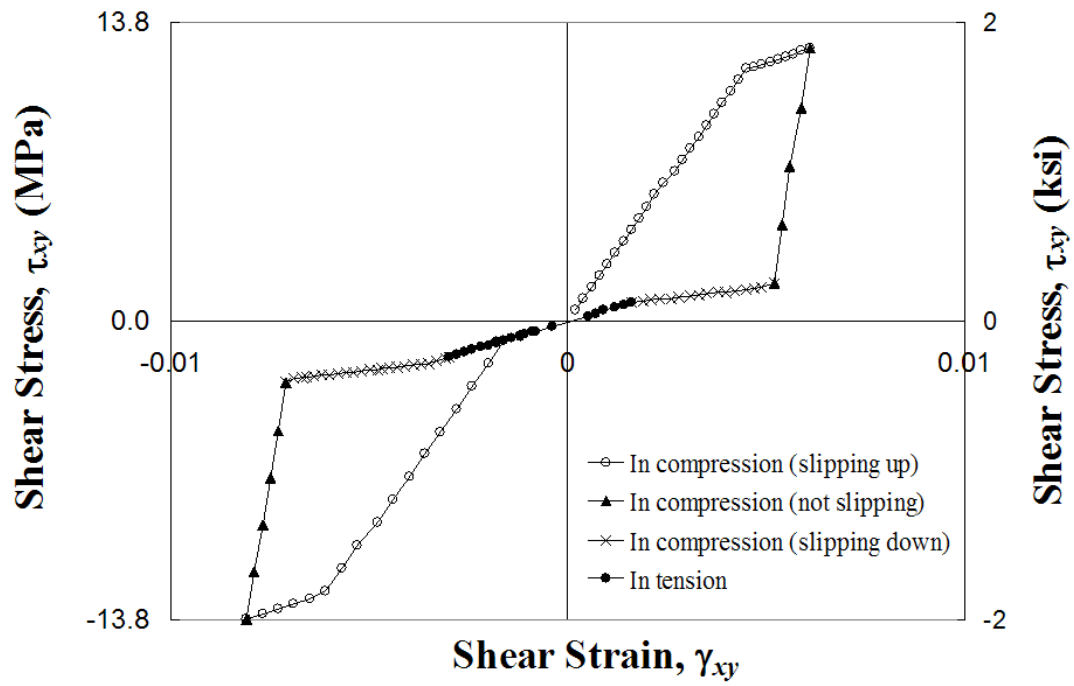


Figure 2.20 Shear Stress vs. Shear Strain [15].

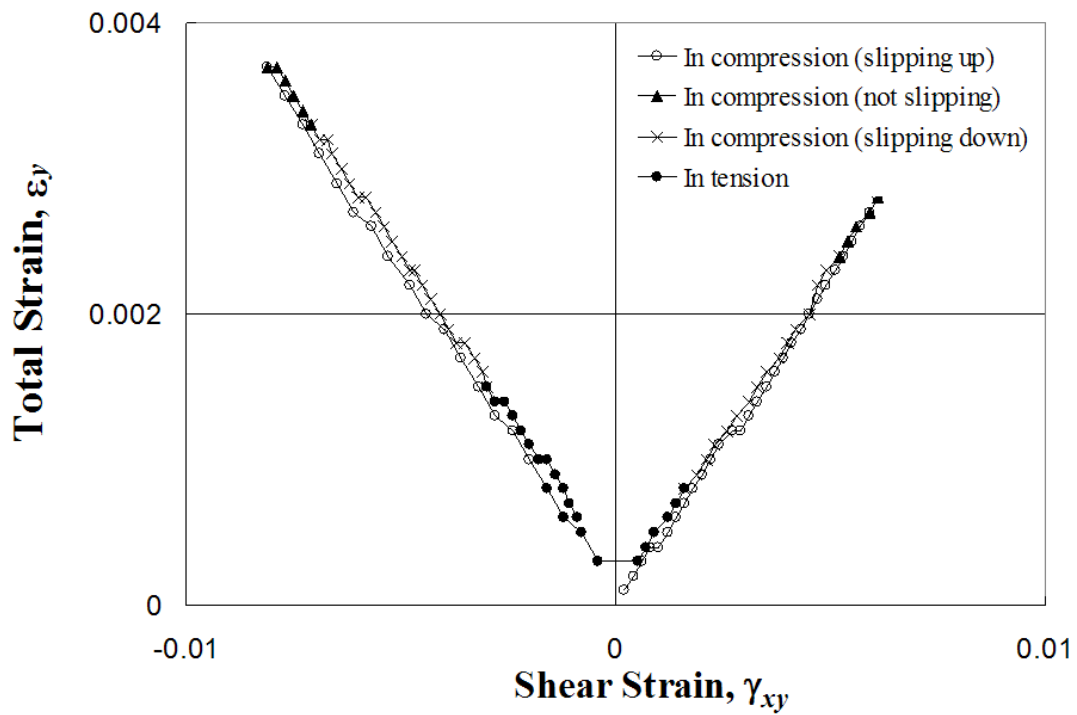


Figure 2.21 Normal Strain vs. Shear Strain (crack-opening path) [15].

## **2.5 Research Direction – Two Crack Orientations**

A new non-linear finite element analytical model that integrates the shear friction concept presented above is developed. The goal is to further generalize the model for a broader range of applications by allowing cracks to form in more than one direction as well as generalize the analysis procedures. The two-directional formulation, analytical difficulties and general procedures are presented in Chapter 3.



## Chapter 3

# Orthogonal Cracking Shear Friction

## Model Iterations

Before the proposed shear friction model can be fully implemented into finite element programs, an analytical model for two-directional orthogonal cracking needs to be developed. The current 1-directional cracking model was successfully implemented in a MATLAB program for a single finite element subjected to a uniform state of cyclical strain using a secant stiffness formulation. Presented in this chapter are the steps taken toward developing a model that allows two-crack directions orthogonal to one another. The first crack will form in the principal tension direction and establish the local material coordinate system. The second crack will be allowed to form orthogonal to the first crack. Multiple iterations of different analysis schemes are presented as developmental phases which document the progress made in understanding the material behavior and modeling issues associated with achieving an orthogonal cracking shear friction model. Formulations, criteria, modeling issues, new understandings and various unique analysis techniques are all presented in this chapter.

## 3.1 Description of Development Procedures

The first step toward generalizing the shear friction method into multiple crack directions was to produce a working single element finite model capable of defining cracks in two directions. The model included non-linear concrete and steel material properties and was capable of cyclical loading. Next the shear friction theory could be inserted into the existing finite element framework. Prior to the insertion of the shear friction method changes to the shear friction theory, analysis methods, and element definitions were necessary. At each stage in the development of the model new considerations of the element's behavior and the current analysis method necessitated new formulations. These new formulations are termed as phases. Each phase yielded a different degree of success and a new set of usable information bringing a working model closer to realization. Listed below are developments and definitions described in this chapter that were necessary for understanding the insertion of the expanded orthogonal cracking shear friction theory:

1. Element definition, degrees of freedom, and material coordinates.
2. Orthogonal cracking definition.
3. Formulating the shear friction theory for two crack directions.
4. Obtaining a state of uniform stress and strain.
5. Obtaining shear stresses in the crack orientation.
6. A detailed description of the phases and finite element models produced.

## 3.2 Element & Simplified Structural Model

In order to understand the derivation of the Orthogonal Shear Friction Theory and its insertion into a finite element frame work, it is important to clearly define the basic parameters of the finite element model. All of the definitions in this section will be kept consistent throughout the thesis.

A bilinear rectangular element was chosen for use in this research. Bilinear rectangular elements are simple four-noded elements that have 8 degrees of freedom (DOF). Each node can translate horizontally and vertically. This type of element was chosen in part because its geometry is suitable for most reinforced concrete structures but also because it is appropriate for plane stress problems, as shown in previous studies such as Vecchio et al. [21]. This type of “low-powered” element was also chosen to increase computational efficiency.

For the purposes of this research the finite element structural model was simplified to one element. Figure 3.1 shows the element, its dimensions, the DOF's, and the boundary conditions. The element is square having dimensions “ $2a$ ” and “ $2b$ ”, with a thickness “ $t$ ”, where in this case  $a=b$ . The bottom left node is pinned (restrained both vertically and laterally) and the bottom right node is a roller, free to translate laterally only. All of the odd numbered DOF's represent lateral translation of the nodes and the even numbered DOF's represent vertical translation. Figure 3.2 shows the element's coordinate definitions. The global coordinate system is “ $x-y$ ” and the local crack direction coordinate system is “ $1-2$ ” which is defined by angle,  $\theta$ . The 1-direction is defined to be orthogonal to the first crack.

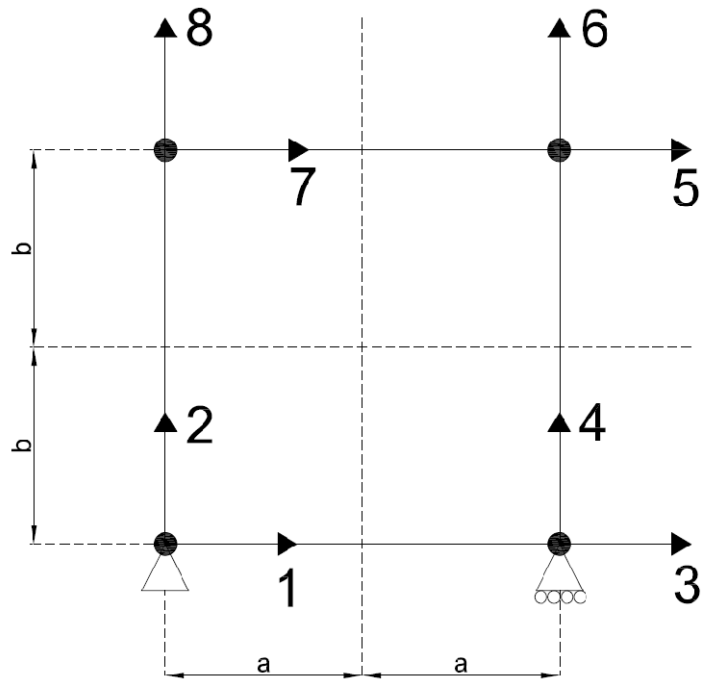


Figure 3.1 Bilinear rectangular element, dimensions, DOF's and boundary conditions.

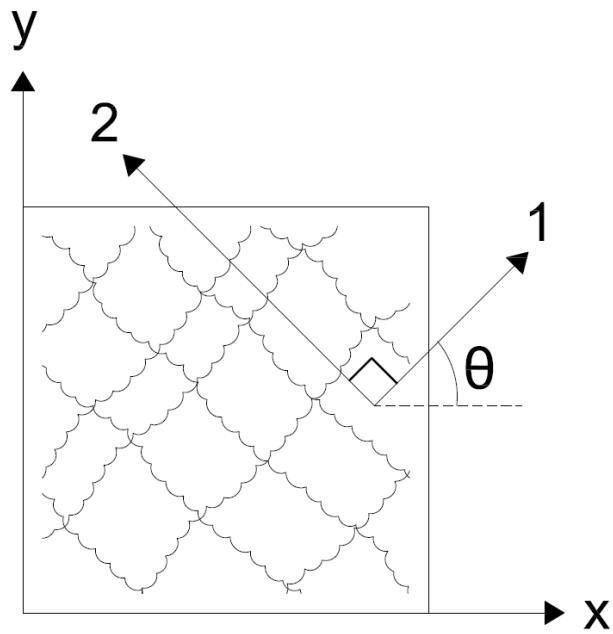


Figure 3.2 Element coordinate systems.

### 3.3 Orthogonal Cracking

To fully implement the shear friction model into a finite element program is to develop a 2-D cracking model. Currently there is a working 1-D model as described in Chapter 2. The simplest 2-D cracking model to start with is orthogonal cracking. This is because a non-orthogonal cracking model would require tracking crack strains in multiple coordinate systems. In the orthogonal model the first crack will form in the principal tension direction and will establish the local material coordinates as shown by coordinate “1” in Figure 3.2. A second crack will be allowed to form orthogonal to the first, coordinate “2” in Figure 3.2. Because the maximum tensile stress may not be in the second crack direction, reasonable cracking criteria will have to be established. This is discussed in a later section of this chapter.

It is important to again discuss the assumptions of smeared material properties and a total strain based model here. For the initial Orthogonal Shear Friction Theory formulation it is assumed that the total strains are almost all crack strains. This reduces computational effort because only total shear slip needs to be tracked as it will be equal to the crack slip. Also, as discussed previously, material properties and cracks are smeared across the element. This coupled with a linear crack opening path eliminates the need to keep track of individual crack spacing. Once two cracks have formed it will be difficult to determine how incremental shear strain is distributed between the two crack directions. For this reason and for simplicity, another important assumption will be that only one crack can slip or be “active” at a time. This assumption is reasonable because it is unlikely that both cracks will be active simultaneously in realistic situations. However, criteria will be established that will allow cracks to slip alternately in the two directions.

## 3.4 The Orthogonal Shear Friction Theory

The relationships of friction and slip and separation originally simplified for the implementation into finite element analysis by So [15] are reformulated for two-directional orthogonal cracking. As established previously, a crack will be allowed to form at any angle,  $\theta$  from the global coordinate system. This angle is defined by the principal tension direction, and the first crack forms normal to the principal tension direction. Once the first crack direction is established a second crack will be allowed to form orthogonal to the first. Once the crack direction (1-2 direction) has been established, shear transfer through shear friction can now be considered. This section details the formulation of the cracked concrete constitutive relationships that allow shear friction behavior.

### 3.4.1 Review of Concepts

As detailed in Section 2.4.3, a linear crack opening path defined by the total shear strain and the total normal strain relative to the crack direction will be assumed to enforce the slip-separation relationship, such that  $\gamma = a\epsilon$ . From the crack opening path effective strain,  $\epsilon^e$ , can be defined. Effective strain is the quantity that defines the state of the crack relative to the crack opening path, as the crack surface could in theory be in contact and compression or completely separated and in tension. Knowing the state of the crack at any given point allows active crack and shear friction criteria to be established. If the crack surfaces are not in contact then shear friction cannot be considered. If the crack surfaces are in contact then shear friction can be considered. A complete formulation of the orthogonal cracking shear friction theory is presented in sections 3.4.2 and 3.4.3.

### 3.4.2 Stress/Strain Formulations

For the purposes of formulation, assume that the concrete element defined in Section 3.2 has been pre-cracked so that there are two cracks. The first crack will be labeled “Crack 1” and set the local crack coordinates “1-2” as shown in Figure 3.3. Note that Crack 1 is defined as the crack normal to the “1” direction. The second crack will be labeled “Crack 2” and will be orthogonal to Crack 1 by definition. Figure 3.3 also shows the element in a deformed state with Crack 1 open. Both cracks are in compression, but only Crack 1 has slipped, inducing separation across the surface. Crack 2 remains in compression and has zero slip. Although Crack 2 has neither slipped nor separated, it could in theory, still be the active crack in a state of “no slip”. For the initial formulation of the Orthogonal Shear Friction Theory stress-strain relationships, only Crack 1 will be considered active.

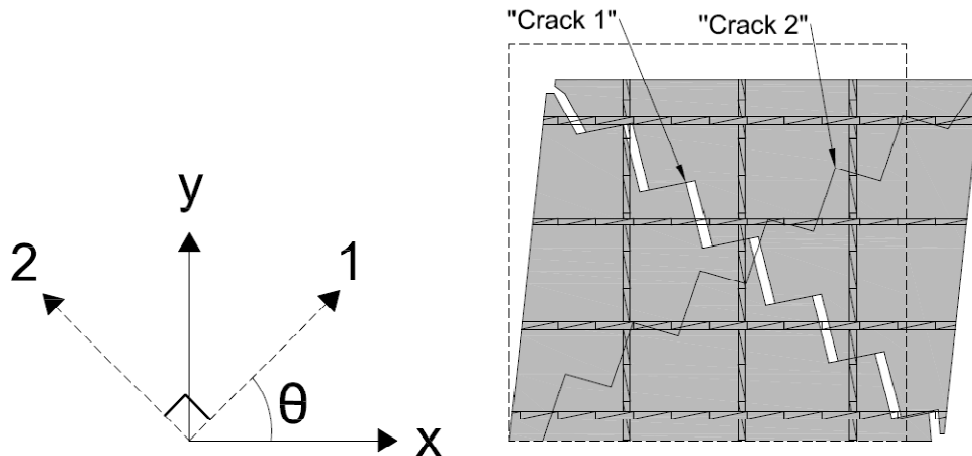


Figure 3.3 Crack definitions and schematic of the slip-separation relationship of the active crack.

#### Effective Strain

For orthogonal cracking, epsilon effective is defined for each crack. This is necessary as effective strain will help define the active crack criteria presented in a later section of this chapter. Equations (3-1) and (3-2) define effective strain by subtracting the

separation strain due to crack slip (crack opening path in the 1-2 direction) from the total strain normal to the crack.

$${}^e\varepsilon_1 = \varepsilon_1 - \frac{|\gamma_{12}|}{a} \quad (3-1)$$

$${}^e\varepsilon_2 = \varepsilon_2 - \frac{|\gamma_{12}|}{a} \quad (3-2)$$

### Normal Concrete Stress

Effective strain is used to define the concrete stresses normal to the crack surfaces,  $\sigma_1$  and  $\sigma_2$ . Positive values of effective strain represent tension across the crack surface and negative values represent compression. As discussed in Section 2.4.3, a tension stiffening curve is used to model the reduced stiffness in the tensile strain region and the full elastic modulus of concrete is used for simplicity in the compressive strain regions. The equations for normal stress in the concrete are listed below and formulated for Crack 1. The equations for Crack two can be obtained by replacing the “1’s” with “2’s” for the stress and strain notations.

(a)  ${}^e\varepsilon_1 \leq \varepsilon_{cr}$  (the cracking strain of concrete):

$$\sigma_1 = E_c {}^e\varepsilon_1 = E_c \left( \varepsilon_1 - \frac{|\gamma_{12}|}{a} \right) \quad (3-3)$$

where  $E_c$  is the full modulus of elasticity of concrete.

(b)  ${}^e\varepsilon_1 > \varepsilon_{cr}$  :

$$\sigma_1 = \frac{f_{cr}}{\sqrt{1+200 {}^e\varepsilon_1}} \quad (3-4)$$

where  $f_{cr}$  is the cracking stress of concrete [15].



### **Maximum and Minimum Shear Stresses**

The shear stress equations are lumped into two major categories: when the normal stress to the crack is tensile and when the normal stress to the crack is compressive. Within the compressive normal stress category shear stress is broken down again into two categories: positive and negative shearing strain relative to the crack. At this point limits on the stresses are introduced to distinguish the physical behavior of the crack. At any given point the crack surface could be slipping up the hill, down the hill or not slipping. All of the equations presented here assume that Crack 1 is the active crack. A sample derivation of the stress limit equations presented below can be found in Appendix A.

### **Tension Across the Crack**

If the normal stress,  $\sigma_1$ , is tensile the shear stress is calculated as follows, assuming that this is the shearing stress resisted by dowel action of the reinforcement crossing the crack:

$$\tau_{12} = \frac{\beta' G \gamma_{12}}{(1 + \beta')} \quad (3-5)$$

The idea is that there is some minimal stiffness when the cracks are not in contact.

### **Compression Across the Crack**

If the normal stress,  $\sigma_1$ , is compressive and the crack surfaces are in contact the shear stress is determined by the following equations:

For positive shearing strain ( $\gamma_{12} > 0$ ), the following three cases are considered.

(a) If the crack surface is slipping down a hill:

$$\tau_{12}^a = \frac{\beta' G \gamma_{12} + \mu^{down} \sigma_1}{(1 + \beta')} \quad (3-6)$$

(b) If the crack surface is not slipping:

$$\tau_{12}^b = \tau_{12,prev} + G(\gamma_{12} - \gamma_{12,prev}) \quad (3-7)$$

In Equation (3-7) “prev” refers to the previously converged stress or strain value.

(c) If the crack surface is slipping up a hill:

$$\tau_{12}^c = \frac{\beta' G \gamma_{12} - \mu^{up} \sigma_1}{(1 + \beta')} \quad (3-8)$$

For negative shearing strain ( $\gamma_{12} < 0$ ), the following three cases are considered:

(a) If the crack surface is slipping up a hill:

$$\tau_{12}^a = \frac{\beta' G \gamma_{12} + \mu^{up} \sigma_1}{(1 + \beta')} \quad (3-9)$$

(b) If the crack surface is not slipping:

$$\tau_{12}^b = \tau_{12,prev} + G(\gamma_{12} - \gamma_{12,prev}) \quad (3-10)$$

In Equation (3-10) “prev” refers to the previously converged stress or strain value.

(c) If the crack surface is slipping down a hill:

$$\tau_{12}^c = \frac{\beta' G \gamma_{12} - \mu^{down} \sigma_1}{(1 + \beta')} \quad (3-11)$$

For any given shear strain,  $\gamma_{12}$ , the shear stress,  $\tau_{12}$ , is determined from the “not slipping equation” but is limited by the minimum and maximum shear stresses,  $\tau_{12}^a$  and  $\tau_{12}^c$  as shown below:

$$\tau_{12} = \tau_{12}^b$$

$$\text{Where, } \tau_{12}^a \leq \tau_{12} \leq \tau_{12}^c$$

These shear stress equations can be formulated for the Crack 2 by replacing the normal stress,  $\sigma_1$ , with the normal stress relative to Crack 2,  $\sigma_2$ .

### 3.4.3 Secant Stiffness Matrix Formulation

The base secant stiffness matrix used to define the concrete stress strain relationship is a 3x3 diagonal matrix shown below. However, this matrix will be altered to include the complete Orthogonal Shear Friction Theory, including effective strain, tension stiffening, the crack opening path and maximum and minimum shear stresses.

$$\begin{Bmatrix} \sigma_1 \\ \sigma_2 \\ \tau_{12} \end{Bmatrix} = \begin{bmatrix} \frac{\sigma_1^{\text{old}}}{\varepsilon_1^{\text{old}}} & 0 & 0 \\ 0 & \frac{\sigma_2^{\text{old}}}{\varepsilon_2^{\text{old}}} & 0 \\ 0 & 0 & \frac{\tau_{12}^{\text{old}}}{\gamma_{12}^{\text{old}}} \end{bmatrix} \begin{Bmatrix} \varepsilon_1 \\ \varepsilon_2 \\ \gamma_{12} \end{Bmatrix} \quad (3-12)$$

Poisson's Ratio is intentionally set to zero for simplicity of formulation and interpretation of results. The Orthogonal Shear Friction Theory stiffness matrices are formulated for all of the possible states of stress parallel and normal to the crack surface.

#### Case 1: Crack Direction 1 Active

Once Crack 1 has formed cases for stiffness must be considered:

1. If the normal stress is tensile, the stress-strain relationship is as follows for positive and negative shearing strain,  $\gamma_{12}$ , respectively.

$$\begin{Bmatrix} \sigma_1 \\ \sigma_2 \\ \tau_{12} \end{Bmatrix} = \begin{bmatrix} E_1 & 0 & \frac{-E_1}{a} \\ 0 & E_2 & 0 \\ 0 & 0 & \frac{\beta'G}{1+\beta'} \end{bmatrix} \begin{Bmatrix} \varepsilon_1 \\ \varepsilon_2 \\ \gamma_{12} \end{Bmatrix} \quad (3-13)$$

$$\begin{Bmatrix} \sigma_1 \\ \sigma_2 \\ \tau_{12} \end{Bmatrix} = \begin{bmatrix} E_1 & 0 & \frac{E_1}{a} \\ 0 & E_2 & 0 \\ 0 & 0 & \frac{\beta'G}{1+\beta'} \end{bmatrix} \begin{Bmatrix} \varepsilon_1 \\ \varepsilon_2 \\ \gamma_{12} \end{Bmatrix} \quad (3-14)$$

Where  $E_1$  is the secant stiffness of concrete defined as the normal stress (Equation 3-4) divided by the current effective strain value,  $\varepsilon_1$ .  $E_2$  can be obtained in the same manner as  $E_1$  by replacing the “1’s” with “2’s” in the stress and strain notations.  $\beta'$  is the dowel action shear retention factor and  $G$  is the shear modulus of concrete.

2. If the normal stress is compressive, the secant stiffness matrix is defined based on the normal compressive stress, Equation 3-3, and the various cases of the shear stress. For positive total shear strain ( $\gamma_{12} > 0$ ), the following cases are considered:

(a) If the crack surface is slipping down a hill:

Equation 3-6 can be rewritten as:

$$\tau_{12}^a = \frac{\beta'G\gamma_{12} + \mu^{down}(E_c\varepsilon_{eff})}{(1 + \beta')} = \frac{\beta'G\gamma_{12} + \mu^{down}E_c\left(\varepsilon_1 - \frac{\gamma_{12}}{a}\right)}{(1 + \beta')}$$

And the secant stiffness matrix then becomes,

$$\begin{Bmatrix} \sigma_1 \\ \sigma_2 \\ \tau_{12} \end{Bmatrix} = \begin{bmatrix} E_c & 0 & \frac{-E_c}{a} \\ 0 & E_c & 0 \\ \frac{\mu^{down}E_c}{1+\beta'} & 0 & \frac{\beta'G - \mu^{down}E_c/a}{1+\beta'} \end{bmatrix} \begin{Bmatrix} \varepsilon_1 \\ \varepsilon_2 \\ \gamma_{12} \end{Bmatrix} \quad (3-15)$$

(b) If the crack surface is not slipping:

Equation 3-7 is written as:

$$\tau_{12}^b = \tau_{12,prev} + G(\gamma_{12} - \gamma_{12,prev})$$

And the secant stiffness matrix becomes,

$$\begin{Bmatrix} \sigma_1 \\ \sigma_2 \\ \tau_{12} \end{Bmatrix} = \begin{bmatrix} E_c & 0 & -\frac{E_c}{a} \\ 0 & E_c & 0 \\ 0 & 0 & \frac{\tau_{12}^b}{\gamma_{12}^{old}} \end{bmatrix} \begin{Bmatrix} \varepsilon_1 \\ \varepsilon_2 \\ \gamma_{12} \end{Bmatrix} \quad (3-16)$$

(c) If the crack surface is slipping up a hill:

Equation 3-8 can be rewritten as:

$$\tau_{12}^c = \frac{\beta' G \gamma_{12} - \mu^{up} (E_c \varepsilon_{eff})}{(1 + \beta')} = \frac{\beta' G \gamma_{12} - \mu^{up} E_c \left( \varepsilon_1 - \frac{\gamma_{12}}{a} \right)}{(1 + \beta')}$$

And the secant stiffness matrix becomes,

$$\begin{Bmatrix} \sigma_1 \\ \sigma_2 \\ \tau_{12} \end{Bmatrix} = \begin{bmatrix} E_c & 0 & -\frac{E_c}{a} \\ 0 & E_c & 0 \\ \frac{-\mu^{up} E_c}{1 + \beta'} & 0 & \frac{\beta' G + \mu^{up} E_c / a}{1 + \beta'} \end{bmatrix} \begin{Bmatrix} \varepsilon_1 \\ \varepsilon_2 \\ \gamma_{12} \end{Bmatrix} \quad (3-17)$$

For negative total shearing strain ( $\gamma_{12} < 0$ ), the following cases are considered:

(a) If the crack surface is slipping up a hill:

Equation 3-9 can be rewritten as:

$$\tau_{12}^a = \frac{\beta' G \gamma_{12} + \mu^{up} (E_c \varepsilon_{eff})}{(1 + \beta')} = \frac{\beta' G \gamma_{12} + \mu^{up} E_c \left( \varepsilon_1 + \frac{\gamma_{12}}{a} \right)}{(1 + \beta')}$$

And the secant stiffness matrix becomes,

$$\begin{Bmatrix} \sigma_1 \\ \sigma_2 \\ \tau_{12} \end{Bmatrix} = \begin{bmatrix} E_c & 0 & \frac{E_c}{a} \\ 0 & E_c & 0 \\ \frac{\mu^{up} E_c}{1+\beta'} & 0 & \frac{\beta' G + \mu^{up} E_c / a}{1+\beta'} \end{bmatrix} \begin{Bmatrix} \varepsilon_1 \\ \varepsilon_2 \\ \gamma_{12} \end{Bmatrix} \quad (3-18)$$

(b) If the crack surface is not slipping:

Equation 3-10 is written:

$$\tau_{12}^b = \tau_{12,prev} + G(\gamma_{12} - \gamma_{12,prev})$$

And the secant stiffness matrix becomes,

$$\begin{Bmatrix} \sigma_1 \\ \sigma_2 \\ \tau_{12} \end{Bmatrix} = \begin{bmatrix} E_c & 0 & \frac{E_c}{a} \\ 0 & E_c & 0 \\ 0 & 0 & \frac{\tau_{12}^b}{\gamma_{12}^{old}} \end{bmatrix} \begin{Bmatrix} \varepsilon_1 \\ \varepsilon_2 \\ \gamma_{12} \end{Bmatrix} \quad (3-$$

19)

(c) If the crack surface is slipping down a hill:

Equation 3-11 can be rewritten as:

$$\tau_{12}^c = \frac{\beta' G \gamma_{12} - \mu^{down} (E_c \varepsilon_{eff})}{(1 + \beta')} = \frac{\beta' G \gamma_{12} - \mu^{down} E_c \left( \varepsilon_1 + \frac{\gamma_{12}}{a} \right)}{(1 + \beta')}$$

And the secant stiffness matrix becomes,

$$\begin{Bmatrix} \sigma_1 \\ \sigma_2 \\ \tau_{12} \end{Bmatrix} = \begin{bmatrix} E_c & 0 & \frac{E_c}{a} \\ 0 & AE_c & 0 \\ \frac{-\mu^{down} E_c}{1+\beta'} & 0 & \frac{\beta' G - \mu^{down} E_c / a}{1+\beta'} \end{bmatrix} \begin{Bmatrix} \varepsilon_1 \\ \varepsilon_2 \\ \gamma_{12} \end{Bmatrix} \quad (3-20)$$

### Case 2: Crack Direction 2 Active

Once Crack 2 has formed the following cases for stiffness must be considered if Crack 2 is the active crack:

1. If the normal stress is tensile, the stress-strain relationship is as follows for positive and negative shearing strain,  $\gamma_{12}$ , respectively:

$$\begin{Bmatrix} \sigma_1 \\ \sigma_2 \\ \tau_{12} \end{Bmatrix} = \begin{bmatrix} E_1 & 0 & 0 \\ 0 & E_2 & \frac{-E_2}{a} \\ 0 & 0 & \frac{\beta' G}{1+\beta'} \end{bmatrix} \begin{Bmatrix} \varepsilon_1 \\ \varepsilon_2 \\ \gamma_{12} \end{Bmatrix} \quad (3-21)$$

$$\begin{Bmatrix} \sigma_1 \\ \sigma_2 \\ \tau_{12} \end{Bmatrix} = \begin{bmatrix} E_1 & 0 & 0 \\ 0 & E_2 & \frac{E_2}{a} \\ 0 & 0 & \frac{\beta' G}{1+\beta'} \end{bmatrix} \begin{Bmatrix} \varepsilon_1 \\ \varepsilon_2 \\ \gamma_{12} \end{Bmatrix} \quad (3-22)$$

2. If the normal stress is compressive, the secant stiffness matrix is defined based on the normal compressive stress and the various cases of the shear stress. For positive total shear strain ( $\gamma_{12} > 0$ ), the following cases are considered:

- (a) If the crack surface is slipping down a hill:

$$\begin{Bmatrix} \sigma_1 \\ \sigma_2 \\ \tau_{12} \end{Bmatrix} = \begin{bmatrix} E_c & 0 & 0 \\ 0 & E_c & -\frac{E_c}{a} \\ 0 & \frac{\mu^{\text{down}} E_c}{1+\beta'} & \frac{\beta' G - \mu^{\text{down}} E_c / a}{1+\beta'} \end{bmatrix} \begin{Bmatrix} \varepsilon_1 \\ \varepsilon_2 \\ \gamma_{12} \end{Bmatrix} \quad (3-23)$$

- (b) If the crack surface is not slipping:

$$\begin{Bmatrix} \sigma_1 \\ \sigma_2 \\ \tau_{12} \end{Bmatrix} = \begin{bmatrix} E_c & 0 & 0 \\ 0 & E_c & -\frac{E_c}{a} \\ 0 & 0 & \frac{\tau_{12}^b}{\gamma_{12}^{\text{old}}} \end{bmatrix} \begin{Bmatrix} \varepsilon_1 \\ \varepsilon_2 \\ \gamma_{12} \end{Bmatrix} \quad (3-24)$$

- (c) If the crack surfaces is slipping up a hill:

$$\begin{Bmatrix} \sigma_1 \\ \sigma_2 \\ \tau_{12} \end{Bmatrix} = \begin{bmatrix} E_c & 0 & 0 \\ 0 & E_c & -\frac{E_c}{a} \\ 0 & \frac{-\mu^{\text{up}} E_c}{1+\beta'} & \frac{\beta' G + \mu^{\text{up}} E_c / a}{1+\beta'} \end{bmatrix} \begin{Bmatrix} \varepsilon_1 \\ \varepsilon_2 \\ \gamma_{12} \end{Bmatrix} \quad (3-25)$$

For negative total shearing strain ( $\gamma_{12} < 0$ ), the following cases are considered:

(a) If the crack surface is slipping up a hill:

$$\begin{Bmatrix} \sigma_1 \\ \sigma_2 \\ \tau_{12} \end{Bmatrix} = \begin{bmatrix} E_c & 0 & 0 \\ 0 & E_c & \frac{E_c}{a} \\ 0 & \frac{\mu^{up} E_c}{1+\beta'} & \frac{\beta' G + \mu^{up} E_c / a}{1+\beta'} \end{bmatrix} \begin{Bmatrix} \varepsilon_1 \\ \varepsilon_2 \\ \gamma_{12} \end{Bmatrix} \quad (3-26)$$

(b) If the crack surface is not slipping:

$$\begin{Bmatrix} \sigma_1 \\ \sigma_2 \\ \tau_{12} \end{Bmatrix} = \begin{bmatrix} E_c & 0 & 0 \\ 0 & E_c & \frac{E_c}{a} \\ 0 & 0 & \frac{\tau_{12}^b}{\gamma_{12}^{old}} \end{bmatrix} \begin{Bmatrix} \varepsilon_1 \\ \varepsilon_2 \\ \gamma_{12} \end{Bmatrix} \quad (3-27)$$

(c) If the crack surface is slipping down a hill:

$$\begin{Bmatrix} \sigma_1 \\ \sigma_2 \\ \tau_{12} \end{Bmatrix} = \begin{bmatrix} E_c & 0 & 0 \\ 0 & E_c & \frac{E_c}{a} \\ 0 & \frac{-\mu^{down} E_c}{1+\beta'} & \frac{\beta' G - \mu^{down} E_c / a}{1+\beta'} \end{bmatrix} \begin{Bmatrix} \varepsilon_1 \\ \varepsilon_2 \\ \gamma_{12} \end{Bmatrix} \quad (3-28)$$

### 3.4.4 Active Crack Criteria

The Orthogonal Shear Friction Theory includes 16 different stiffness formulations to model the concrete behavior at any given state of stress and strain for two crack directions. These 16 formulations become pertinent once orthogonal cracking has occurred as defined in Section 3.3. As stated previously, only one established crack direction can be active at time. In order to implement the Orthogonal Shear Friction Theory into a finite element program, rational criteria for active crack and the current state of the crack surface needs to be established.



At any given state of stress and strain the crack surface may be in tension or compression. This is defined by the crack opening path, specifically effective strain. Positive values of effective strain represent tension across the crack surface, more specifically meaning that the rough surfaces of the crack are not in contact. Negative values of effective strain represent compression across the crack, more specifically meaning that the rough surfaces of the crack are in contact and shear friction can be developed. Once it is established that the crack is either in compression or tension for the current state, more detailed criteria are necessary to further define the material stiffness.

If both cracks are in tension then crack slip, or  $\gamma_{12}$ , is split between the cracks. However, this case is unlikely for most realistic loading situations. If Crack 1 is in tension and Crack 2 is in compression, then the active crack is defined as Crack 1. This is because slip would tend to be focused on the open crack as it can only be resisted by tension in the reinforcement crossing the crack. Just the same if Crack 2 is in tension and Crack 1 is in compression, the active crack will be Crack 2. The last possible case is both cracks in compression. To determine the active crack for this situation requires the maximum and minimum shear stress limits. The upper and lower limits on the shear stress,  $\tau^a$  and  $\tau^c$ , represent the stress necessary to overcome the force of friction across the crack and initiate slip. If the current value of shear stress,  $\tau^b$ , is between these limits then the crack is not slipping. However, if the current value of shear stress is above or below the limits then by definition the shear stress is the limit that was exceeded, as the stress is sufficient to initiate slip across the crack. This definition is utilized to formulate the active crack criteria for the double compression case.

The shear stress limits for both cracks are necessary to determine the active crack ( $\tau^a$ ,  $\tau^c$ ,  $\tau^a_2$ ,  $\tau^c_1$ , and  $\tau^c_2$ ). The active crack will be defined as the crack that has the limits that would be reached first. This is because slip would be initiated in this crack first, controlling the behavior. To better understand this idea it is useful to view the shear stress limits on one dimensional plot as shown in Figure 3.4.



Figure 3.4 Example shear stress limits on a one-dimensional plot.

From the example presented in Figure 3.4 it is clear that the shear stress,  $\tau^b$ , for the current iteration is outside the upper limits,  $\tau_1^c$  and  $\tau_2^c$ . Because the upper slip limit for Crack 1,  $\tau_1^c$ , would have been reached first, Crack 1 will be defined as the active crack in this case. Similarly if  $\tau^b$  had been located outside of either of the lower bounds,  $\tau_1^a$  and  $\tau_2^a$ , Crack 1 would be the active crack. If  $\tau^b$  had been located between all of the limits in Figure 3.4, Crack 1 would still be the active crack because both of its slip limits would be reached before Crack 2's. However, in this case there would be no crack slip as neither of the limits would have been reached. A summary of the active crack criteria is presented in Table 3.1.

Table 3.1 Summary of Active Crack Criteria

$\epsilon_1$	$\epsilon_2$	Crack 1 Surface State	Crack 2 Surface State	Active Crack
+	+	Tension	Tension	Split – both cracks
+	-	Tension	Compression	Crack 1
-	+	Compression	Tension	Crack 2
-	-	Compression	Compression	Requires analysis of shear stress limits

### **3.5 Uniform State of Stress and Strain**

Obtaining a uniform state of stress and strain was an important consideration in the development of the finite element analysis program and the insertion of the orthogonal shear friction model. A uniform state of strain is defined as strain remains consistent across the dimensions of the element. For a rectangular element, like the membrane being analyzed here, this means that straight lines before strain remain straight after strain and parallel lines before strain remain parallel after strain. Thus a rectangular element subjected to uniform strain could, for example, deform into a parallelogram. A uniform state of stress follows suit, as stresses will be consistent across the dimensions of the element.

Without a uniform state of stress and strain, analyzing and interpreting the results would become too cumbersome and critical material behavior may be lost. In addition verification would be impossible as previous testing of membrane elements and shear transfer across crack surfaces were performed under a uniform state of stress and strain. Obtaining a uniform state of stress and strain consequently becomes a major constraint on the design of the finite element program. Creating this uniform state in a deflection controlled analysis is discussed in detail in the developmental phases of the finite element program.

### **3.6 Shear Stress across the Crack Surface**

As discussed previously, cracks will tend to form perpendicular to the direction of the principal tensile stress. Once orthogonal cracking has been established, the two principal stress directions (orthogonal to one another by definition) define the two crack directions. In order to consider shear transfer by shear friction, there needs to be shear stress across the surface of the crack. In the previous shear friction model created by So [15], the element was subjected to a state of pure shear and was pre-cracked in the

orientation of the applied shear force. This applied shear stress across the surface of the crack directly.

To generalize the shear friction model to include orthogonal cracking at any angle, the concrete cannot be pre-cracked, but allowed to crack in the direction of the principal stresses. Consider, for example, an element subjected to pure shear as shown in Figure 3.5. The orientation of the principal stresses, 1 and 2, will be at an angle,  $\theta$ , of  $45^\circ$  with respect to the x-y coordinate system. In this case the 1-direction is the principal tensile stress, therefore creating a crack parallel to the 2-direction. The shear stress transformed at an angle of  $45^\circ$  to the x-y coordinate system will be equal to zero. With no shear across the surface of the crack, transfer by shear friction becomes irrelevant. The only way to obtain shear across the crack is to apply normal stress to the element. Obtaining shear across the crack surface while maintaining a uniform state of strain is discussed in detail in the developmental phases of the finite element program.

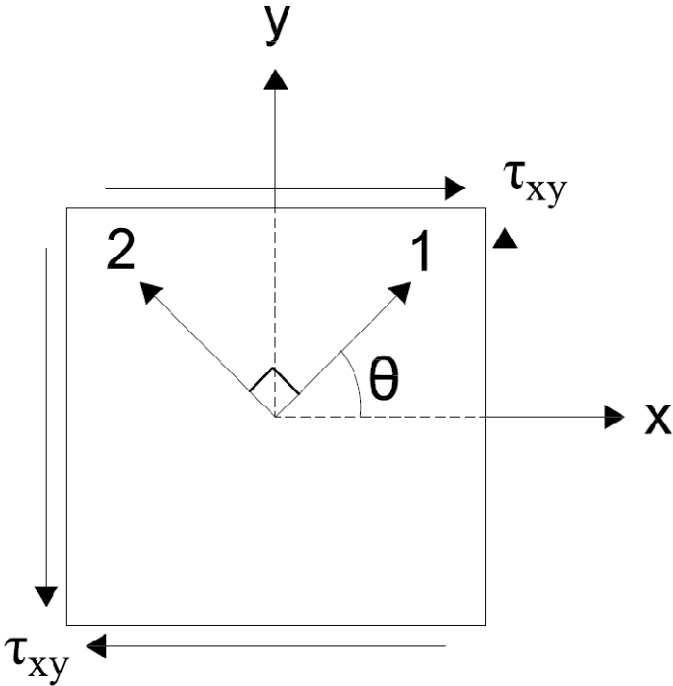


Figure 3.5 Element subjected to pure shear.

## **3.7 Developmental Phases of the Finite Element Model**

There were six phases in the development process of the finite element model for the Orthogonal Shear Friction Theory. At each phase new understandings toward a working model were gained. This section details the formulations, results, and problems encountered with each model.

### **3.7.1 Phase One: Non-Linear Cyclical Model Framework**

This first step toward a working orthogonal cracking shear friction model was to produce a non-linear finite element framework. Once the framework was created, the shear friction model could simply be inserted into the program. The framework was an analysis of a single bi-linear rectangular element that was simply supported on the bottom two nodes. Refer back to Figure 3.1 for a diagram of the element dimensions, degrees of freedom and boundary conditions. The element was subjected to uniform state of stress and strain by deflection controlled procedures. Equal lateral displacements were enforced cyclically to the top two nodes. To ensure a uniform state of stress and strain the vertical displacements of the top two nodes were slaved to one another, making them equal, to prevent bending of the element.

This initial framework included non-linear steel and concrete material properties. The non-linear concrete properties were previously established in Section 3.4.2, including the tension stiffening curve. The non-linear steel model is presented here in Figure 3.6 and was kept consistent in all phases of the model development. The “smeared” steel stress is simply the strain multiplied by the steel modulus of elasticity times the reinforcement ration until the steel yields. Once the steel yields, the “smeared” stress is equal to the

yield strength of the steel times the reinforcement ratio. For unloading the steel from the maximum excursion strain, the slope of the steel modulus of elasticity is used.

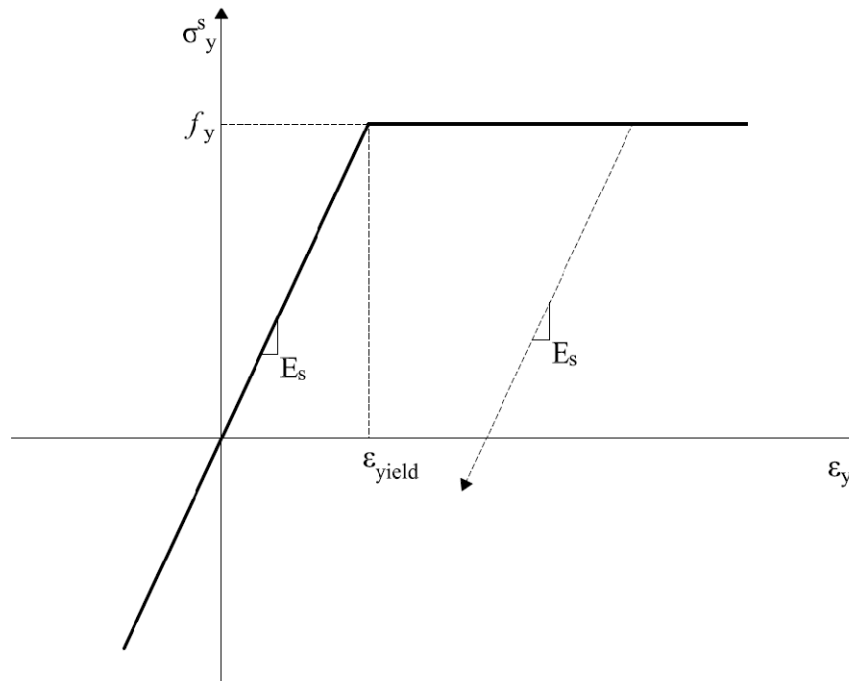


Figure 3.6 Non-linear steel stress-strain relationship.

A working cyclical finite element framework was achieved with the given parameters and material models. Crack directions were established orthogonally and kept constant throughout the cyclical displacements. Convergence was achieved by iteratively checking and updating the secant material properties of steel and concrete individually until the difference between properties between two iterations was within a tolerance. This initial framework, displacement method and convergence scheme were changed throughout the developmental phases as necessary to implement the Orthogonal Shear Friction Theory.

### **3.7.2 Phase Two: Initial Shear Friction Implementation**

The Orthogonal Shear Friction Theory as presented in Section 3.4 was inserted into the initial finite element framework. Displacements were incremented monotonically until the strain was sufficient to crack the concrete. As stated previously, the displacements were enforced to create a uniform state of stress and strain. Once the crack angle was established, the Orthogonal Shear Friction Theory was activated to define the concrete stress-strain relationships and stiffness. These relationships were formulated in the crack coordinate system (1-2 direction) and then rotated to the global coordinate system (x-y direction) for analysis.

Upon review of the incremental converged stress and strain state after cracking, two main problems were observed. The first problem, as previously discussed, was that the applied displacements induced a state of pure shear, with the crack orientation in the direction of the principal stress. By definition the shear stress is zero in the direction of the principal stresses. Therefore, no shear was present across the crack, causing the shear transfer by shear friction irrelevant. The second problem was that the effective strain was always positive, meaning that the crack surfaces were never in contact. Again, without contact or compression across the crack shear friction cannot be developed. The simple reason for this is that loading was such that there was no vertical applied load based on the induced displacements. In realistic situations there would be some vertical load, either applied or induced by the self weight of the element itself. In addition to the two major problems, convergence became an issue as it was not suitable for all the possible stiffness cases in the shear friction theory.

### **3.7.3 Phase Three: Proportional Load Vector (PLV)**

Due to the problems encountered during the initial implementation of the Orthogonal Shear Friction Theory the finite element framework, specifically loading, needed to be reworked. Because the shear friction behavior was never tested during the initial

implementation, the Orthogonal Shear Friction Theory was not altered during this phase. However, alterations were made to the analysis portion of the program. To obtain shear across the crack surface and apply a compressive vertical load on the element, a proportional load vector was used to obtain the desired displacements. The proportional load vector ensured a uniform state of stress and strain, while still allowing a displacement controlled analysis. Formulations of the PLV, a new convergence method, results and difficulties are presented in the subsets of this section.

### Formulation of the Proportional Load Vector

Previously, for a displacement controlled analysis, the global stiffness matrix was partitioned into the “Free”, “Restrained” and “Prescribed” degrees of freedom as shown in Equation 3-29.

$$\begin{Bmatrix} A_F \\ A_P \\ A_R \end{Bmatrix} = \begin{bmatrix} S_{FF} & S_{FP} & S_{FR} \\ S_{PF} & S_{PP} & S_{PR} \\ S_{RF} & S_{RP} & S_{RR} \end{bmatrix} \begin{Bmatrix} D_F \\ D_P \\ D_R \end{Bmatrix} \quad (3-29)$$

Where “A” refers to action or force, “S” refers to the global stiffness matrix terms, and “D” refers to nodal displacements. The subscripts “F”, “P” and “R” denote the free, prescribed and restrained degrees of freedom respectively. The free DOF’s were 6&8 and the prescribed DOF’s were 5&7. The remaining DOF’s were restrained as defined by the boundary conditions. By performing the matrix multiplication of Equation 3-29 the following three equations can be obtained:

$$A_F = S_{FF}D_F + S_{FP}D_P + S_{FR}D_R \quad (3-30)$$

$$A_P = S_{PF}D_F + S_{PP}D_P + S_{PR}D_R \quad (3-31)$$

$$A_R = S_{RF}D_F + S_{RP}D_P + S_{RR}D_R \quad (3-32)$$

For the displacement controlled analysis the free DOF’s were slaved by summing the rows and columns in the stiffness equation corresponding to those DOF’s to obtain a



single “master” free DOF in place of two. To keep a uniform state of stress and strain the free actions must be equal and opposite. Therefore, when adding the free DOF’s together  $A_F$ , the load vector component corresponding to the master free DOF will equal zero. In addition the restrained displacements,  $D_R$ , are equal to zero. Now Equation 3-30 can be solved for the free displacements,  $D_F$ . Once the free displacements are known the full displacement column vector can be populated and all of the actions computed by using the partitioned global stiffness matrix.

The PLV formulation similarly requires partitioning the global stiffness matrix into free, prescribed and restrained DOF’s. However, as shown in Figure 3.7, the partitioned DOF’s are slightly different. The PLV states that there is some shape vector,  $\tilde{A}$ , that defines the shape of the loads on the DOF such that:

$$A = \tilde{A}a \tag{3-33}$$

where  $A$  represents the global actions and  $a$  is a constant.

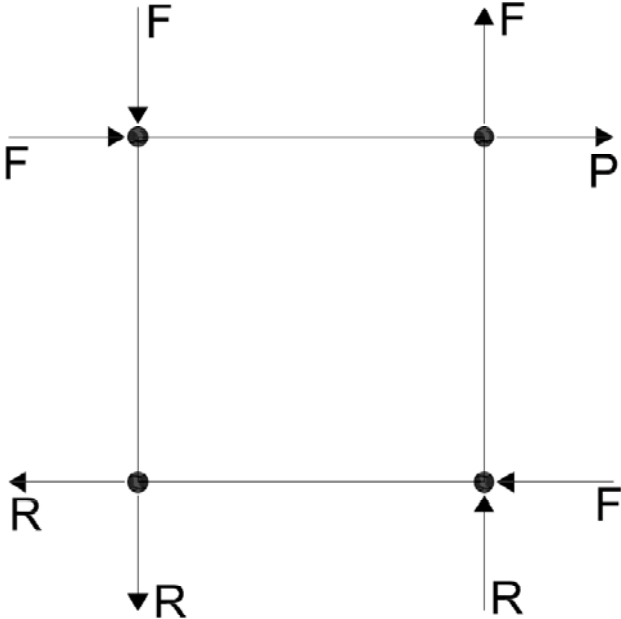


Figure 3.7 Partitioned DOF’s for the PLV.

To ensure a state of uniform stress and strain the shape vector is defined as follows:

$$\tilde{\mathbf{A}} = \begin{Bmatrix} -1 \\ -1 \\ -1 \\ 1 \\ 1 \\ 1 \\ 1 \\ -1 \end{Bmatrix} \text{ where the DOF's are : } \begin{matrix} 1 \\ 2 \\ 3 \\ 4 \\ 5 \\ 6 \\ 7 \\ 8 \end{matrix}$$

Figure 3.8 shows the shape vector applied to the element's DOF's. Now by applying Equation 3-33 to Equation 3-29, and performing the matrix multiplication the following equations can be written:

$$a\tilde{\mathbf{A}}_F = S_{FF}D_F + S_{FP}D_P + S_{FR}D_R \quad (3-34)$$

$$a\tilde{\mathbf{A}}_P = S_{PF}D_F + S_{PP}D_P + S_{PR}D_R \quad (3-35)$$

$$a\tilde{\mathbf{A}}_R = S_{RF}D_F + S_{RP}D_P + S_{RR}D_R \quad (3-36)$$

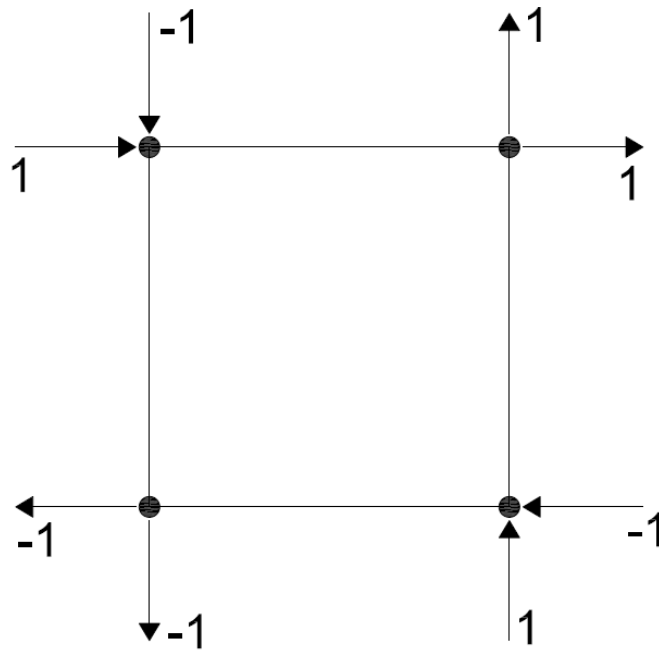


Figure 3.8 Shape vector applied to the element.

Applying the boundary conditions,  $D_R=0$ , and plugging Equation 3-34 into Equation 3-35, and solving for  $a$  yields,

$$a = \frac{S_{PP}D_P - S_{PF}S_{FF}^{-1}S_{FP}D_P}{\tilde{A}_P - S_{PF}S_{FF}^{-1}\tilde{A}_F}$$

Notice that the solution for  $a$  is driven by the prescribed displacement. That is, the PLV still allows for a displacement controlled analysis. However, the shape vector as defined produces a state of pure shear and therefore shear across the crack surfaces and net vertical compression are not guaranteed. To accomplish this, a vertical load,  $v$ , can be applied to the shape vector as shown in Figure 3.9.

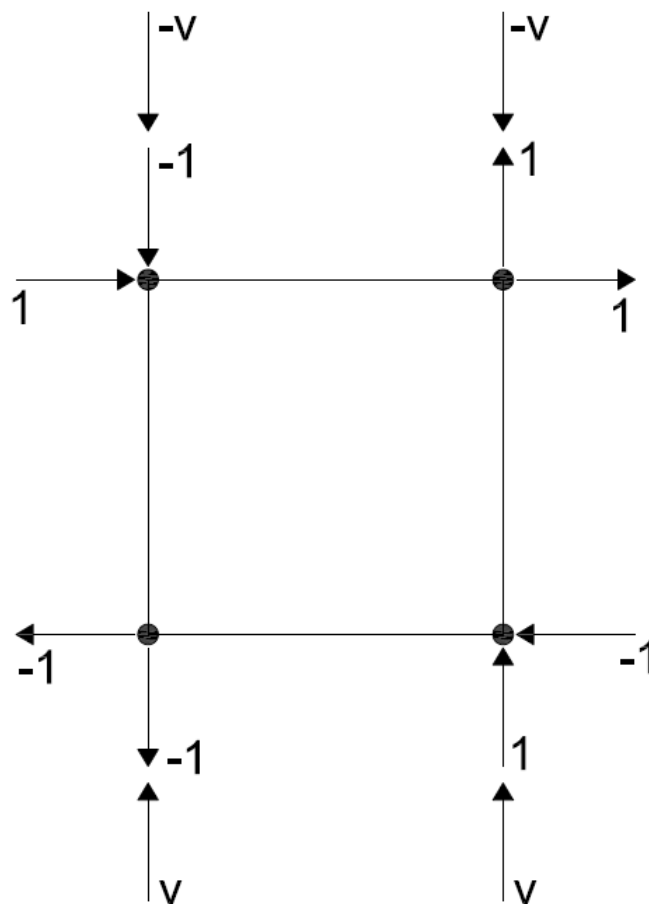


Figure 3.9 Shape vector and vertical load,  $v$ , applied to element.

Now the shape vector can be defined as follows:

$$\tilde{\mathbf{A}} = \begin{Bmatrix} -1 \\ -1 + v \\ -1 \\ 1 + v \\ 1 \\ 1 - v \\ 1 \\ -1 - v \end{Bmatrix} \left. \vphantom{\begin{Bmatrix} -1 \\ -1 + v \\ -1 \\ 1 + v \\ 1 \\ 1 - v \\ 1 \\ -1 - v \end{Bmatrix}} \right\} \text{where the DOF's are : } \begin{matrix} 1 \\ 2 \\ 3 \\ 4 \\ 5 \\ 6 \\ 7 \\ 8 \end{matrix}$$

The solution for  $a$  remains the same and the vertical load,  $v$ , can be defined to ensure compression across the crack surface. Notice that the vertical compression applied to the element is not constant in this formulation, but will change depending on the solution for  $a$ .

### **Convergence on $a$**

Previously, convergence was achieved on the individual material secant values within an iteration. With the new formulation of the PLV, it is convenient to converge on the constant,  $a$ , while still updating the material secant values within an iteration. First a displacement is applied to the prescribed DOF. The previous converged stiffness matrix is used to estimate the new displacements and an initial value for  $a$ . Stresses and strains are then determined from the displacements. The state of stress and strain yields new material secant values which are in turn used to resolve. If the new solution yields a value of  $a$  that is within a tolerance of the previous value for  $a$ , the solution has converged. Figure 3.10 shows a flowchart of the PLV algorithm to illustrate the convergence method.

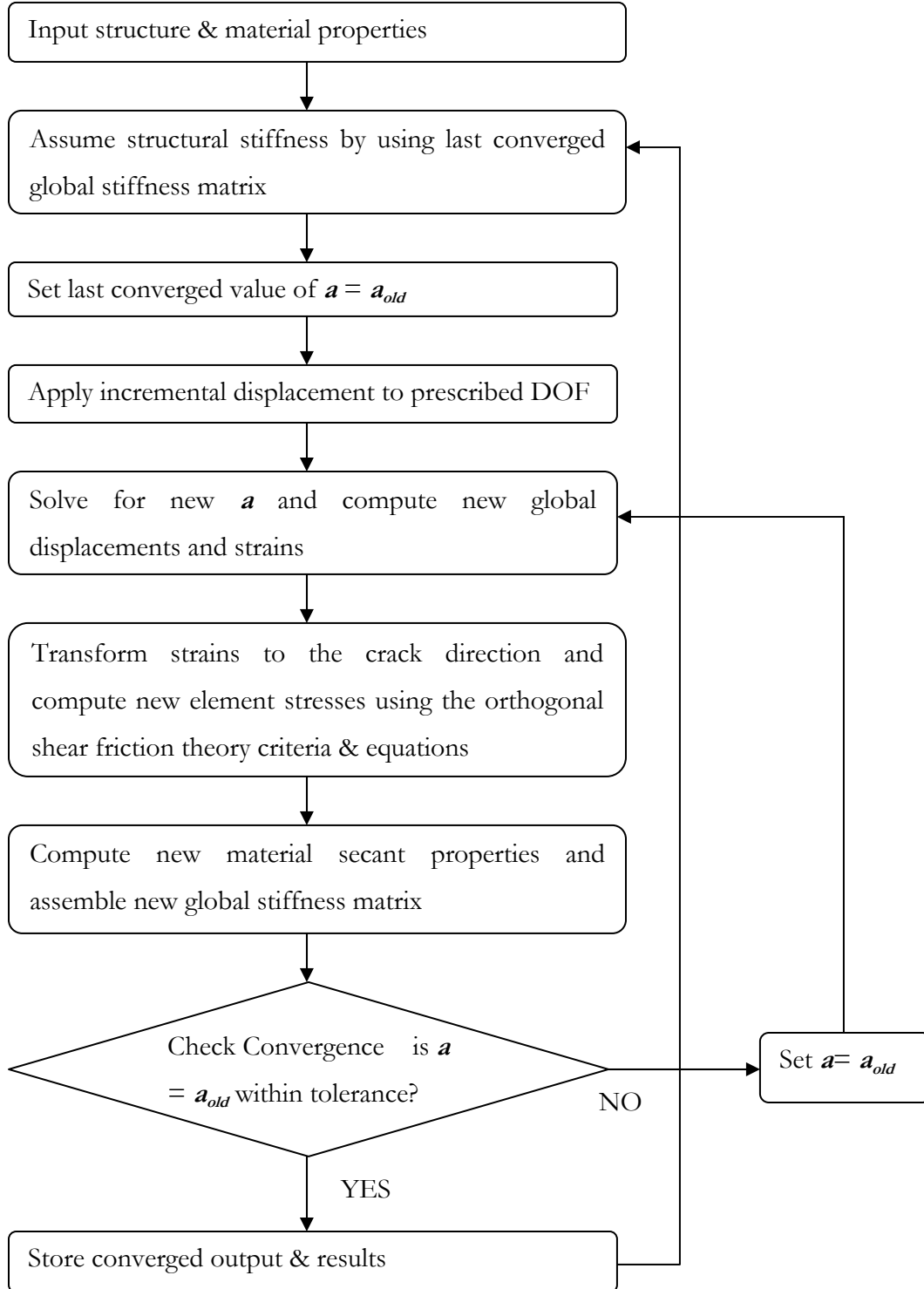


Figure 3.10 Flowchart of the PLV Algorithm.

## Results and Discussion

The PLV formulation was successful in developing shear across the crack surface as well applying vertical compression while keeping a uniform state of stress and strain. In addition the analysis was displacement controlled, allowing the element to cycle through a series of lateral displacements. However, as the element was cycled, various issues presented themselves. These issues will be discussed as the results are presented.

A single four-node rectangular element was analyzed under the loading imposed by the proportional load vector. The concrete membrane was 10 inches tall by 10 inches wide and 2 inches thick. The concrete compressive strength,  $f'_c$ , was 6 ksi. The elastic modulus  $E_c$  and shear modulus,  $G$ , were 4000 ksi and 2000 ksi respectively. The shear retention factor,  $\beta'$ , was 0.05. The reinforcement yield strength was 60 ksi and the modulus of elasticity of steel,  $E_s$ , was 30000 ksi. The reinforcement ratio was 2% in the horizontal direction and 0.5% in the vertical direction. The concrete was pre-cracked at an angle,  $\theta$ , of  $45^\circ$  setting the orthogonal cracking direction (1-2 direction). This was done by assigning the maximum experienced tensile strain, exceeding that of the cracking strain in the direction of the crack. The friction coefficients,  $\mu^{\text{up}}$  and  $\mu^{\text{down}}$ , were 1.2 and 0.2 respectively and the inverse slope of the linear crack opening path,  $a$  (Figure 2.11), was set equal to 2.0. The vertical load,  $v$ , was initially set equal to 2.0 kips.

Results of the analysis are presented in Figures 3.11-3.16. Analysis was successful in loading and unloading in one direction. The element was incrementally forced to displace to 0.06 inches in the  $x$ -direction at the prescribed DOF (see Figure 3.7). Then the element was incrementally unloaded until the solution diverged around zero as will be discussed later. Throughout the analysis only Crack 1 was the active crack. Figure 3.11 shows the normal strain to the crack,  $\epsilon_1$ , versus the shear strain,  $\gamma_{12}$ . This figure shows that the crack opening path relationship was enforced during the analysis.

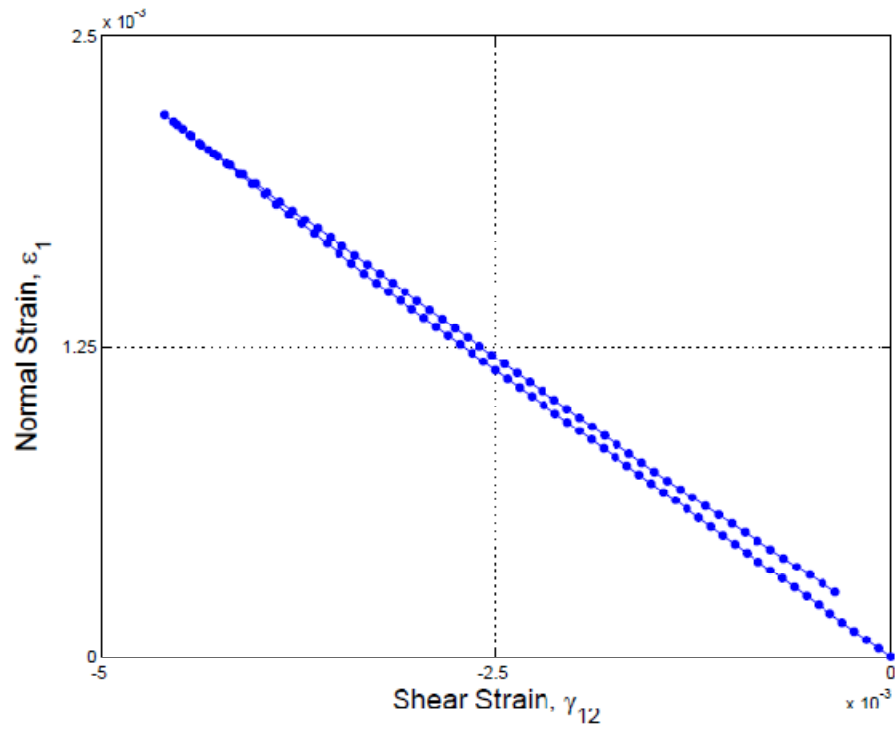


Figure 3.11 Normal Strain (to Crack 1) vs. Shear Strain (PLV).

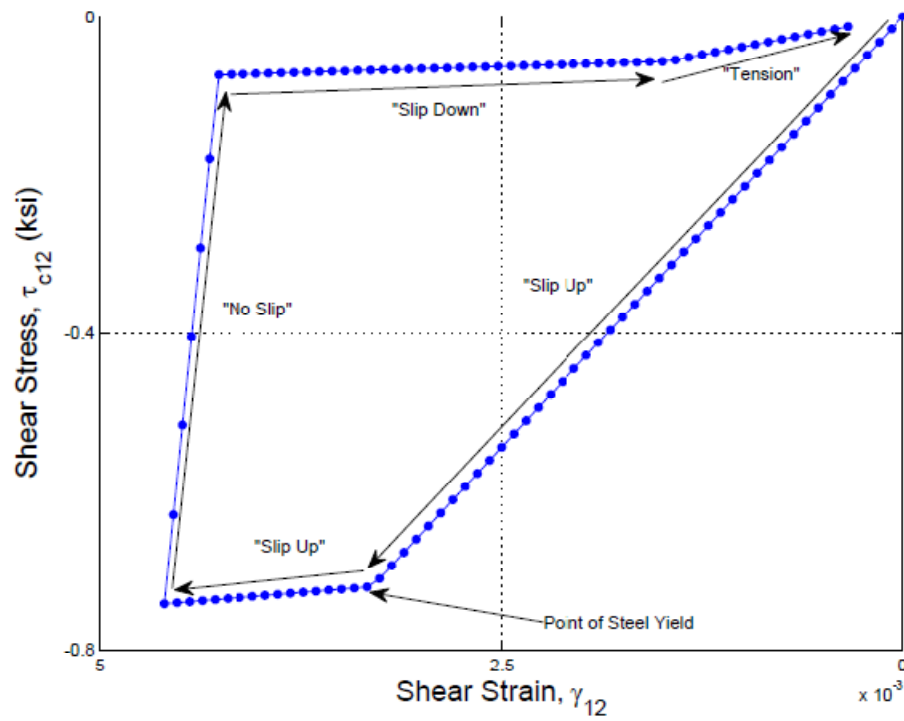


Figure 3.12 Concrete Shear Stress (Crack 1) vs. Shear Strain (PLV).

Figure 3.12 shows the relationship between shear stress and shear strain in the crack orientation for loading and unloading in one direction. The analysis starts with the cracked concrete from zero, as the cracks are closed and have not yet strained. As displacements are enforced and shear slip occurs across the crack surface, the crack begins to “slip up the hill” in the negative direction. It can be seen that shear stress becomes more negative with increasingly negative shear strain. This represents the stiffness attributed to the  $\beta'G$  portion of the “slip up” equation and the shear friction force associated with “slip up.” Shear friction resistance is due to the fact that as the crack surface slips it separates, causing tensile stresses in the steel. The tension in the reinforcement places compression on the crack surface causing shear friction stress to be developed. This shear friction stress is directly proportional to the increasing compressive stress caused by the reinforcement. Once the steel is strained to its yield point, compressive stresses can no longer be increased across the crack surface and the only increase in shear stress is due to the  $\beta'G$  term. This can be seen as the slope of the curve begins to flatten out.

Once the direction of the shear slip reverses, the shear stress drops dramatically. This is represented as the “no slip” case and the stiffness of the shear stress vs shear strain relationship just becomes the shear modulus,  $G$ . Once the shear stress has been reduced sufficiently the crack surface begins to slide “down the hill”. The shear stresses in the “slip down” case are attributed to the  $\beta'G$  term as well as the friction force. Notice that the slope is smaller than the “slip up” case. This is reflective of the fact that it is easier to slip down the hill than up the hill. Eventually the concrete goes into tension and the shear stiffness is again just due to the  $\beta'G$  term. The reason the concrete goes into tension is because of the residual strains in the steel due to yielding.

Figure 3.13 shows the relationship between stress in the x-direction reinforcing steel and the total strain in the x-direction. As can be seen the steel model is enforced as the steel yields and follows the slope of the modulus of elasticity as it unloads, reflecting the residual strains due to yield. Figure 3.14 shows the normal concrete stress relative to the active crack versus the total strain in the same direction. The curve is not reflective of



the concrete stress strain relationship presented in Section 3.4.2. However, when the normal concrete stress relative to the active crack is plotted against effective strain in Figure 3.15, a more reasonable curve is obtained. The compressive region stiffness is represented by the un-cracked modulus of elasticity of concrete  $E_c$ , while the tensile region is represented by the reduced modulus obtained from the tension stiffening curve (see Figure 2.13).

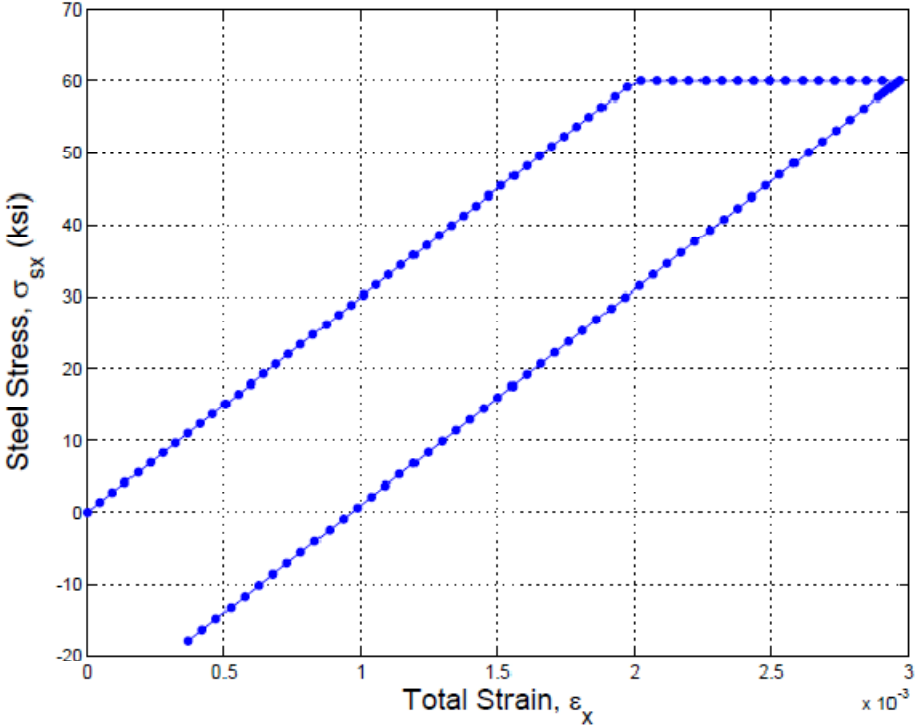


Figure 3.13 Steel Stress vs. Total Strain (PLV).

The usable results from the PLV formulation presented here show that the desired shear friction behavior was captured for a crack at an angle corresponding to the principal stress directions. Resistance to shear was developed by shear friction due to compression across the crack surface and shear strength was limited by the yield strength of the reinforcement. However, full cyclical loading and unloading was not achieved. This is primarily due to the proportional load vector.

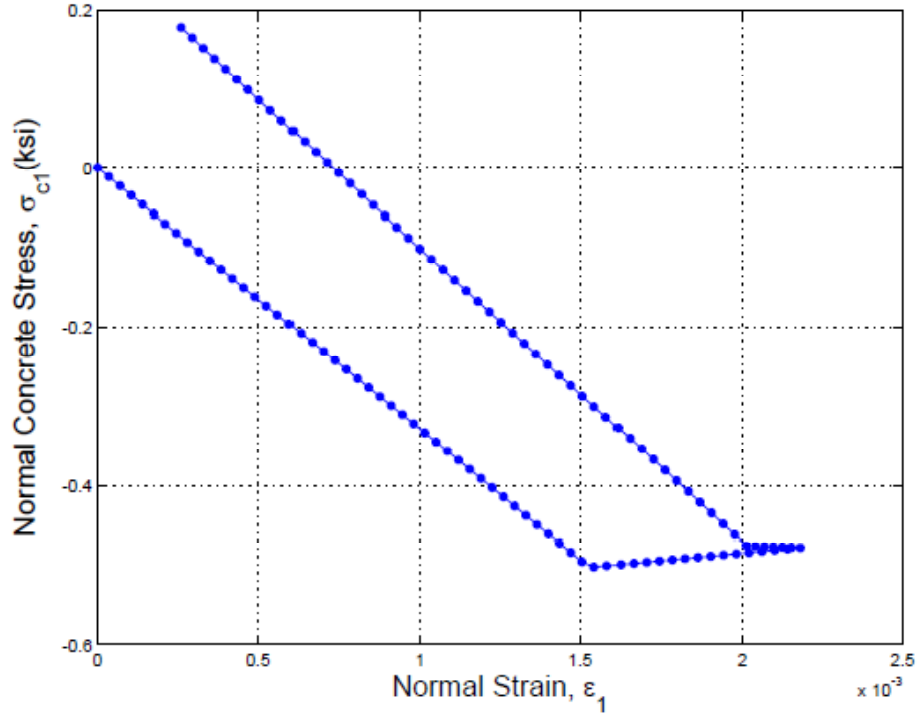


Figure 3.14 Concrete Normal Stress (Crack 1) vs. Normal Strain (PLV).

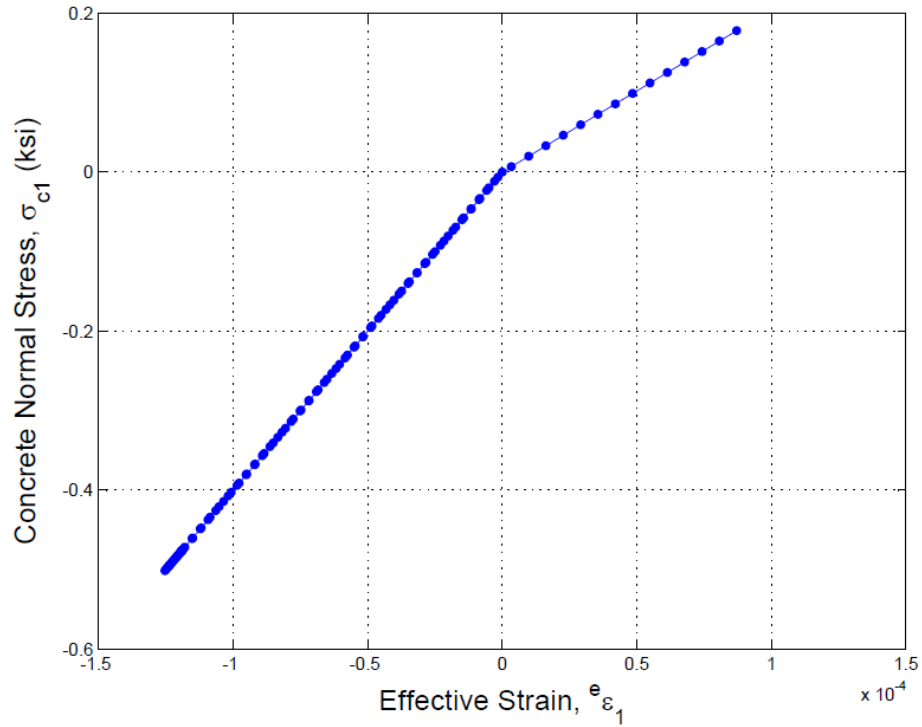


Figure 3.15 Concrete Normal Stress (Crack 1) vs. Effective Strain (PLV).

Figure 3.16 shows the relationship between converged values of  $a$ , the multiplier of the shape vector, and the displacement,  $du$ . Only positive values for  $a$  yield the correct forces in the proportional load vector as the element would be subjected to vertical tension once  $a$  exceeded the value of the applied load,  $v$ . This yields an undesirable state of stress as the crack surfaces would always be in tension and shear friction could no longer be developed. This “flipped” state of  $a$  begins to happen as the displacement approaches zero. Figure 3.16 shows the last converged point before the value of  $a$  exceeds the applied load,  $v$ . When that happens, the element is subjected to a state of tension and the solution diverges. In addition, once  $a$  has “flipped” sign, the direction of the horizontal loads also becomes “flipped”, even though a converged solution for  $a$  produces the desired displacement.

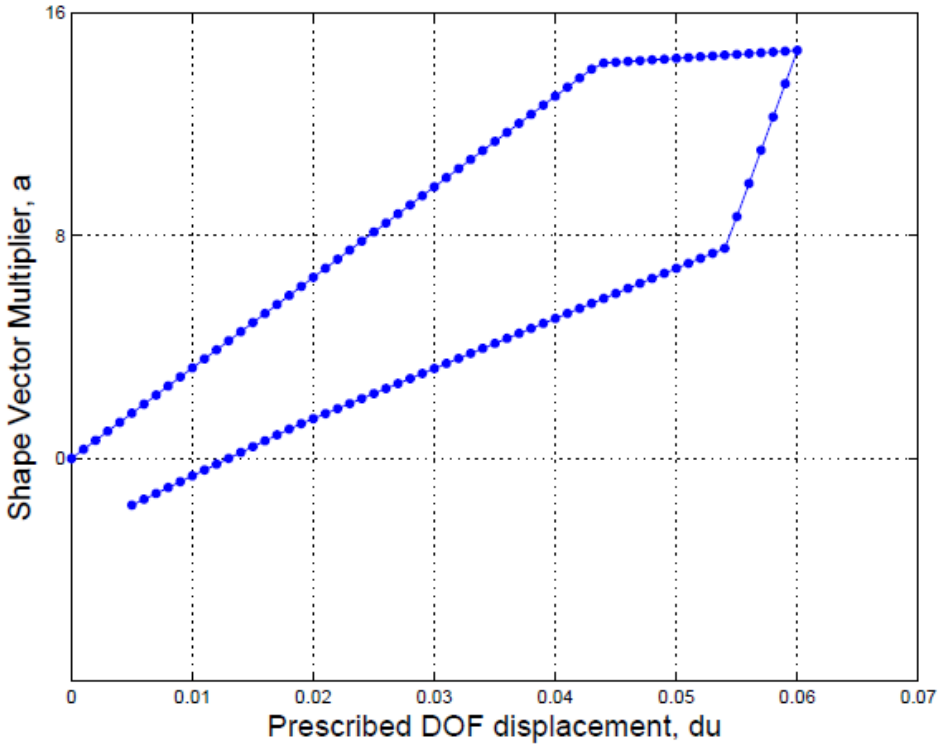


Figure 3.16 Shape Vector Multiplier vs. Prescribed Displacement (PLV).

The program was reformulated to switch the direction of the load vector once  $a$  reached zero or became negative. However, the solved value of  $a$  continued to “flip” to the wrong sign for the desired load vector. The only reasonable explanation is that the solution, given the stiffness matrix at that point, wants to converge to the state of vertical tension. Given the results, the PLV algorithm was modified into a constant vertical load as detailed in the following section.

### 3.7.4 Phase Four: Constant Vertical Load (CVL)

The PLV formulation applied a net vertical compressive load to the element. However, the vertical compressive load is proportional with  $a$ , increasing and decreasing with  $a$ . This may be the reason that the solution converged to a net state of vertical tension in the PLV algorithm. In order to fix this the vertical compressive load needs to be independent of  $a$ . This is also more reasonable as realistic structures generally have a constant vertical load for design, not a variable one. To accomplish this Equation 3-33 was modified as follows:

$$A = \tilde{A}a + \tilde{B} \quad (3-37)$$

$$\text{Where, } \tilde{A} = \begin{Bmatrix} -1 \\ -1 \\ -1 \\ 1 \\ 1 \\ 1 \\ 1 \\ -1 \end{Bmatrix} \text{ and } \tilde{B} = \begin{Bmatrix} 0 \\ 0 \\ 0 \\ 0 \\ 0 \\ -v \\ 0 \\ -v \end{Bmatrix} \text{ and the DOF's are: } \begin{matrix} 1 \\ 2 \\ 3 \\ 4 \\ 5 \\ 6 \\ 7 \\ 8 \end{matrix}$$

In addition Equations 3-34 through 3-36 need to be modified to account for the changes to Equation 3-33. The DOF's and the two load vectors,  $\tilde{A}$  and  $\tilde{B}$ , will be partitioned again into free, prescribed and restrained portions as follows:

$$a\tilde{A}_F + \tilde{B}_F = S_{FF}D_F + S_{FP}D_P + S_{FR}D_R \quad (3-38)$$

$$a\tilde{A}_P + \tilde{B}_P = S_{PF}D_F + S_{PP}D_P + S_{PR}D_R \quad (3-39)$$

$$a\tilde{A}_R + \tilde{B}_R = S_{RF}D_F + S_{RP}D_P + S_{RR}D_R \quad (3-40)$$

By applying the boundary conditions Equation 3-38 can be solved for  $D_F$  and plugged into Equation 3-39. Now  $a$  can be solved for, such that:

$$a = \frac{S_{PF}S_{FF}^{-1}(\tilde{B}_F - S_{FP}D_P) + S_{PP}D_P}{\tilde{A}_P - S_{PF}S_{FF}^{-1}\tilde{A}_F}$$

Notice again that the solution for  $a$  is driven by the prescribed displacement. That is, the addition of the constant load vector still allows for a displacement controlled analysis. The convergence scheme and program algorithm were the same as the PLV (refer to Figure 3.10). Figure 3.17 diagrams the loading imposed on the element from the CVL formulation.

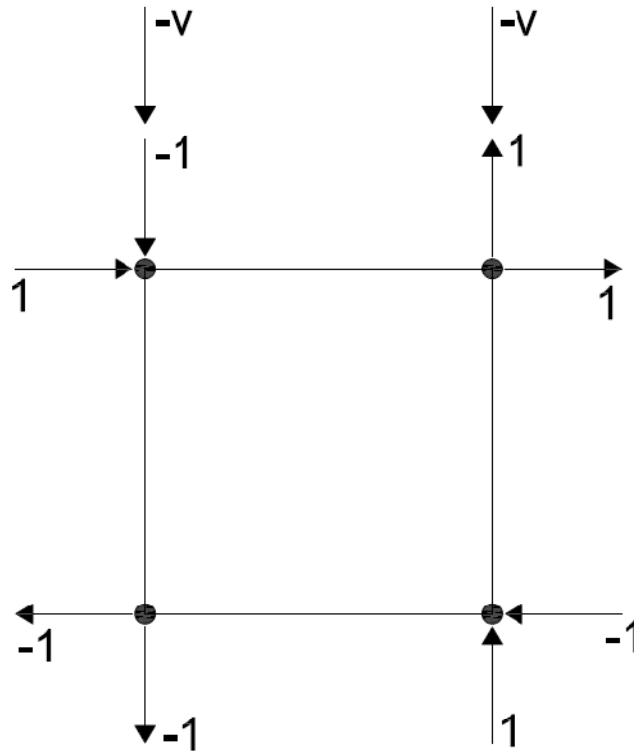


Figure 3.17 Diagram of loading for the CVL formulation.

## Results and Discussion

The CVL formulation was again successful in developing shear across the crack surface as well applying vertical compression while keeping a uniform state of stress and strain. In addition the applied vertical load was separated from  $a$ , keeping it constant throughout the analysis. However, as the element was analyzed with the CVL formulation, various issues presented themselves. These issues will be discussed as the results are presented.

Again a single four-node rectangular element was analyzed under the loading imposed by the CVL. All of the material properties, the crack orientation, the friction coefficients and crack opening path angle were kept the same as the PLV analysis. The reinforcement ratio was 2% in the horizontal direction and 0.2% in the vertical direction. The constant vertical load,  $v$ , was set equal to 18 kips. Results of the analysis are presented in Figures 3.18-3.23. Analysis was successful in incrementally loading the element in one direction. The solution diverged at the unloading stage. Throughout the analysis only Crack 1 was active. Figure 3.18 shows the normal strain to the crack,  $\epsilon_1$ , versus the shear strain,  $\gamma_{12}$ . This figure shows that the crack opening path relationship was enforced during the analysis.

Figure 3.19 shows the relationship between shear stress and shear strain in the crack orientation for loading in one direction. The analysis starts with the cracked concrete from zero, as the cracks are closed and have not yet strained. As the analysis starts the shear stress becomes very negative due to the applied vertical load. At this point the crack surface is not slipping as the shear stresses are not sufficient to overcome the force of friction and initiate slip. As displacements continue to be enforced the shear stress eventually overcomes the force of friction and the crack surface begins to “slip up the hill”. When strain becomes sufficient to yield the reinforcing steel, the curve flattens out, limiting the shear strength. The solution diverged at the point of unloading, so only the monotonic loading case is presented here in the results.

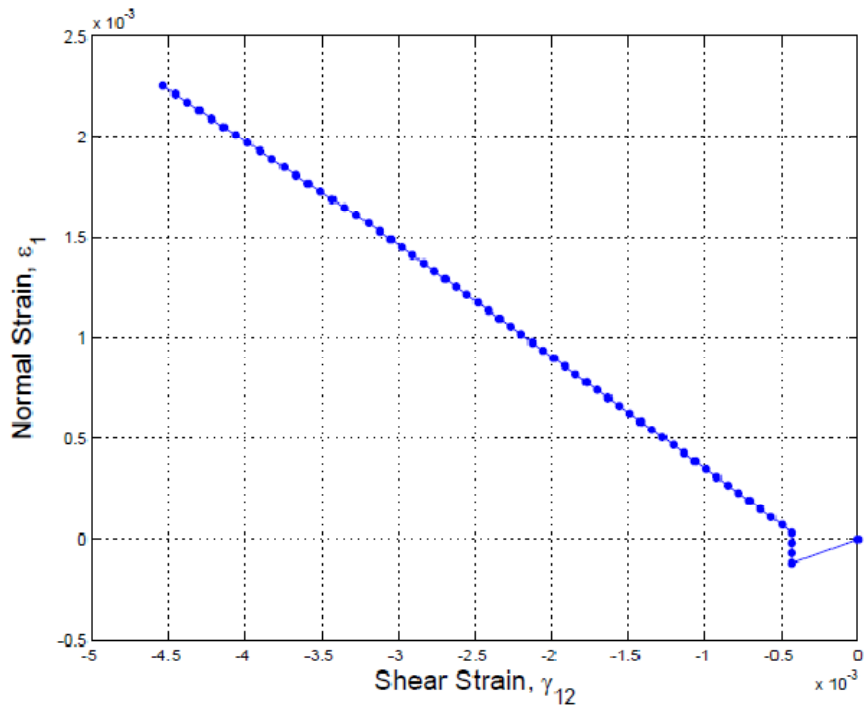


Figure 3.18 Normal Strain (to Crack 1) vs. Shear Strain (CVL).

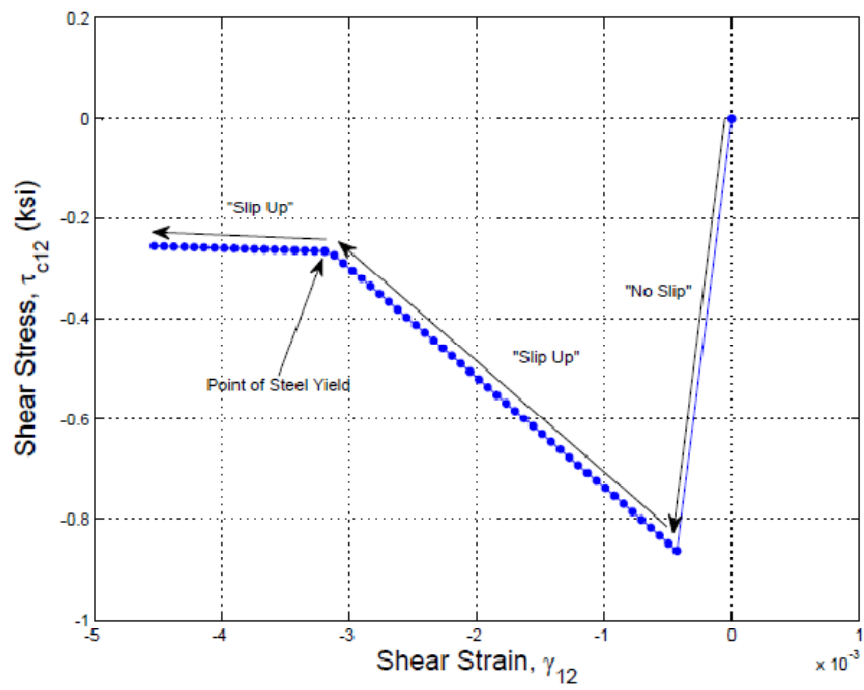


Figure 3.19 Concrete Shear Stress (Crack 1) vs. Shear Strain (CVL).

Notice in Figure 3.19 that the shear stress in the concrete begins to become smaller as the crack surface “slips up the hill”. This is due to the steel and concrete interaction for resisting shear in the direction of the crack. Referring back to the loading shown in Figure 3.17, it can be seen that only the applied vertical load,  $v$ , imposes shear across the crack surface. Because the applied vertical load is constant, the shear force across the crack also must remain constant throughout the analysis. Keeping this in mind, Figure 3.20 shows that the sum of the concrete and shear stresses remains constant. At first the concrete takes almost all of the shear, as the “no slip” case provides the same shear stiffness of un-cracked concrete. Once the crack surface begins to slip the concrete shear stiffness is reduced and the steel begins to resist more of the shear as can be seen from the curves in Figure 3.20. Once the steel yields, the curves flatten out limiting the shear strength. The program’s ability to capture the interaction between the two materials shows its potential power for modeling cracked concrete membrane structures resisting shear forces.

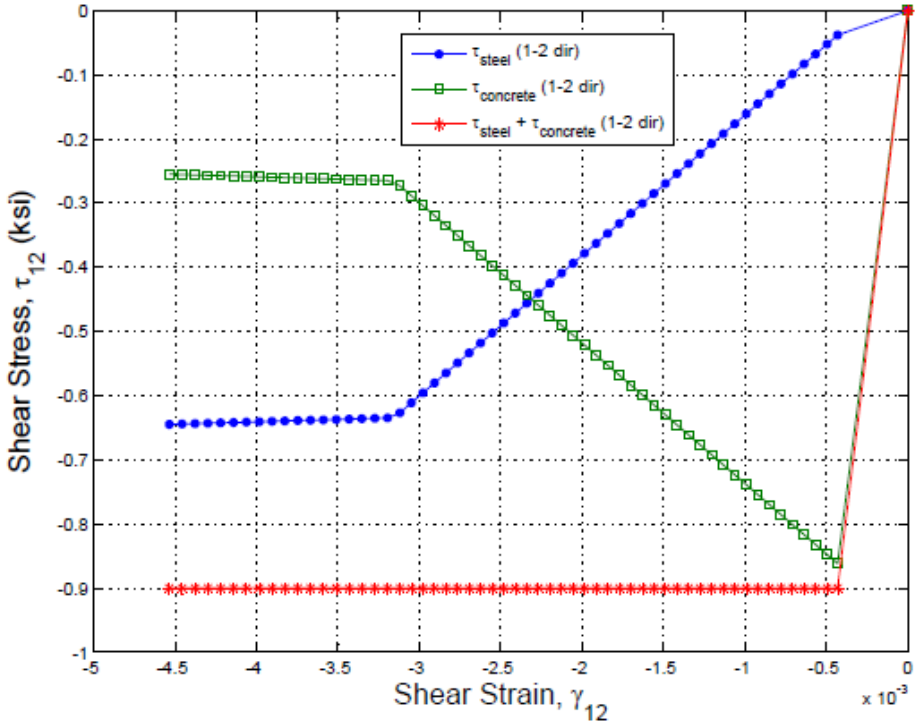


Figure 3.20 Interaction between steel and concrete shearing stresses (CVL).



Similar results to the PLV formulation results are presented here for comparative purposes. Figure 3.21 show the steel stress versus the total strain in the x-direction. As can be seen, the steel model is enforced in the analysis, including yield. Figure 3.22 shows normal concrete stress versus normal strain relative to Crack 1. Again this does not reflect a traditional concrete curve. However, when the normal stress is plotted against effective strain a more realistic curve is obtained showing that the concrete model is enforced during the analysis (see Figure 3.23).

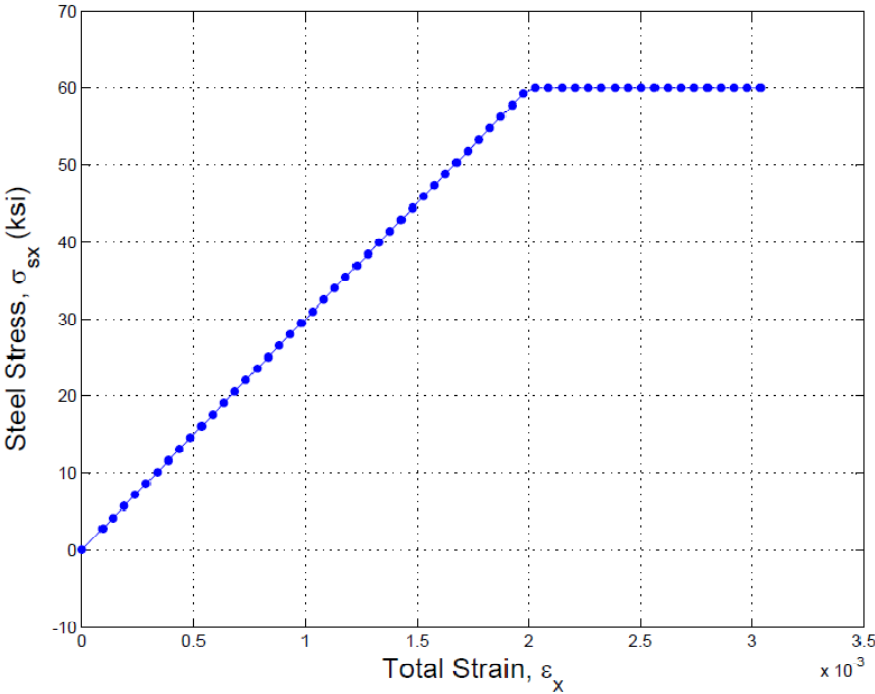


Figure 3.21 Steel Stress vs. Total Strain (CVL).

The reasons the model diverged at the onset of unloading are not completely understood. Based on the results and the new formulation, the reason for divergence might be due to the current convergence method. Converging on  $a$ , may not be robust enough to handle the various non-linear material properties. Based on this fact a more robust modified Newton-Raphson convergence scheme was implemented, as described in the next section.

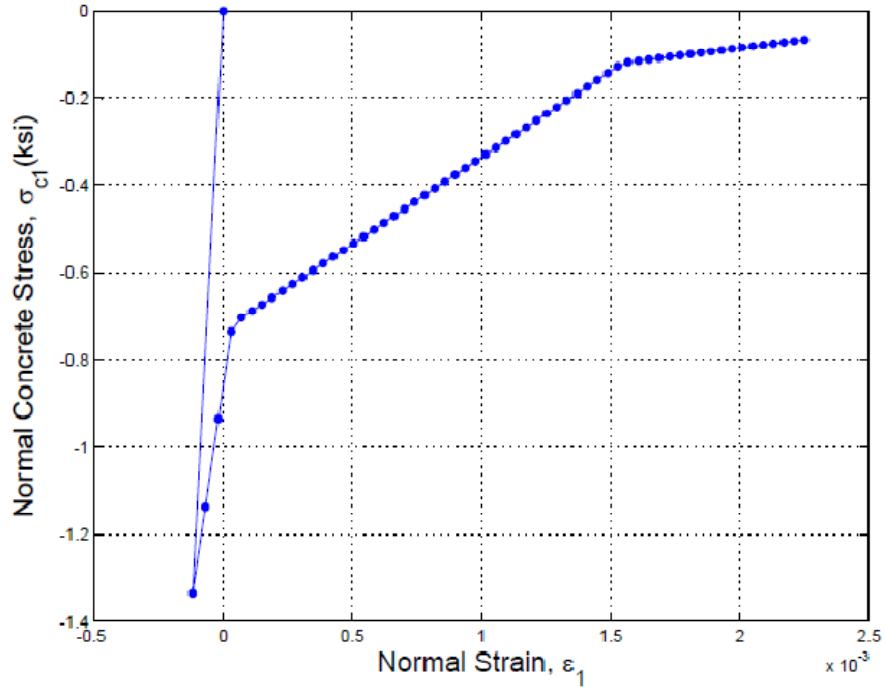


Figure 3.22 Normal Concrete Stress (Crack 1) vs. Normal Strain (CVL).

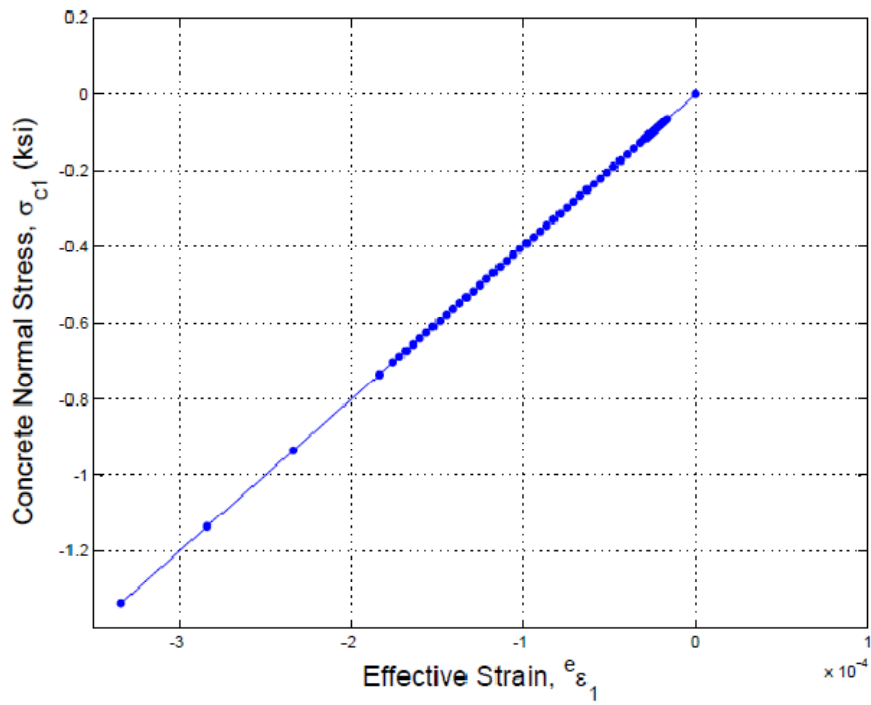


Figure 3.23 Concrete Normal Stress (Crack 1) vs. Effective Strain (CVL).

### 3.7.5 Phase Five: Modified Newton-Raphson Method (MNRM)

In an attempt to obtain convergence over cyclical loading of the current model, a new convergence algorithm was developed. The MNRM works by releasing and re-enforcing the prescribed DOF within an individual convergence iteration until the forces are consistent with the state of stress. The new convergence algorithm was applied to the CVL model, preserving the loading, shear friction parameters, general analysis procedures and other inputs. Presented below are the Modified Newton-Raphson formulations and procedures, the results of the analysis and discussions.

#### Procedures and Formulation

An example procedure for the MNRM can be seen in Figure 3.24. The algorithm is based on ensuring consistency between the forces and the state of stress. The procedure starts at the last set of converged displacements and forces,  $D^{\text{old}}$  and  $F^{\text{old}}$ , respectively. This point, “0”, lies on a representative curve of the force-displacement relationship, which includes all of the model’s properties contained within the global stiffness matrix,  $S$ . From point “0” a new incremental displacement is enforced. Also, the strains and stresses from this last converged point will define the state of the crack. The state of the crack defines which crack is active, forcing the program to only allow that crack to be active for the current iteration. As the state of active crack could, in theory, change within an iteration, the increment of enforced displacement will be made small enough to obtain reasonable results.

A first estimate is then made by using the previously converged stiffness matrix,  $S^0$ , to obtain point “1”. From this new set of displacements,  $D^0$ , first strains and then stresses are calculated. The set of displacements,  $D^0$ , contains at least the correct prescribed displacement, while the other DOF may be incorrect at this point. From the new state of stress and strain a new stiffness matrix,  $S^i$ , is obtained. At this point the forces and stresses are checked for consistency. Using the element’s geometry nodal forces,  $A^0$ , are

calculated from the current state of stress. Then point “2” can be obtained by finding  $\Delta A$ .  $\Delta A$  is calculated by removing the vertical load ( $v$ ) from  $A^0$  such that:

$$\Delta A = (A^0 - v) - A^0(PDOF) \cdot (\tilde{A}) \quad (3-41)$$

Where PDOF is the prescribed degree of freedom and  $\tilde{A}$  is the shape vector.

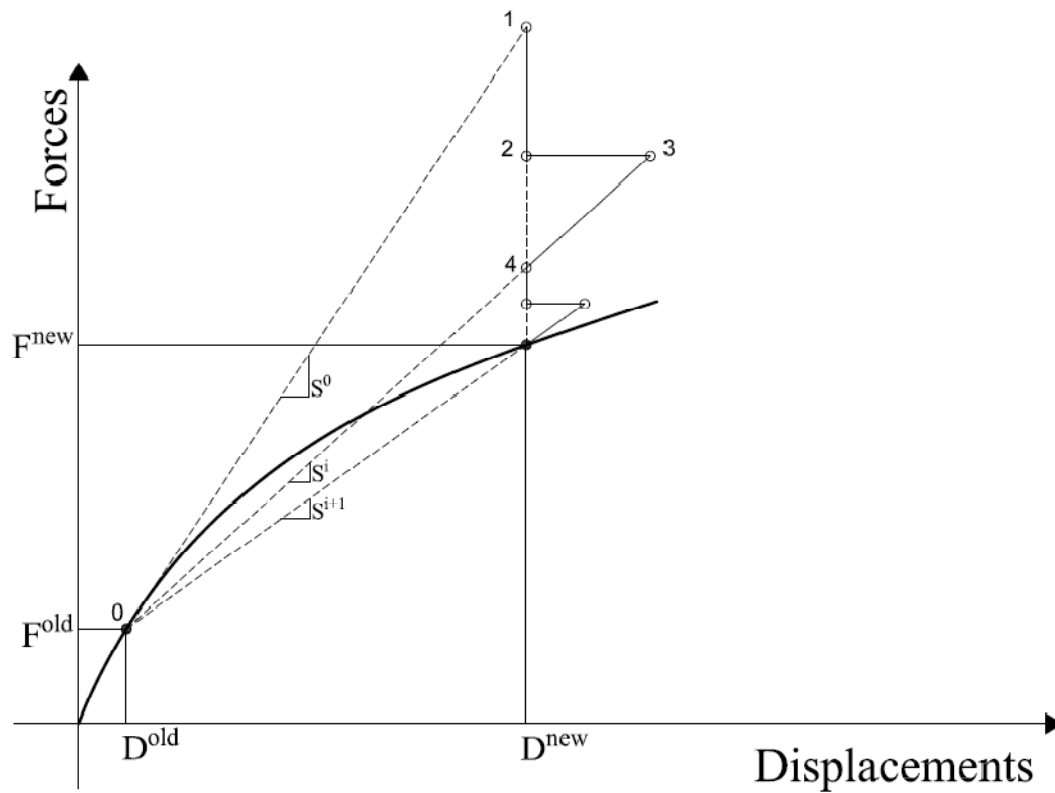


Figure 3.24 Example procedure for the Modified Newton-Raphson Convergence Method

Next the prescribed DOF is released and the change in the displacements,  $\Delta D'$ , can be calculated from the new stiffness matrix and  $\Delta A$  such that:

$$\Delta D' = (S^i)^{-1} \Delta A \quad (3-42)$$

Now point “3” can be obtained by solving for  $D'$  by subtracting  $\Delta D'$  from the displacements at point “1”,  $D^0$ . The prescribed DOF is now enforced again by running the analysis by imputing the prescribed DOF from  $\Delta D'$ . This yields a new change in displacement  $\Delta D''$  from which point “4”, represented as  $D''$ , can be obtained using the following equation:

$$D'' = D' + \Delta D'' \quad (3-43)$$

At this point one full convergence iteration has taken place. Convergence is achieved when  $\Delta A$  is below a tolerance. If  $\Delta A$  is below the tolerance the results are stored and the next displacement increment is analyzed. If not then  $D''$  (point “4”) is set equal to  $D^0$  and iterations are run until convergence is achieved or the model diverges. Figure 3.25 shows a flowchart of the MNRM used.

### **Results and Discussions**

The MNRM was successful in converging for loading in one direction. The analysis was run with the same inputs as the CVL formulation. The results of the analysis were consistent with the results obtained from the CVL. Like the CVL analysis the MNRM diverged at the onset of unloading. Presented in Figures 3.26 & 3.27 are results from the analysis for comparison to the CVL analysis. Figure 3.26 shows shearing stress versus shearing strain relative to Crack 1, which was the active crack throughout the analysis. Comparing this figure with Figure 3.19 shows consistency in the results of the two methods. Figure 3.27 can be compared to Figure 3.20, showing again the interaction between steel and concrete for shear resistance in the orientation of the crack.

Due to convergence issues at unloading with both the MNRM and CVL, focus was placed back on the formulation of the Orthogonal Shear Friction Theory. The assumption that total strains are solely crack strains made in the Orthogonal Shear Friction Theory may be the cause of the divergence in the model.

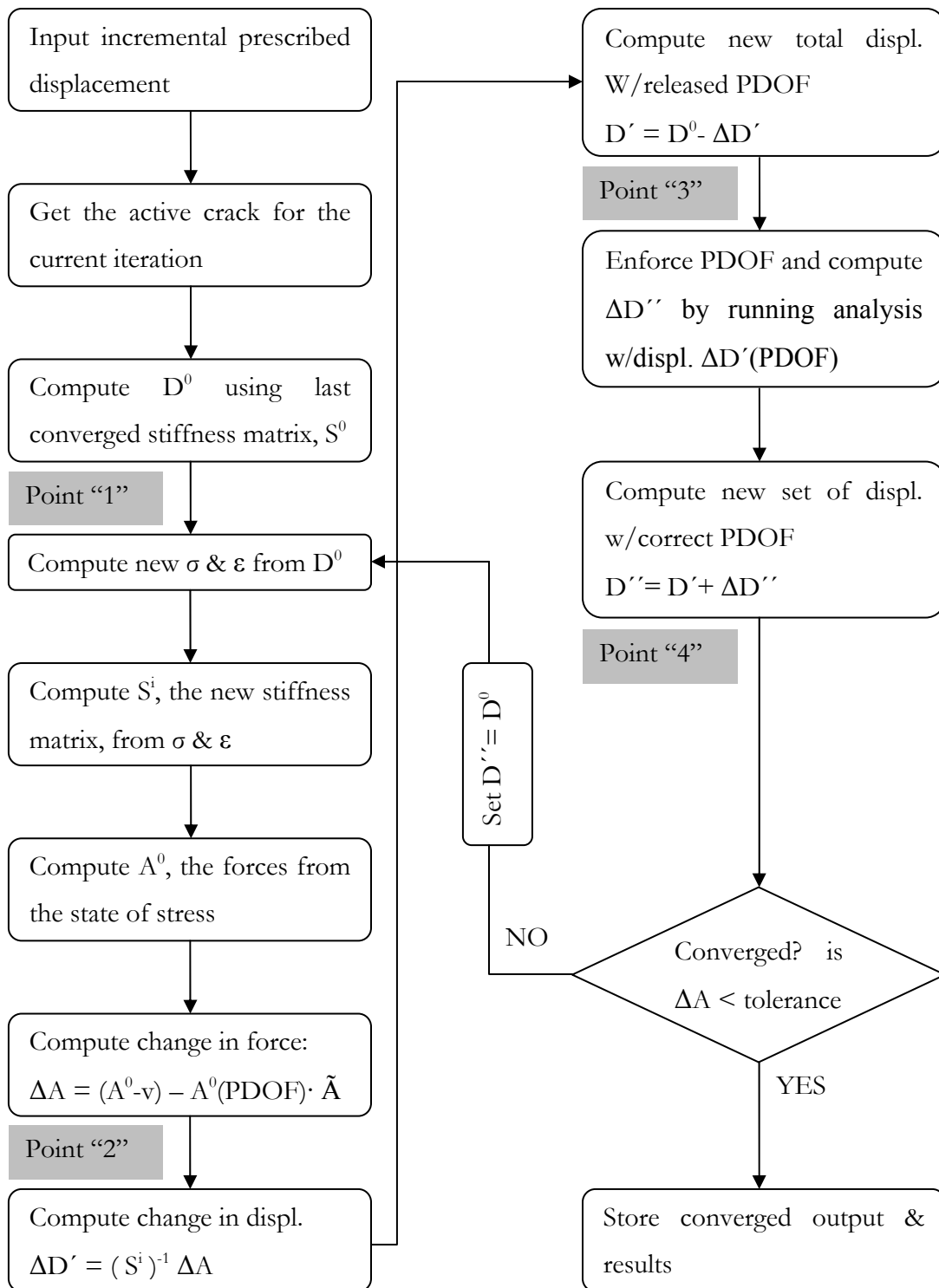


Figure 3.25 Flowchart of the Modified Newton-Raphson Algorithm

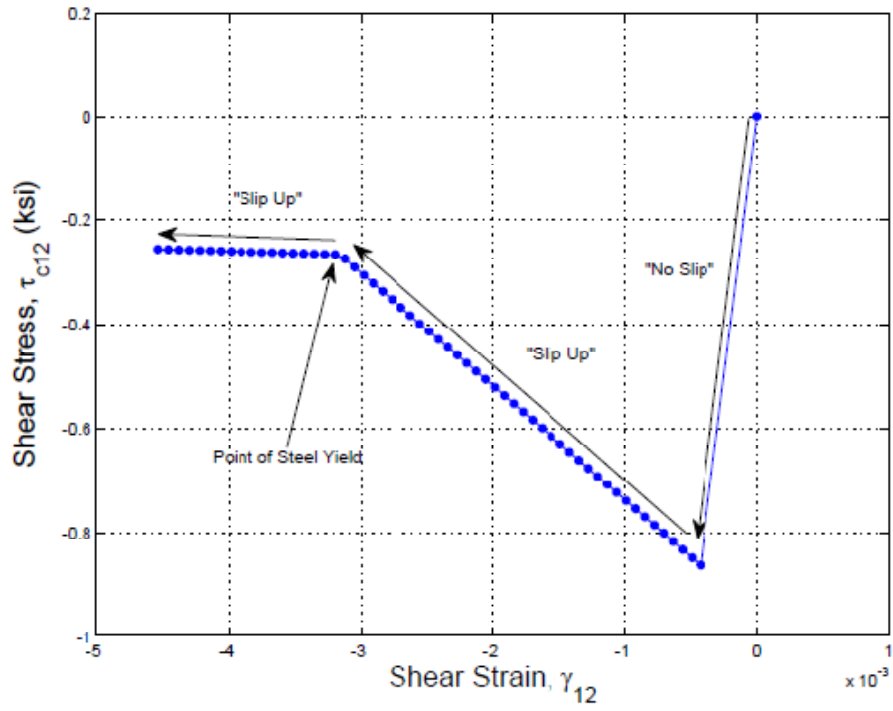


Figure 3.26 Concrete Shear Stress (Crack 1) vs. Shear Strain (MNRM).

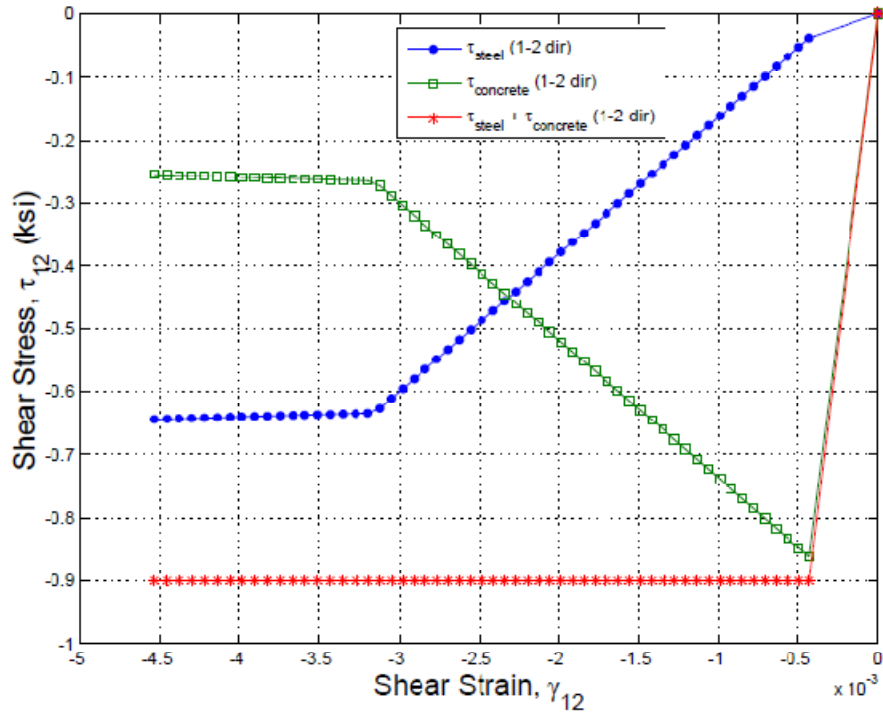


Figure 3.27 Interaction between concrete and steel shearing stresses (MNRM).

This assumption about crack strains was based on results presented by So, see Figure 2.10. Making this assumption discounts the fact that a portion of the strains may be from the un-cracked portions of the concrete. This simplification becomes problematic when computing the shear stress limits for slip,  $\tau^a$  and  $\tau^c$ . This is because the limits should be based solely on the crack slip not the total slip, as the crack may be in the no slip case. For computing the “no slip” shear stress this does not matter as the equation is assumed to be that of un-cracked concrete,  $\tau^b = G\gamma_{\text{total}}$ . However, the slip limits may be incorrect when solved for by using total strains instead of crack strains. This may cause the model to flip-flop states of slip and diverge. This means that crack strains must be separated from total strains and tracked throughout the analysis. The current Orthogonal Shear Friction Theory must be formulated to separate out crack strains. These formulations are presented in Chapter Four.



## Chapter 4

# Orthogonal Shear Friction Theory: Crack Strain Separated (CSS)

An analytical model for two-directional orthogonal cracking needs to be developed that allows separating and tracking individual crack strains. The previous formulation for the Orthogonal Shear Friction Theory was successfully implemented with a variety of loading types and convergence methods; the Proportional Load Vector, the Constant Vertical Load and the Modified Newton-Raphson Method. However, these models were only able to obtain partial cyclic behavior. Presented in this chapter is a new formulation for the Orthogonal Shear Friction Theory that is able to account for strains due to the crack, strains due to the un-cracked portions of concrete, and locked in crack strains. This formulation of separated crack strains was produced in hopes of obtaining greater accuracy as well as full cyclical loading. Definitions, formulations, results and discussions are all presented in the sections of this chapter.

## 4.1 Model Definitions

In order to understand the new formulations for separated crack strains it is important to define the key concepts of the model. As before, a bilinear rectangular element was used for the model. All of the model's DOF's, boundary conditions and geometries were kept consistent with previous models. The global coordinate system remains the "x-y" direction and the crack coordinate system is the "1-2" direction. Orthogonal cracking definitions are kept the same such that Crack 1 is allowed to form at an angle,  $\theta$ , from the global coordinate system and is defined by the principal tension direction. Crack 2 will be allowed to form only perpendicular to Crack 1, eliminating the need for multiple crack coordinate systems. Again material properties and cracks are smeared across the element. However, now crack strains are not considered equal to total strains. This idea will be discussed in detail in a subsequent section of this chapter.

Again it is assumed that only one crack can be active at a time. However, now the model will be able to account for locked in crack slip. A linear crack opening path will be integrated into the model to enforce the slip-separation relationship. From the crack opening path, effective strain will be defined and will account for the state of the crack surface. Limits on shearing stresses will be enforced again to determine if the crack surface is slipping and define the shear stiffness of the crack due to friction.

Convergence on the non-linear properties contained in the model will be achieved by the MNRM. Also the loading from the MNRM will be kept consistent. The loading from the MNRM is a pure shear loading applied to constant vertical load. The pure shear loading will be driven by applied displacements and enforced by a proportional load vector. This assures that a uniform state of stress and strain is maintained. Further details about the model definitions will be presented as the separated crack strain formulations are presented.

## 4.2 Crack Strain Separated Stress-Strain Formulations

For the purposes of formulation, the concrete is assumed to be pre-cracked and cases for each crack being active will be discussed. All of the equations from the Orthogonal Shear Friction Theory need to be changed to include the separation of crack strain and total strain. In addition, new definitions will be necessary. The goal of the reformulation is to put the stress-strain relationships in terms of crack strains while still being able to formulate the secant stiffness matrices in terms of the total strains for analysis.

### 4.2.1 Crack Strains

Previously a reasonable simplification that crack strains were equal to the total strains was made. This simplification comes into question when defining the slip along the surface of the crack. Before, the slip along the crack was defined as the total shearing strain in the orientation of the crack,  $\gamma_{12}$ . To separate out the cracking shear strain, the total shear strain needs to be defined as such:

$$\gamma_{12} = \gamma_{cr} + \gamma_c \quad (4-1)$$

where  $\gamma_{cr}$  is the cracking shear strain and  $\gamma_c$  is the concrete shear strain.

The concrete shearing strain can be defined as:

$$\gamma_c = \tau_{12}/G \quad (4-2)$$

Applying Equation 4-2 to Equation 4-1 and solving for the cracking shear strain yields the following:

$$\gamma_{cr} = \gamma_{12} - \tau_{12}/G \quad (4-3)$$

In order to account for the locked in slip of the cracks, the concept of net shearing strain,  $\gamma_n$ , is introduced. Net shearing strain is obtained by calculating the portion of the total shearing strain that is not already locked into the crack as shown in Equation 4-4.

$$\gamma_n = \gamma_{12} - \gamma_{cr}^{old} \quad (4-4)$$

where  $\gamma_{cr}^{old}$  is the previous converged value of locked in crack slip.

The introduction of net shearing strain changes the definition for cracking strain such that:

$$\gamma_{cr} = \gamma_n - \tau_{12}/G \quad (4-5)$$

However, these definitions only apply to a case where there is one crack direction. In order to consider locked in shear strain in two crack directions net shearing strain must be considered for two cracks such that:

$$\gamma_{n(1)} = \gamma_{12} - \gamma_{cr(2)}^{old} \quad (4-6a)$$

$$\gamma_{n(2)} = \gamma_{12} - \gamma_{cr(1)}^{old} \quad (4-6b)$$

where the number denotes either Crack 1 or Crack 2.

This allows the crack shear strain to only be updated for the active crack. For example, if Crack 1 is the active crack Equation (4-6a) would be used to define the net shear strain so that a new crack shear strain can be obtained for Crack 1. In other words if Crack 1 is active, crack shear strain can be defined by Equation 4-7a and if Crack 2 was the active crack, shear strain can be defined by Equation 4-7b.

$$\gamma_{cr(1)} = \gamma_{n(1)} - \gamma_c \quad (4-7a)$$

$$\gamma_{cr(2)} = \gamma_{n(2)} - \gamma_c \quad (4-7b)$$

With individual crack strains now separated from total strains the Orthogonal Shear Friction Theory can be reformulated.

### 4.2.2 Effective Strain

The concept of effective strain is necessary to enforce the slip-separations relationship. This is done with a linear crack opening path as before. Effective strain is essential for defining the state of the crack surface, either tension or compression. The crack state is what allows the shear friction behavior to be determined. Because the crack opening path is driven by the crack slip, the formulas for effective strain need to be changed. Effective strain should only include crack shear strain, not total shear strain. Therefore effective strain can now be defined by subtracting the separation due to crack slip from the normal strain to the crack as shown in Equations 4-8a and 4-8b.

$${}^e\varepsilon_1 = \varepsilon_1 - \frac{|\gamma_{cr(1)}|}{a} \quad (4-8a)$$

$${}^e\varepsilon_2 = \varepsilon_2 - \frac{|\gamma_{cr(2)}|}{a} \quad (4-8b)$$

### 4.2.3 Normal Concrete Stress

Effective strain is used to define the normal concrete stress curves. Positive values for effective strain mean that the crack surface is not touching and that there is tension across the crack. Negative values of effective strain represent compression across the crack surface. The stress curves for normal concrete in tension and compression are kept the same as in the Orthogonal Shear Friction Theory. However, the equations need to be changed to include the separation of crack strains from total strains. The equations for normal stress in the concrete are listed below and formulated for Crack 1. The equations for Crack two can be obtained by replacing the “1’s” with “2’s” for the stress and strain notations.

(a)  $\epsilon_1 \leq \epsilon_{cr}$  (the cracking strain of concrete):

$$\sigma_1 = E_c \epsilon_1 = E_c \left( \epsilon_1 - \frac{|\gamma_{cr(1)}|}{a} \right) \quad (4-9)$$

(b)  $\epsilon_1 > \epsilon_{cr}$ :

$$\sigma_1 = \frac{f_{cr}}{\sqrt{1+200 \epsilon_1}} \quad (4-10)$$

## 4.2.4 Shearing Stresses

The equations for shearing stress are reformulated from the Orthogonal Shear Friction Theory to include the separation of crack strain from total strain. The shearing stresses are again lumped into two major categories: when the normal stress to the crack is tensile and when the normal stress to the crack is compressive. The limits for shear friction, considered only when the crack is compressive, are also presented here.

### Tension Across the Crack

If the crack surface is determined to be in tension the shear stress is determined as follows, assuming that this is the shearing stress resisted by dowel action of the reinforcement crossing the crack:

$$\tau_{12} = \frac{\beta' G \gamma_{n(1)}}{(1+\beta')} \quad (4-11a)$$

if Crack 1 is the active crack and,

$$\tau_{12} = \frac{\beta' G \gamma_{n(2)}}{(1+\beta')} \quad (4-11b)$$

if Crack 2 is the active crack.

This is the idea that there is some minimal stiffness when the cracks are not in contact and can be thought of as a weak spring. Now that the shear stress is defined, the equations for normal stress to the crack can be reformulated for tension across the crack. Assuming that the shear strain is positive the following equation can be written:

$$\sigma_1 = E_1 \left( \varepsilon_1 - \frac{\gamma_{cr(1)}}{a} \right) = E_1 \varepsilon_1 - \frac{E_1}{a} \left( \gamma_{n(1)} - \frac{\tau_{12}}{G} \right) \quad (4-12a)$$

where  $E_1$  is the secant modulus of concrete.

By plugging the Equation 4-11a into 4-12a the equation for normal stress can be rewritten as:

$$\sigma_1 = E_1 \varepsilon_1 - \frac{E_1}{a} \left( 1 - \frac{\beta'}{1+\beta'} \right) \gamma_{n(1)} \quad (4-12b)$$

The equation for  $\sigma_2$  can be obtained by replacing the “1’s” for “2’s” in Equation 4-12b.

### Compression Across the Crack

If the crack surfaces are in contact and there is compression across the crack the shear stress is determined by the equations presented in this section. The following derivations are for Crack 1. Crack 2 formulations can be obtained by replacing the “1’s” with “2’s” in the equations. First for positive shearing strain ( $\gamma_{12} > 0$ ), the following three cases are considered.

(a) If the crack surface is slipping down a hill:

$$\tau_{12} = \beta G \gamma_{cr(1)} + \mu^{down} \sigma_1 = \beta G \gamma_{cr(1)} + \mu^{down} E_c \left( \varepsilon_1 - \frac{\gamma_{cr(1)}}{a} \right) \quad (4-13a)$$

Rearranging Equation 4-13a yields the following:

$$\tau_{12} = \mu^{down} E_c \varepsilon_1 + \gamma_{cr(1)} \left( \beta G - \frac{\mu^{down} E_c}{a} \right) \quad (4-13b)$$

Substituting for  $\gamma_{cr(1)}$  in Equation 4-13b using Equation 4-7a yields the following:

$$\tau_{12} = \mu^{down} E_c \varepsilon_1 + \left( \gamma_{n(1)} - \frac{\tau_{12}}{G} \right) \left( \beta G - \frac{\mu^{down} E_c}{a} \right) \quad (4-13c)$$

Expanding Equation 4-13c and rearranging yields the following:

$$\tau_{12} \left[ 1 + \frac{\beta G - \frac{\mu^{down} E_c}{a}}{G} \right] = \mu^{down} E_c \varepsilon_1 + \left( \beta G - \frac{\mu^{down} E_c}{a} \right) \gamma_{n(1)} \quad (4-13d)$$

Equation 4-12d yields the shear stress limit for “slip down”:

$$\tau_{12}^a = \left( \frac{B}{A} \right) \varepsilon_1 + \left( \frac{C}{A} \right) \gamma_{n(1)} \quad (4-13e)$$

where,

$$A = 1 + \frac{\beta G - \frac{\mu^{down} E_c}{a}}{G}$$

$$B = \mu^{down} E_c$$

and,

$$C = \beta G - \frac{\mu^{down} E_c}{a}$$

Now the equation for the normal concrete stress needs to be reformulated to include the limit definition  $\tau_{12}^a$ . Rearranging Equation 4-9 and substituting for  $\gamma_{cr}$  yields:

$$\sigma_1 = E_c \varepsilon_1 - \frac{E_c}{a} \left( \gamma_{n(1)} - \frac{\tau_{12}}{G} \right) \quad (4-14a)$$

When the crack is slipping down the hill, the shear stress,  $\tau_{12}$ , is equal to the limit shear stress,  $\tau_{12}^a$ . Plugging Equation 4-13e in to Equation 4-14a yields:

$$\sigma_1 = E_c \varepsilon_1 - \frac{E_c}{a} \left[ \gamma_{n(1)} - \frac{1}{G} \left( \left( \frac{B}{A} \right) \varepsilon_1 + \left( \frac{C}{A} \right) \gamma_{n(1)} \right) \right] \quad (4-14b)$$



where A, B, and C were defined previously.

Equation 4-14b can also be written as:

$$\sigma_1 = \left( E_c + \frac{E_c B}{aAG} \right) \varepsilon_1 - \left( \frac{E_c}{a} - \frac{E_c C}{aAG} \right) \gamma_{n(1)} \quad (4-14c)$$

Equations 4-13e and 4-14c are now written in a usable format and formulated with respect to the net shearing strain, allowing the crack shearing strain to be separated from the total. For the sake of brevity, the rest of the shearing stress limits are not derived in detail as the previous limit,  $\tau_{12}^a$  for  $\gamma_{12} > 0$ , was presented. However, their derivations can be obtained in a similar manner.

(b) If the crack surface is not slipping:

$$\tau_{12}^b = \tau_{12,prev} + G(\gamma_{n(1)} - \gamma_{n(1),prev}) \quad (4-15)$$

where “prev” refers to the previously converged stress or strain value.

Because the crack surface is not slipping there is no change in the crack shear strain. Thus the equation for the normal concrete stress to the crack becomes:

$$\sigma_1 = E_c \varepsilon_1 - \frac{E_c}{a} |\gamma_{cr(1)}^{old}| \quad (4-16)$$

(c) If the crack surface is slipping up a hill

$$\tau_{12}^c = -\left(\frac{B}{A}\right) \varepsilon_1 + \left(\frac{C}{A}\right) \gamma_{n(1)} \quad (4-17)$$

where,

$$A = 1 + \frac{\beta G + \frac{\mu^{up} E_c}{a}}{G}$$

$$B = \mu^{up} E_c$$

and,

$$C = \beta G + \frac{\mu^{up} E_c}{a}$$

The normal concrete stress can now be defined as:

$$\sigma_1 = \left( E_c - \frac{E_c B}{aAG} \right) \varepsilon_1 - \left( \frac{E_c}{a} - \frac{E_c C}{aAG} \right) \gamma_{n(1)} \quad (4-18)$$

For negative shearing strain ( $\gamma_{12} < 0$ ), the following three cases are considered:

(a) If the crack surface is slipping up a hill:

$$\tau_{12}^a = \left( \frac{B}{A} \right) \varepsilon_1 + \left( \frac{C}{A} \right) \gamma_{n(1)} \quad (4-19)$$

where,

$$A = 1 + \frac{\beta G + \frac{\mu^{up} E_c}{a}}{G}$$

$$B = \mu^{up} E_c$$

and,

$$C = \beta G + \frac{\mu^{up} E_c}{a}$$

The normal concrete stress can now be defined as:

$$\sigma_1 = \left( E_c - \frac{E_c B}{aAG} \right) \varepsilon_1 + \left( \frac{E_c}{a} - \frac{E_c C}{aAG} \right) \gamma_{n(1)} \quad (4-20)$$

(b) If the crack surface is not slipping:

$$\tau_{12}^b = \tau_{12,prev} + G(\gamma_{n(1)} - \gamma_{n(1),prev}) \quad (4-21)$$

where “prev” refers to the previously converged stress or strain value.

The equation for the normal concrete stress to the crack becomes:

$$\sigma_1 = E_c \varepsilon_1 - \frac{E_c}{a} |\gamma_{cr(1)}^{old}| \quad (4-22)$$

(c) If the crack surface is slipping down a hill:

$$\tau_{12}^c = -\left(\frac{B}{A}\right) \varepsilon_1 + \left(\frac{C}{A}\right) \gamma_{n(1)} \quad (4-23)$$

where,

$$A = 1 + \frac{\beta G - \frac{\mu^{down} E_c}{a}}{G}$$

$$B = \mu^{down} E_c$$

and,

$$C = \beta G - \frac{\mu^{down} E_c}{a}$$

The normal concrete stress can now be defined as:

$$\sigma_1 = \left(E_c + \frac{E_c B}{aAG}\right) \varepsilon_1 + \left(\frac{E_c}{a} - \frac{E_c C}{aAG}\right) \gamma_{n(1)} \quad (4-24)$$

For any given shear strain,  $\gamma_{12}$ , the shear stress,  $\tau_{12}$ , is determined from the “not slipping equation” but is limited by the minimum and maximum shear stresses,  $\tau_{12}^a$  and  $\tau_{12}^c$  as shown below:

$$\tau_{12} = \tau_{12}^b$$

$$\text{Where, } \tau_{12}^a \leq \tau_{12} \leq \tau_{12}^c$$

## 4.2.5 Secant Stiffness Matrix Formulation: Net Shearing Strain

The shearing and normal stresses have all been formulated in terms of net shearing strain. This was done to separate out the crack strain from the total strain and allow the secant stiffness matrices to be formed. The secant stiffness matrices are broken down into two main categories: Crack 1 active and Crack 2 active. The matrices are further broken down by the state of the crack surface. In the following equations  $E_1$  and  $E_2$  are the secant moduli of concrete for the two crack directions. Also, in the following equations  $\gamma_n$  is pre multiplied by the total shear strain,  $\gamma_{12}$ , to be able to write the stress equations in terms of total strain.

### Case 1: Crack Direction 1 Active

Once Crack 1 has formed cases for stiffness must be considered:

1. If crack surface is determined to be in tension, the stress-strain relationship is as follows for positive and negative shearing strain,  $\gamma_{12}$ , respectively.

$$\begin{Bmatrix} \sigma_1 \\ \sigma_2 \\ \tau_{12} \end{Bmatrix} = \begin{bmatrix} E_1 & 0 & \frac{-E_1}{a} \left(1 - \frac{\beta'}{1+\beta'}\right) \left(\frac{\gamma_{n(1)}}{\gamma_{12}}\right) \\ 0 & E_2 & 0 \\ 0 & 0 & \frac{\beta'G}{1+\beta'} \left(\frac{\gamma_{n(1)}}{\gamma_{12}}\right) \end{bmatrix} \begin{Bmatrix} \varepsilon_1 \\ \varepsilon_2 \\ \gamma_{12} \end{Bmatrix} \quad (4-25)$$

$$\begin{Bmatrix} \sigma_1 \\ \sigma_2 \\ \tau_{12} \end{Bmatrix} = \begin{bmatrix} E_1 & 0 & \frac{E_1}{a} \left(1 - \frac{\beta'}{1+\beta'}\right) \left(\frac{\gamma_{n(1)}}{\gamma_{12}}\right) \\ 0 & E_2 & 0 \\ 0 & 0 & \frac{\beta'G}{1+\beta'} \left(\frac{\gamma_{n(1)}}{\gamma_{12}}\right) \end{bmatrix} \begin{Bmatrix} \varepsilon_1 \\ \varepsilon_2 \\ \gamma_{12} \end{Bmatrix} \quad (4-26)$$

2. If the crack surface is in compression, the secant stiffness matrix is defined based on the various cases for shear stress. The constants A, B and C were determined in the derivations for the shear stress cases in Section 4.2.4. The equations for shearing stress and normal stress can also be referenced there. For positive total shear strain ( $\gamma_{12} > 0$ ), the following cases are considered:

(a) If the crack surface is slipping down a hill the secant stiffness matrix becomes:

$$\begin{Bmatrix} \sigma_1 \\ \sigma_2 \\ \tau_{12} \end{Bmatrix} = \begin{bmatrix} E_c + \frac{E_c B}{aAG} & 0 & \left( \frac{-E_c}{a} + \frac{E_c C}{aAG} \right) \left( \frac{\gamma_{n(1)}}{\gamma_{12}^{old}} \right) \\ 0 & E_c & 0 \\ \frac{B}{A} & 0 & \frac{C}{A} \left( \frac{\gamma_{n(1)}}{\gamma_{12}^{old}} \right) \end{bmatrix} \begin{Bmatrix} \varepsilon_1 \\ \varepsilon_2 \\ \gamma_{12} \end{Bmatrix} \quad (4-27)$$

(b) If the crack surface is not slipping the secant stiffness matrix becomes:

$$\begin{Bmatrix} \sigma_1 \\ \sigma_2 \\ \tau_{12} \end{Bmatrix} = \begin{bmatrix} E_c & 0 & -\left( \frac{E_c}{a} \right) \left( \frac{\gamma_{cr(1)}^{old}}{\gamma_{12}^{old}} \right) \\ 0 & E_c & 0 \\ 0 & 0 & \left( \frac{\tau_{12}^b}{\gamma_{12}^{old}} \right) \end{bmatrix} \begin{Bmatrix} \varepsilon_1 \\ \varepsilon_2 \\ \gamma_{12} \end{Bmatrix} \quad (4-28)$$

(c) If the crack surface is slipping up a hill the secant stiffness matrix becomes:

$$\begin{Bmatrix} \sigma_1 \\ \sigma_2 \\ \tau_{12} \end{Bmatrix} = \begin{bmatrix} E_c - \frac{E_c B}{aAG} & 0 & \left( \frac{-E_c}{a} + \frac{E_c C}{aAG} \right) \left( \frac{\gamma_{n(1)}}{\gamma_{12}^{old}} \right) \\ 0 & E_c & 0 \\ -\frac{B}{A} & 0 & \frac{C}{A} \left( \frac{\gamma_{n(1)}}{\gamma_{12}^{old}} \right) \end{bmatrix} \begin{Bmatrix} \varepsilon_1 \\ \varepsilon_2 \\ \gamma_{12} \end{Bmatrix} \quad (4-29)$$

For negative total shear strain ( $\gamma_{12} < 0$ ), the following cases are considered:

(a) If the crack surface is slipping up a hill the secant stiffness matrix becomes:

$$\begin{Bmatrix} \sigma_1 \\ \sigma_2 \\ \tau_{12} \end{Bmatrix} = \begin{bmatrix} E_c - \frac{E_c B}{aAG} & 0 & \left( \frac{E_c}{a} - \frac{E_c C}{aAG} \right) \left( \frac{\gamma_{n(1)}}{\gamma_{12}^{old}} \right) \\ 0 & E_c & 0 \\ \frac{B}{A} & 0 & \frac{C}{A} \left( \frac{\gamma_{n(1)}}{\gamma_{12}^{old}} \right) \end{bmatrix} \begin{Bmatrix} \varepsilon_1 \\ \varepsilon_2 \\ \gamma_{12} \end{Bmatrix} \quad (4-30)$$

(b) If the crack surface is not slipping the secant stiffness matrix becomes:

$$\begin{Bmatrix} \sigma_1 \\ \sigma_2 \\ \tau_{12} \end{Bmatrix} = \begin{bmatrix} E_c & 0 & \left( \frac{E_c}{a} \right) \left( \frac{\gamma_{cr(1)}^{old}}{\gamma_{12}^{old}} \right) \\ 0 & E_c & 0 \\ 0 & 0 & \left( \frac{\tau_{12}^b}{\gamma_{12}^{old}} \right) \end{bmatrix} \begin{Bmatrix} \varepsilon_1 \\ \varepsilon_2 \\ \gamma_{12} \end{Bmatrix} \quad (4-31)$$

(c) If the crack surface is slipping down a hill the secant stiffness matrix becomes:

$$\begin{Bmatrix} \sigma_1 \\ \sigma_2 \\ \tau_{12} \end{Bmatrix} = \begin{bmatrix} E_c + \frac{E_c B}{aAG} & 0 & \left(\frac{E_c}{a} - \frac{E_c C}{aAG}\right) \left(\frac{\gamma_{n(1)}}{\gamma_{12}^{old}}\right) \\ 0 & E_c & 0 \\ -\frac{B}{A} & 0 & \frac{C}{A} \left(\frac{\gamma_{n(1)}}{\gamma_{12}^{old}}\right) \end{bmatrix} \begin{Bmatrix} \varepsilon_1 \\ \varepsilon_2 \\ \gamma_{12} \end{Bmatrix} \quad (4-32)$$

### Case 2: Crack Direction 2 Active

Once Crack 2 has formed the following cases for stiffness must be considered if Crack 2 is the active crack:

1. If crack surface is determined to be in tension, the stress-strain relationship is as follows for positive and negative shearing strain,  $\gamma_{12}$ , respectively.

$$\begin{Bmatrix} \sigma_1 \\ \sigma_2 \\ \tau_{12} \end{Bmatrix} = \begin{bmatrix} E_1 & 0 & 0 \\ 0 & E_c & \frac{-E_2}{a} \left(1 - \frac{\beta'}{1+\beta'}\right) \left(\frac{\gamma_{n(1)}}{\gamma_{12}^{old}}\right) \\ 0 & 0 & \frac{\beta' G}{1+\beta'} \left(\frac{\gamma_{n(1)}}{\gamma_{12}^{old}}\right) \end{bmatrix} \begin{Bmatrix} \varepsilon_1 \\ \varepsilon_2 \\ \gamma_{12} \end{Bmatrix} \quad (4-33)$$

$$\begin{Bmatrix} \sigma_1 \\ \sigma_2 \\ \tau_{12} \end{Bmatrix} = \begin{bmatrix} E_1 & 0 & 0 \\ 0 & E_c & \frac{E_2}{a} \left(1 - \frac{\beta'}{1+\beta'}\right) \left(\frac{\gamma_{n(1)}}{\gamma_{12}^{old}}\right) \\ 0 & 0 & \frac{\beta' G}{1+\beta'} \left(\frac{\gamma_{n(1)}}{\gamma_{12}^{old}}\right) \end{bmatrix} \begin{Bmatrix} \varepsilon_1 \\ \varepsilon_2 \\ \gamma_{12} \end{Bmatrix} \quad (4-34)$$

2. If the crack surface is in compression, the secant stiffness matrix is defined based on the various cases for shear stress. The constants A, B and C were determined in the derivations for the shear stress cases in Section 4.2.4. The equations for shearing stress and normal stress can also be referenced there. For positive total shear strain ( $\gamma_{12} > 0$ ), the following cases are considered:

(d) If the crack surface is slipping down a hill the secant stiffness matrix becomes:

$$\begin{Bmatrix} \sigma_1 \\ \sigma_2 \\ \tau_{12} \end{Bmatrix} = \begin{bmatrix} E_c & 0 & 0 \\ 0 & E_c + \frac{E_c B}{aAG} & \left(\frac{-E_c}{a} + \frac{E_c C}{aAG}\right) \left(\frac{\gamma_{n(1)}}{\gamma_{12}^{old}}\right) \\ 0 & \frac{B}{A} & \frac{C}{A} \left(\frac{\gamma_{n(1)}}{\gamma_{12}^{old}}\right) \end{bmatrix} \begin{Bmatrix} \varepsilon_1 \\ \varepsilon_2 \\ \gamma_{12} \end{Bmatrix} \quad (4-35)$$

(e) If the crack surface is not slipping the secant stiffness matrix becomes:

$$\begin{Bmatrix} \sigma_1 \\ \sigma_2 \\ \tau_{12} \end{Bmatrix} = \begin{bmatrix} E_c & 0 & 0 \\ 0 & E_c & -\left(\frac{E_c}{a}\right) \left(\frac{\gamma_{cr(1)}^{old}}{\gamma_{12}^{old}}\right) \\ 0 & 0 & \left(\frac{\tau_{12}^b}{\gamma_{12}^{old}}\right) \end{bmatrix} \begin{Bmatrix} \varepsilon_1 \\ \varepsilon_2 \\ \gamma_{12} \end{Bmatrix} \quad (4-36)$$

(f) If the crack surface is slipping up a hill the secant stiffness matrix becomes:

$$\begin{Bmatrix} \sigma_1 \\ \sigma_2 \\ \tau_{12} \end{Bmatrix} = \begin{bmatrix} E_c & 0 & 0 \\ 0 & E_c - \frac{E_c B}{aAG} & \left(\frac{-E_c}{a} + \frac{E_c C}{aAG}\right) \left(\frac{\gamma_{n(1)}}{\gamma_{12}^{old}}\right) \\ 0 & -\frac{B}{A} & \frac{C}{A} \left(\frac{\gamma_{n(1)}}{\gamma_{12}^{old}}\right) \end{bmatrix} \begin{Bmatrix} \varepsilon_1 \\ \varepsilon_2 \\ \gamma_{12} \end{Bmatrix} \quad (4-37)$$

For negative total shear strain ( $\gamma_{12} < 0$ ), the following cases are considered:

(d) If the crack surface is slipping up a hill the secant stiffness matrix becomes:

$$\begin{Bmatrix} \sigma_1 \\ \sigma_2 \\ \tau_{12} \end{Bmatrix} = \begin{bmatrix} E_c & 0 & 0 \\ 0 & E_c - \frac{E_c B}{aAG} & \left(\frac{E_c}{a} - \frac{E_c C}{aAG}\right) \left(\frac{\gamma_{n(1)}}{\gamma_{12}^{old}}\right) \\ 0 & \frac{B}{A} & \frac{C}{A} \left(\frac{\gamma_{n(1)}}{\gamma_{12}^{old}}\right) \end{bmatrix} \begin{Bmatrix} \varepsilon_1 \\ \varepsilon_2 \\ \gamma_{12} \end{Bmatrix} \quad (4-38)$$

(e) If the crack surface is not slipping the secant stiffness matrix becomes:

$$\begin{Bmatrix} \sigma_1 \\ \sigma_2 \\ \tau_{12} \end{Bmatrix} = \begin{bmatrix} E_c & 0 & 0 \\ 0 & E_c & \left(\frac{E_c}{a}\right) \left(\frac{\gamma_{cr(1)}^{old}}{\gamma_{12}^{old}}\right) \\ 0 & 0 & \left(\frac{\tau_{12}^b}{\gamma_{12}^{old}}\right) \end{bmatrix} \begin{Bmatrix} \varepsilon_1 \\ \varepsilon_2 \\ \gamma_{12} \end{Bmatrix} \quad (4-39)$$

(f) If the crack surface is slipping down a hill the secant stiffness matrix becomes:

$$\begin{Bmatrix} \sigma_1 \\ \sigma_2 \\ \tau_{12} \end{Bmatrix} = \begin{bmatrix} E_c & 0 & 0 \\ 0 & E_c + \frac{E_c B}{aAG} & \left(\frac{E_c}{a} - \frac{E_c C}{aAG}\right) \left(\frac{\gamma_{n(1)}}{\gamma_{12}^{old}}\right) \\ 0 & -\frac{B}{A} & \frac{C}{A} \left(\frac{\gamma_{n(1)}}{\gamma_{12}^{old}}\right) \end{bmatrix} \begin{Bmatrix} \varepsilon_1 \\ \varepsilon_2 \\ \gamma_{12} \end{Bmatrix} \quad (4-40)$$

## 4.2.6 Active Crack Criteria

As state previously, only one established crack direction can be active at a time. Because of this reasonable active crack criteria need to be established. With the new formulation of the Orthogonal Shear Friction Theory to separate crack strain from total strain, some of the previously established criteria need to be changed. Epsilon effective was used to determine whether or not the crack is in tension or compression. However, the new formulation of effective strain requires that the crack shear strain is known. The crack shear strain cannot be determined until the correct shear stress equation is determined. Because of this fact new criteria to determine the state of the crack are as follows.

Assume the crack surface is in tension such that:

$$\tau_{12} = \beta' G \gamma_{cr} \text{ and } \gamma_n = \frac{\tau_{12}}{G} + \gamma_{cr}$$

The equation for  $\gamma_n$  can be rewritten as:

$$\gamma_n = \frac{\tau_{12}}{G} + \frac{\tau_{12}}{\beta' G} = \frac{\tau_{12}(1+\beta')}{\beta' G}$$

Now the shear stress can be rewritten as:

$$\tau_{12} = \frac{\gamma_n \beta' G}{(1+\beta')} = \beta' G \gamma_{cr}$$

Solving for the cracking shear stress yields:

$$\gamma_{cr} = \frac{\gamma_n}{(1+\beta')}$$



Plugging this into the equation for epsilon effective yields:

$${}^e\varepsilon = \varepsilon - \frac{|\gamma_n|}{a(1+\beta')} \quad (4-41)$$

If the assumption of tension was correct, Equation 4-41 will yield a positive value. If the assumption was wrong a negative value will be obtained and the crack surface will therefore be in compression. Once this is established the same active crack criteria used for the Orthogonal Shear Friction Theory is applicable.

## 4.3 Analysis of the Orthogonal Shear Friction Model: Crack Strain Separated

A single four-noded element was analyzed using the Crack Strain Separated formulation of the Orthogonal Shear Friction Theory (CSS). The CSS theory was inserted into the MNRM framework, so that all inputs and the convergence scheme were identical. Again the concrete was pre-cracked and the crack coordinates were set at an angle of 45° from the global coordinate system. The analysis successfully converged for loading in one direction and the solution diverged at the onset of unloading.

### 4.3.1 Results and Discussions

Results of the CSS analysis are presented in Figures 4.1 through 4.4. Figure 4.1 shows the normal strain,  $\varepsilon_1$ , versus the crack shear strain,  $\gamma_{cr}$ , and the total shear strain,  $\gamma_{12}$ . This relationship shows the crack opening path. Notice that when the normal strain is plotted against the total shear strain there are two different slopes. However, when plotted against the crack shear strain there is only one slope, which is the crack opening path. This verifies that the crack shear strain enforces the crack opening path. Figure 4.2 shows the crack and concrete shear strains versus the total shear strain. At the start

of the analysis the state of the crack is “no slip” and the crack shear strain remains zero while concrete shear strain increases. Eventually the crack surface begins to “slip up the hill” and the crack shear strain increases while the concrete shear strain goes toward zero. This enforces the idea that almost all strains in cracked concrete are crack strains.

Figure 4.3 shows a comparison of the concrete shear stress versus the total shear strain for both the CSS analysis and the MNRM analysis. The results of the CSS analysis are almost identical to the results from the MNRM analysis. The crack strain starts from zero and as the element is loaded the shears stresses are not sufficient to initiate slip. At this point all of strains are that of the concrete not the cracks as the crack surface is in a state of “no slip”. Figure 4.4 shows the concrete shear stress versus the concrete, crack and total shear strains. Here it can be seen that the concrete shear strains only follow the “no slip” portion of the curve (the shear modulus,  $G$ ). As in Figure 4.2 the concrete shear strains reach a maximum value at the beginning of the analysis and then move back toward zero.

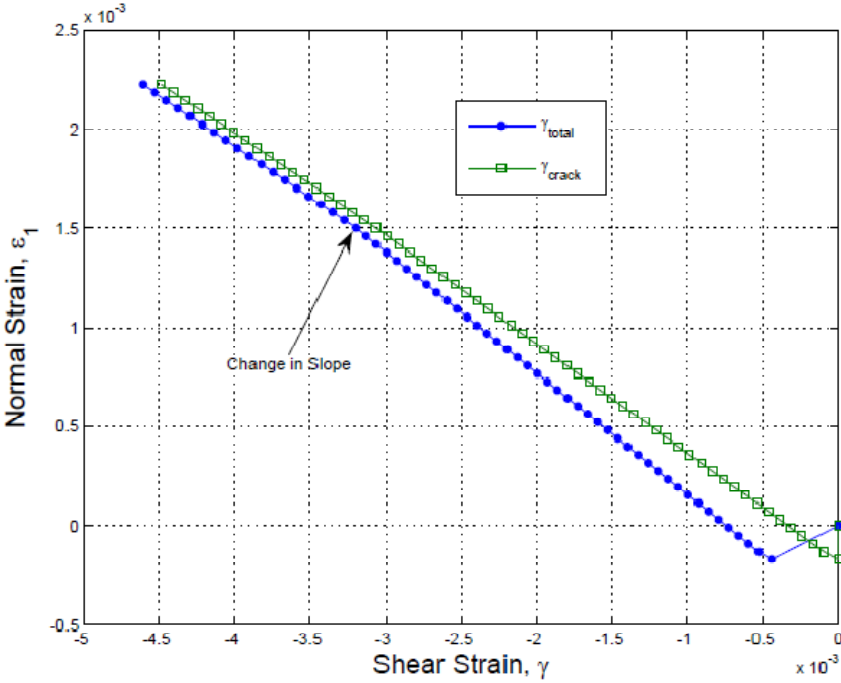


Figure 4.1 Normal Strain vs. Crack Shear Strain and Total Shear Strain.

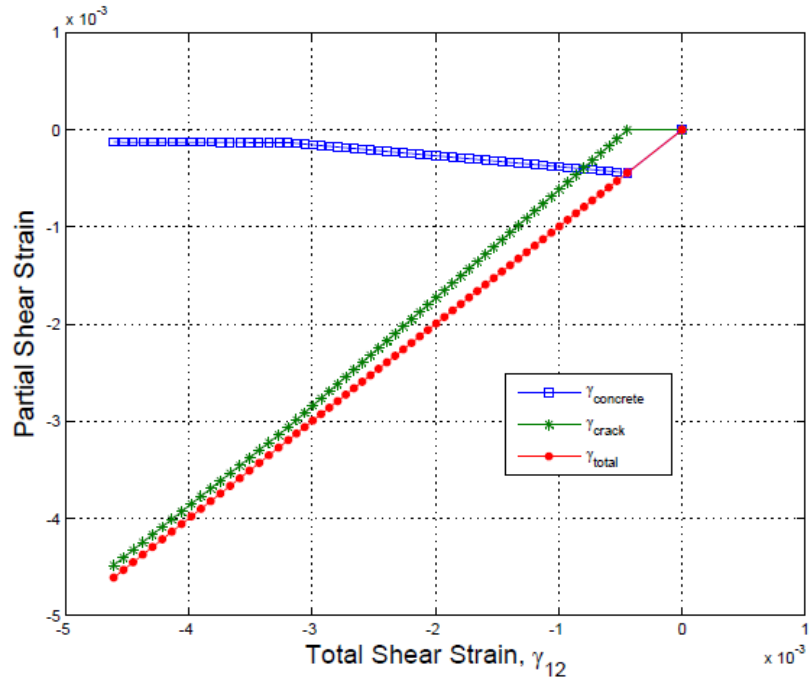


Figure 4.2 Crack Shear Strain and Concrete Shear Strain vs. Total Shear Strain.

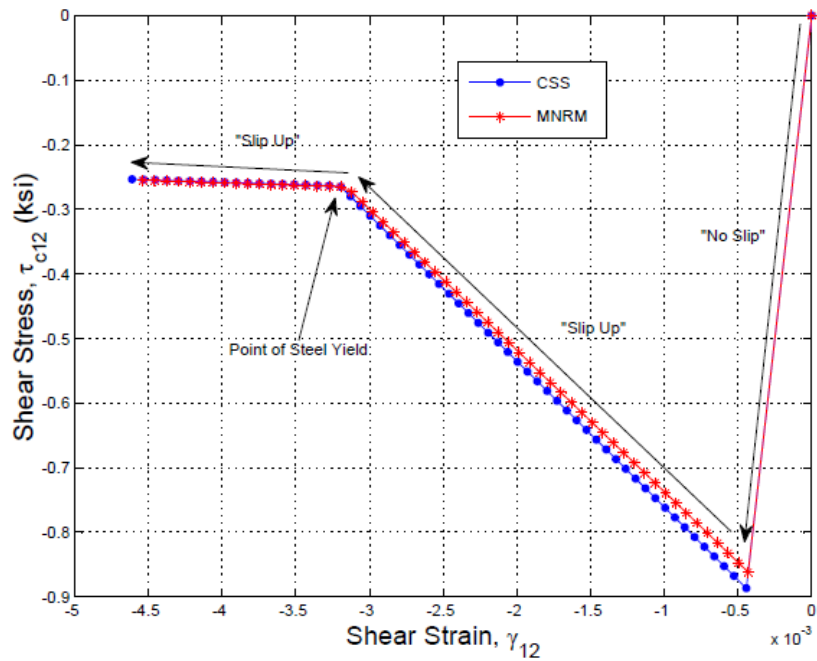


Figure 4.3 Comparison of Concrete Shear Stress vs Shear Strain for the CSS and MNRM analysis's.

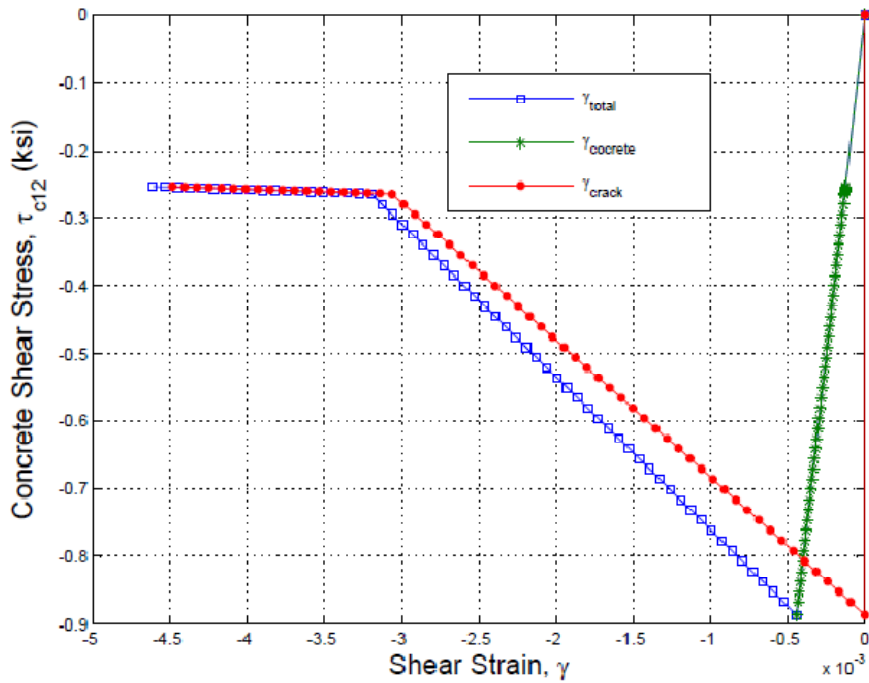


Figure 4.4 Concrete Shear Stress vs. Total, Concrete and Crack Shear Strains.

Figure 4.4 also shows that the crack strains start at zero and increase once the crack surface begins to slip. At this point the shear strength becomes of function the shear friction developed across the crack. Figure 4.4 also shows that the additions of the concrete and crack shear strains are equal to the total shear strains, which verifies the relationship imposed by the CSS theory (Equation 4-1).

Even though the CSS model was unsuccessful for cyclical loading, it is able to capture the fundamental shear friction behavior. The model was also successful in separating out strains due to the cracks as well as the un-cracked concrete. This fact creates an increase in overall model accuracy. In addition the model is capable of handling various crack orientations. The results of the CSS analysis will be compared to other models commonly used for modeling the reduced shear stiffness of cracked reinforced concrete in the next section.

## 4.4 Study of CSS Results

The results of the CSS analysis were compared to the results of two other models for cracked reinforced concrete. Significant differences in the observed results were found. The two models used for comparison were a basic  $\beta G$  model and an alternate procedure for the Modified Compression Field Theory (MCFT) proposed by Vecchio [22]. Both models assume the same tension stiffening curve as the CSS analysis to approximate the non-linear behavior of cracked concrete. Both models are also secant stiffness formulations, like the CSS formulation. The  $\beta G$  model handles the reduced shear stiffness of cracked concrete by multiplying the shear modulus,  $G$ , by an arbitrary factor,  $\beta$ , which in theory can vary from 0 to 1. The model proposed by Vecchio [22], varies the secant shear stiffness such that it is a function of the secant stiffness values for the principal stress directions as shown below and previously presented as Equation 2-3:

$$\bar{G} = \frac{\bar{E}_1 \cdot \bar{E}_2}{\bar{E}_1 + \bar{E}_2} \quad \text{where, } \bar{E}_1 = \frac{\sigma_1}{\varepsilon_1} \text{ and } \bar{E}_2 = \frac{\sigma_2}{\varepsilon_2}$$

Like the CSS analysis a single element was analyzed under a specific set of loads controlled by a prescribed displacement. A constant vertical load of 18 kips was applied to the element as well as horizontal shear by means of the proportional load vector to ensure a uniform state of stress (See Section 3.7.4 for a complete description of loading). Reinforcement was provided in both the global horizontal and vertical directions. The reinforcement ratio for the horizontal direction was 2% and 0.2% for the vertical direction. For the  $\beta G$  model,  $\beta$  was set equal to 0.2. Poisson's ratio was ignored for ease of implementation and interpretation of results. All other material constants and stress strain relationships were the same as the CSS analysis.

Initially the model was analyzed with prescribed DOF's displacement set equal to zero (see Figure 3.7 for the location of the partitioned DOF). This was done to initially

determine the differences in behavior for a simple case. Figures 4.5-4.7 show the deformed shape for the three models for zero prescribed displacement. The open circles represent the un-deformed position of the nodes and the solid circles represent the deformed position of the nodes. The displacements are all in inches and are multiplied by a factor of 100.

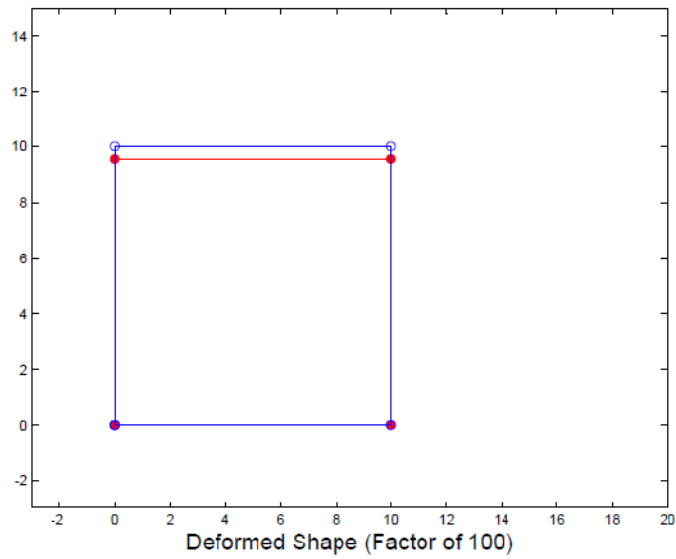


Figure 4.5 Deformed Shape for zero prescribed displacement, CSS model (in).

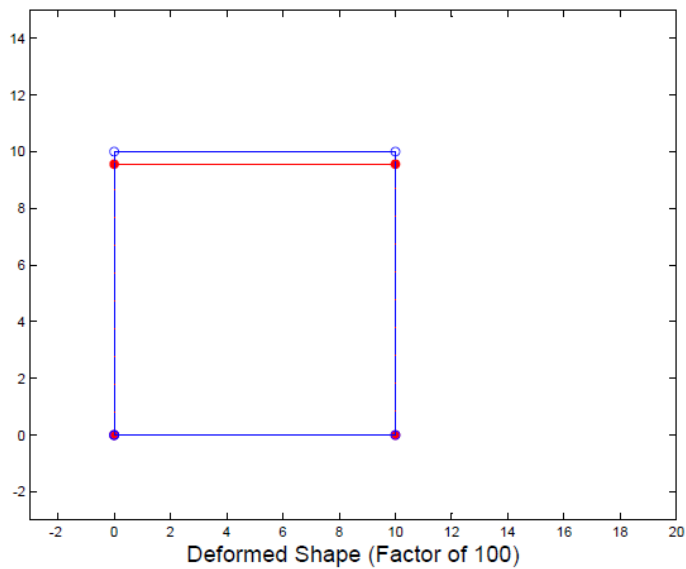
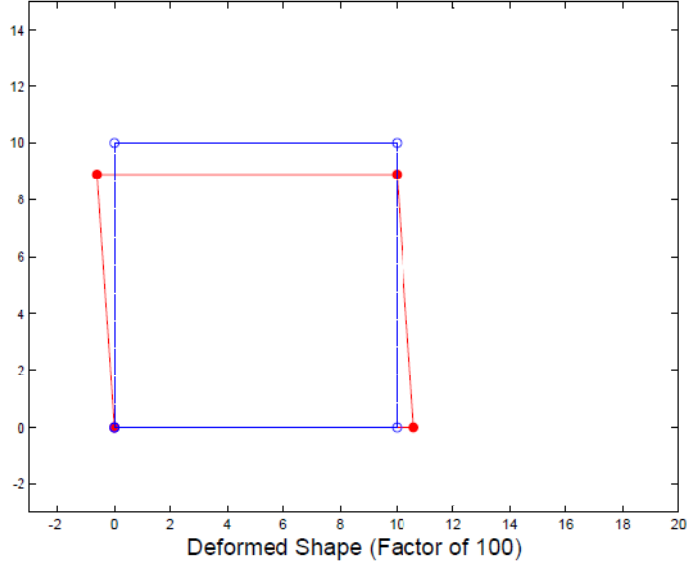


Figure 4.6 Deformed Shape for zero prescribed displacement, Vecchio model (in).



**Figure 4.7 Deformed Shape for zero prescribed displacement,  $\beta G$  model (in).**

It is clear that the CSS and Vecchio models have near identical behavior, while the  $\beta G$  model has very different results. The difference in the  $\beta G$  model is due to a false Poisson's ratio effect caused by the reduced shear stiffness. This is because the reduction in the shear modulus violates the elastic relationships between the shear modulus, the elastic modulus and Poisson's ratio. Even though Poisson's ratio is ignored in the crack orientation's stiffness formulation, when the stiffness matrix is rotated into the global direction a non-diagonal stiffness matrix is produced. If the elastic relationships between the shear modulus, the elastic modulus and Poisson's ratio are held true, the rotation of the diagonal stiffness matrix from the crack orientation to the global direction will produce a diagonal stiffness matrix as well. This is why the CSS and Vecchio models do not have any horizontal expansion with the vertical contraction caused by the compressive load. The CSS model is in a state of no crack slip, so the stiffness matrix in the crack orientation has both the full elastic and shear modulus's of un-cracked concrete. The Vecchio model is similar in that there is no reduction in the elastic modulus of concrete for the given state of loading, so that shear modulus

remains the true shear modulus of un-cracked concrete. This is also why the results of the CSS and Vecchio models are nearly identical for the given state of loading.

Next the three models were compared over identical sets of horizontal displacements. The prescribed DOF of the element in each model was incrementally displaced to 0.06 inches. The results of the three different models are presented in Figures 4.8-4.13.

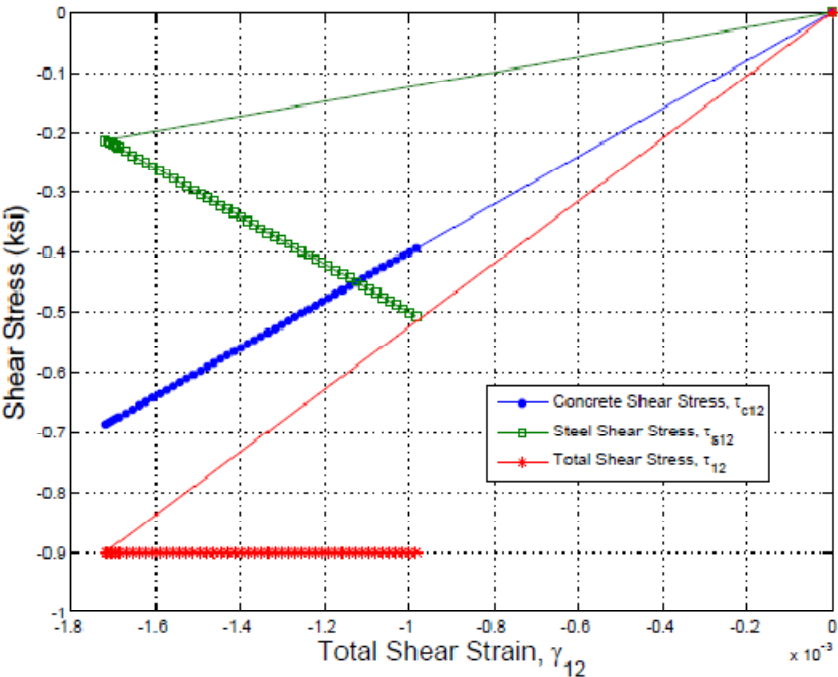


Figure 4.8 Concrete, Steel and Total Shear Stresses vs. Total Shear Strain,  $\beta G$  model.

Figure 4.8 shows the concrete, steel and total shear stresses versus the total shear stress for the  $\beta G$  model. The large first step is due to the applied vertical load. Notice that the steel begins to take more of the shear stress as the element is displaced further, while the concrete follows the slope of the reduced shear modulus,  $\beta G$ . Also the shear strain or “slip” decreases with increased horizontal displacement. This is due to the fact that the steel ratio is greater in the horizontal direction than the vertical and is reflected in the deformed shape. Figure 4.9 shows the final deformed shape at a factor of 100 at the prescribed displacement of 0.06 inches.



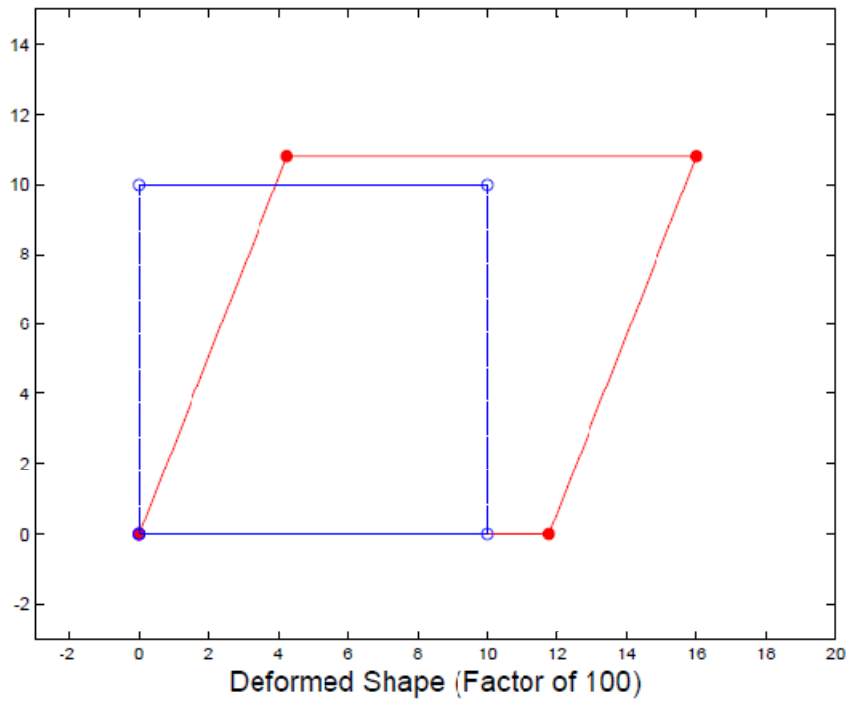


Figure 4.9 Deformed Shape for a prescribed displacement of 0.06 (in),  $\beta G$  model.

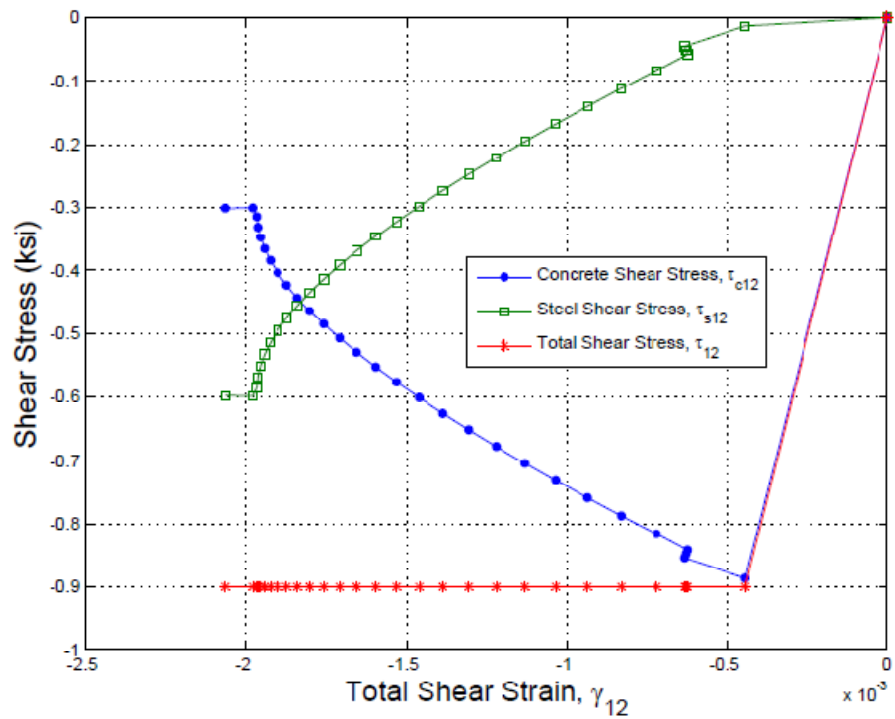


Figure 4.10 Concrete, Steel and Total Shear Stresses vs. Total Shear Strain, Vecchio model.

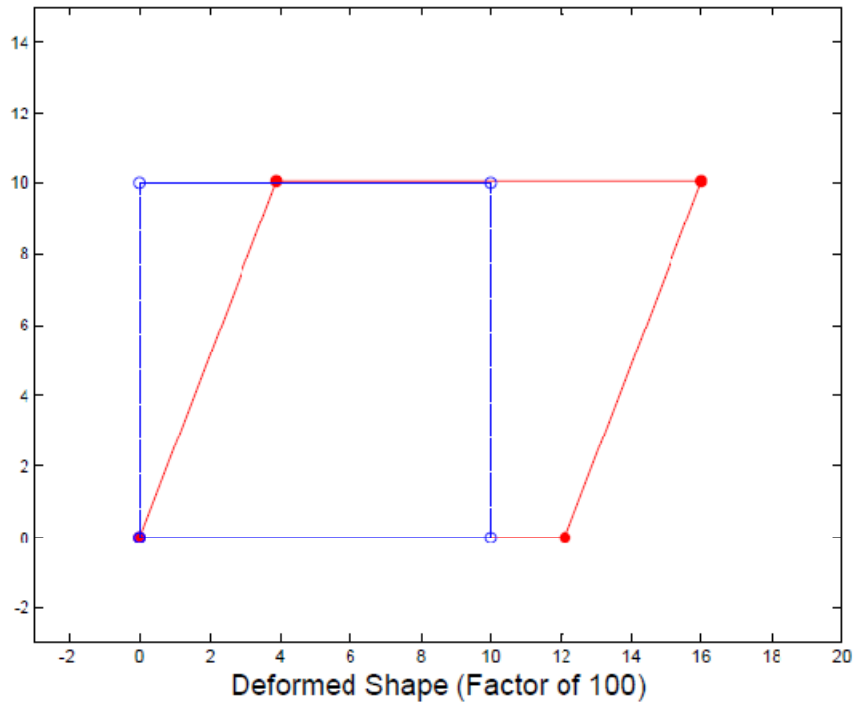


Figure 4.11 Deformed Shape for a prescribed displacement of 0.06 (in), Vecchio model.

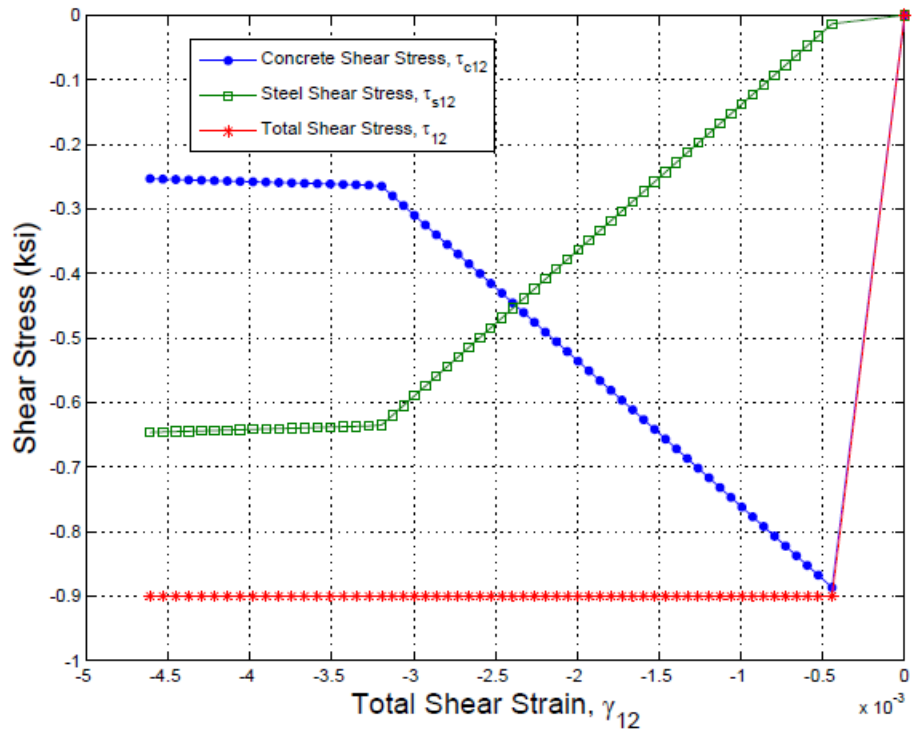


Figure 4.12 Concrete, Steel and Total Shear Stresses vs. Total Shear Strain, CSS model.

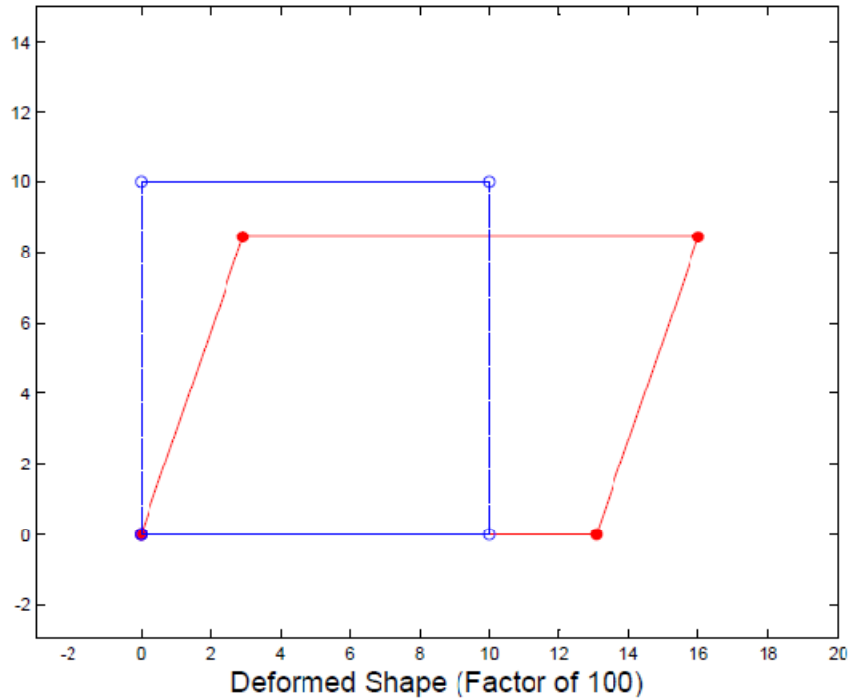


Figure 4.13 Deformed Shape for a prescribed displacement of 0.06 (in), CSS model.

Figures 4.10 and 4.11 show the data from the Vecchio analysis while Figures 4.12 and 4.13 show the data from the CSS analysis. Comparing Figures 4.10 and 4.12 shows there is some agreement with the shear stresses in the crack orientation between the Vecchio and CSS models. However, the shear strains in the CSS model are almost twice the shear strains in the Vecchio model. In addition the predicted displacements are drastically different as can be seen by comparing Figures 4.11 and 4.13. In general it can be clearly seen that three different models for cracked reinforced concrete produce very different results.

The difference between the three models can further be seen in Figure 4.14, which shows the global shear stress versus the prescribed displacement for each model. This shows the predicted shear stress for each model over the same displacements. It can be seen that maximum predicted shear stress is similar for the  $\beta G$  and Vecchio models, while the CSS shear stress is much lower. The displacement at which the steel yields is

also different between the models and can be seen where the slope of the curves becomes smaller. Although Figure 4.14 shows a comparison of results for identical horizontal displacements of the prescribed DOF, the difference in vertical displacements for this DOF were very different. This comparison of results is important as there are significant differences in predicted design values between the models for a seemingly important load case, similar to that which a shear wall may see. These results display the need to establish a testing program to validate the accuracy of finite element models for cracked reinforced concrete membranes subjected to this loading pattern frequently seen by this type of structure.

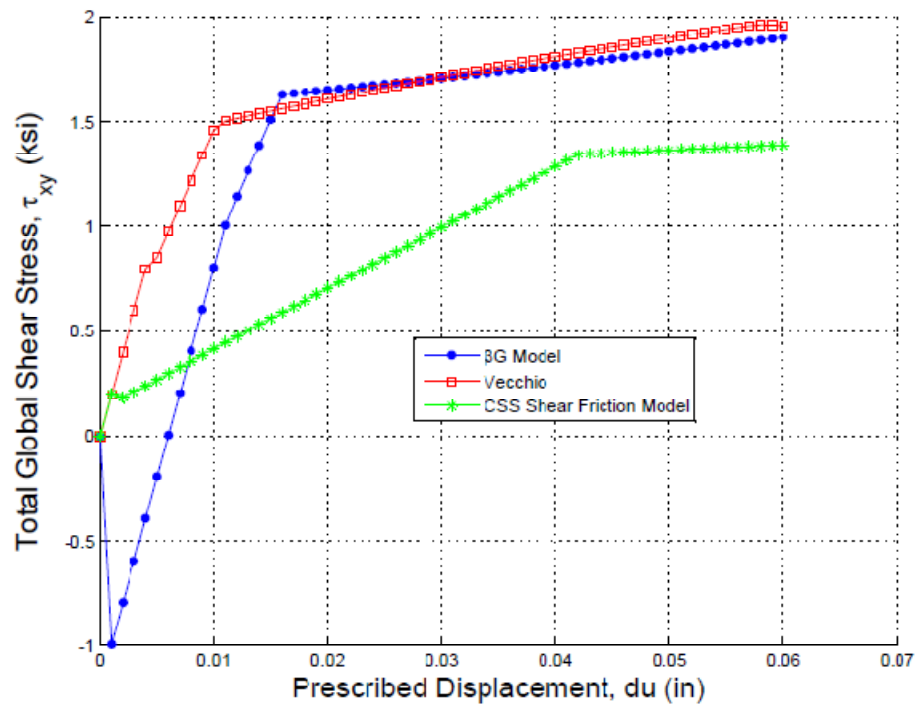


Figure 4.14 Comparison of Global Shear Stress vs. Prescribed Displacement for  $\beta G$ , Vecchio and CSS models.

## Chapter 5

### Conclusions and Future Work

An analytical model for reinforced concrete membranes was recently developed to include a rational shear strength model based on the shear friction provisions in the ACI code [15]. This model was able to limit the shear strength of crack surfaces by implementing the shear friction theory into a total strain based model. However, this proposed model was only formulated for one crack direction that was assigned parallel to the applied shear loads. This research aimed to extend the model to two-directional, orthogonal cracking at any angle to the applied shear loading. The ultimate goal was to further generalize and test the theory's applicability to common design applications such as shear walls. Evaluations of existing finite element models for shear strength of crack reinforced concrete, including the shear friction theory proposed by So, are presented in Chapter 2. In addition, code provisions for shear friction present in the ACI Building Code as well as the original testing the provisions are based on are reviewed. A new formulation for the shear friction theory to include orthogonal cracking, the Orthogonal Shear Friction Theory, is presented in Chapter 3. The phases of the Orthogonal Shear Friction Theory's models development and discussions of results are also presented there. An attempt to fix convergence issues and improve the overall models accuracy by separating crack strains from total strains is presented in Chapter 4 as the Crack Strain Separated Model. This includes formulations, discussions of results and finally comparisons to existing models.

## 5.1 Objectives

The original objectives of this research progressively changed with development of the model and serve as a track of what was accomplished. Listed here is summary of the main research objectives and to what extent they were met.

1. A working finite element analysis model that includes a shear friction model that enforces a crack opening path and limits the materials strength in shear.

This objective was accomplished previously by So [15]. However, a new finite element framework was required for the implementation of multi-directional cracking. Because of this a new framework was developed successfully and results of the analysis showed that the shear friction model was able to enforce the crack opening path and limit the strength in shear by yielding in the reinforcement.

2. Implementation of multi-directional orthogonal cracking into the shear friction model.

The Orthogonal Shear Friction Theory was developed and implemented into the finite element framework. The theory includes criteria and formulations to handle multi-directional cracking. However, due to convergence issues only one crack was able to be analyzed, as the second crack was never stressed such that shear friction would be a consideration of stiffness. In an attempt to obtain convergence the Orthogonal Shear Friction Theory was expanded to the Crack Strain Separated Theory, which improved the model's overall accuracy but was also unable to obtain cyclical convergence.

3. A deflection controlled analysis.

A deflection controlled analysis was successfully obtained in all phases of model development. A deflection controlled analysis is necessary to produce useful and comparable results for arbitrary loading, such as cyclical loading.

4. A uniform state of stress and strain across the element in order to be able to interpret the results.

A uniform state of stress and strain was successfully obtained in all phases of model development. First it was obtained by applying equal incremental displacements to the top two nodes. In addition the top two nodes vertical displacements were slaved together. In later phases of the model development, a uniform state of stress and strain was obtained by a proportional load vector, which ensured this state while still allowing a displacement controlled analysis.

5. Shear stress across the surface of the crack.

Shear stress was successfully obtained across the surface of the crack. This was a major consideration as the crack directions are defined by the orientation of the principal tensile stress. By definition there is no shear in the direction of the principal stresses. Without shear being transferred across the surface of the crack the consideration of shear friction for shear transfer becomes irrelevant. In order to obtain shear across the crack surface a vertical compressive load was required. This was accomplished by means of a proportional load vector and later a constant vertical load combined with a proportional load vector (the PLV and CVL formulations respectively).

6. Variable steel reinforcement ratios in the reinforcement directions.

Variations in the steel reinforcing are necessary considerations as reinforcing required by design is not necessarily uniform in all directions. This was accomplished by smeared steel reinforcing ratios in the two major global directions of the element.

7. Cyclical loading allowing more than one crack direction to be active throughout the analysis.

This objective was not met due to convergence issues. Only monotonic loading was achieved by all models. The PLV model obtained full convergence on loading and

unloading in one direction. Full cyclical convergence is necessary to successfully analyze and implement multi-directional cracking.

8. Analysis of larger structures requiring multiple elements.

Due to the fact that cyclical convergence was not achieved, no larger structures were analyzed or tested.

## 5.2 Conclusions

Even though full cyclical convergence was not achieved, and subsequently multi-directional cracking and analysis of larger structures were not accomplished, the research still produced notable results. The models using the Orthogonal Shear Friction Theory and the Crack Strain Separated Theory were able capture some unique and complex behavior of reinforced concrete. The models are unique in that they predict the stiffness of cracked reinforced concrete using rational physical behavior, not arbitrary constants. They are also able to limit the strength in shear as a function of the yielding of the reinforcing steel provided across the cracks, which is in accordance with the provisions in the ACI Building Code and recognized concrete behavior [12]. The models are also able to capture the complex interaction between reinforcing steel and concrete. This complex behavior is captured using a simple model.

A comparison of the Crack Strain Separated Theory to other existing models shows a high degree of inconsistency. Predicted shear stresses, and displacements were very different for the three models that were compared. Each model predicted different interactions between the concrete and the steel, most importantly the point at which the steel yields. This is due to differences in predicted stiffness of the cracked concrete. This inconsistency necessitates further testing and analysis to determine what the actual behavior is. This also becomes important as the difference in results was found under a seemingly important loading condition. The element analyzed by the three models was



subjected to vertical compression as well as horizontal shear, and previously developed diagonal cracks. This loading on reinforced concrete membranes is directly applicable to the design of shear walls and predicting their behavior.

## 5.3 Future Work

This research has added to the limited knowledge concerning the finite modeling of the shear stiffness and strength of reinforced concrete. Specifically this research has brought to light the discrepancy between the predicted results of existing models for a loading case mostly untouched by other research. The CSS shear friction theory rationally predicts the stiffness of cracked concrete utilizing a simple procedure, however there are a number of areas for improvement and future work stemming from this research. The areas for improvement and future work are described under three main categories: obtaining a cyclical analytical model, improving the models overall accuracy and experiments to obtain the actual physical behavior.

Cyclical Model:

1. A fully cyclical model is necessary to test the CSS shear friction model's criteria and formulation for multi-directional cracking.
2. The current stiffness formulation is a secant formulation; a tangent formulation may be required to achieve full cyclical convergence.
3. Alternative methods for convergence should be tried, such as the arc length method.

#### Model Accuracy:

1. Currently there is no compression curve for concrete. A compression curve that limits the concrete's strength in compression should be added to improve the model's applicability for all loading types.
2. An improved cyclical steel model should be implemented again to improve overall model accuracy. The current model is a simplification of more sophisticated existing steel models.
3. Currently the shear friction model does not include any damage parameter for cyclical loading or fatigue of materials. Specifically the degradation of the crack opening path should be included as the rough protrusions on the crack surface will tend to smooth out under cyclical loading. This will change the "up" and "down" coefficients of friction as well as the angle of the crack opening path.

#### Experiments:

1. An experimental program is necessary to determine and verify the shear friction behavior under cyclical loading. This should be done for the loading case presented in this thesis, vertical compression and horizontal shear with a pre-existing diagonal crack. In addition the crack orientation and steel ratios should be varied.
2. Additional experiments are needed to verify the sliding friction coefficients presented for the shear friction theory. The crack opening path should also be verified as it may tend to degrade under cyclical loading and may not be explicitly followed for loading and unloading.
3. Further comparative studies of the current loading condition and CSS model should be performed on other existing reduced shear stiffness models for cracked concrete.

4. Additional parameter studies should be performed on the model, testing various reinforcement ratios, loading cases and crack orientations.

# Appendix A

## Derivations

### A.1 Sample Derivation of Shear Stress Limit

A sample derivation of a shear stress limit is presented here. The specific case is “slip up” for negative total shearing strain ( $\gamma < 0$ ).

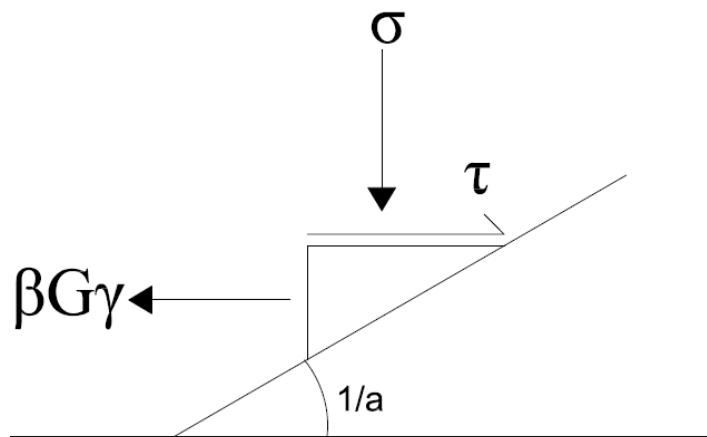


Figure A.1 Schematic of a block being pushed “up the hill”.

Based on Figure A.1 the following equation can be written:

$$\tau = -\mu^{up} \sigma + \beta G \gamma_{cr} \quad (A-1)$$

Rearranging Equation A-1 and solving for  $\gamma_{cr}$  yields:

$$\gamma_{cr} = \frac{\tau + \mu^{up}}{\beta G} \quad (A-2)$$

In addition the concrete shearing strain can be defined as:

$$\gamma_{concrete} = \frac{\tau}{G} \quad (A-3)$$

Combining Equations A-2 and A-3 to get the total shearing strain yields the following equation:

$$\gamma_{total} = \gamma_{concrete} + \gamma_{cr} = \frac{\tau}{G} + \frac{\tau + \mu^{up}}{\beta G} = \frac{\tau\beta + \tau}{\beta G} + \frac{\mu^{up}\sigma}{\beta G} \quad (A-4)$$

Rearranging Equation A-4 and solving for  $\tau$  yields:

$$\tau = \frac{\gamma\beta G + \mu^{up}\sigma}{1 + \beta} \quad (A-5)$$

Where,

$$\sigma = E\varepsilon - \frac{E\gamma}{a} \quad (A-6)$$

Now Equation A-5 can be re-written as:

$$\tau = \frac{\gamma\beta G + \mu^{up}\left(E\varepsilon - \frac{E\gamma}{a}\right)}{1 + \beta} \quad (A-7)$$

## A.1 Derivation of “Slip Up” Coefficient of Friction

In a case where the crack surface is slipping “up the hill”, the coefficient of friction,  $\mu^{\text{up}}$ , needs to be defined. The derivation of  $\mu^{\text{up}}$  is presented here.

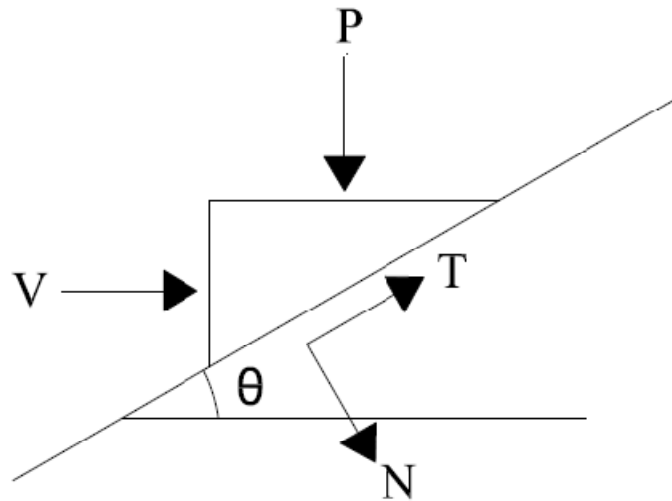


Figure A.2 Schematic of a block slipping “up the hill” at an inclination,  $\theta$ .

Based on Figure A.2 the following relationships can be established:

$$\mu' = \frac{T}{N} \text{ and } \mu = \frac{V}{P}$$

Where  $\mu'$  is the coefficient of friction relative to the surface of the hill and  $\mu$  is the coefficient of friction corresponding to the applied forces  $V$  and  $P$ . Because of previous test results presented in Section 2.4.1, it is convenient to define the friction coefficient,  $\mu$ , in terms of the friction coefficient relative to the crack opening path,  $\mu'$ .

The forces  $P$  and  $V$  can be written in terms of the crack opening path and the normal forces,  $T$  and  $N$  such that:

$$P = -T \sin \theta + N \cos \theta \tag{A-8}$$

$$V = T \cos \theta + N \sin \theta \quad (\text{A-9})$$

Now the equation for the coefficient of friction,  $\mu$ , can be written in terms of Equations A-8 and A-9.

$$\frac{V}{P} = \frac{T \cos \theta + N \sin \theta}{-T \sin \theta + N \cos \theta} \quad (\text{A-10})$$

Equation A-10 can be rearranged in terms of the coefficient of friction,  $\mu'$ , as shown below:

$$\frac{V}{P} = \frac{T \cos \theta + N \sin \theta}{-T \sin \theta + N \cos \theta} \left( \frac{1/N}{1/N} \right) = \frac{\sin \theta + \frac{T}{N} \cos \theta}{\cos \theta - \frac{T}{N} \sin \theta} = \frac{\sin \theta + \mu' \cos \theta}{\cos \theta - \mu' \sin \theta}$$

Finally the desired equation can be written as:

$$\mu^{up} = \frac{\sin \theta + \mu' \cos \theta}{\cos \theta - \mu' \sin \theta} \quad (\text{A-11})$$

# Appendix B

## MATLAB Source Codes

### B.1 Proportional Load Vector (PLV) Master File

```
%%%%%%%%%%%%%%%%%%%%%%%%%%%%%%%%%%%%%%%%%%%%%%%%%%%%%%%%%%%%%%%%%%%%%%%%%%%%%%
%%%%%%%%%
%%%PROPORTIONAL LOAD VECTOR (PLV) MASTER FILE
%%%DISPLACEMENT-CONTROLLED ANALYSIS
%%%RECTANGULAR MEMBRANE USING 4-NODED BI-LINEAR RECTANGULAR ELEMENT
      %BY JEFFREY MITCHELL % JULY 2010 %MATLAB 7.4.0 (R2007a)
%%%%%%%%%%%%%%%%%%%%%%%%%%%%%%%%%%%%%%%%%%%%%%%%%%%%%%%%%%%%%%%%%%%%%%%%%%%%%%
%%%%%%%%%
clear all;

%INITIALIZE
MATRICES%%%%%%%%%%%%%%%%%%%%%%%%%%%%%%%%%%%%%%%%%%%%%%%%%%%%%%%%%%%%%%%%%%%%%%%%%
I.NE=1; % Number of elements
I.NGDF=8; % Number of Global Degrees of Freedom
I.NLDF=8; % Number of Local Degrees of Freedom
%I.NC = 4; % Number of constraints
I.ESM=zeros(I.NLDF,I.NLDF); %Initialize element stiffness matrix
I.GSM=zeros(I.NGDF,I.NGDF); %Initialize global stiffness matrix
I.GSMs=zeros(I.NGDF,I.NGDF); %Initialize global stiffness matrix for
%steel
I.GSMc=zeros(I.NGDF,I.NGDF); %Initialize global stiffness matrix for
%concr.
I.IG=zeros(I.NE,I.NLDF); %Initialize connectivity matrix
%I.IBC = zeros(NC); %Initialize boundary conditions matrix
I.q = zeros(I.NGDF,1); %Initialize displacement vector
I.IG = [1 2 3 4 5 6 7 8]; %Connectivity Matrix

% ELEMENT
GEOMETRY%%%%%%%%%%%%%%%%%%%%%%%%%%%%%%%%%%%%%%%%%%%%%%%%%%%%%%%%%%%%%%%%%%%%%%%%%
%Unit: kip-in
Geo.a=10; Geo.b=10; Geo.t=2; %in

% MATERIAL PROPERTIES
%%%%%%%%%%%%%%%%%%%%%%%%%%%%%%%%%%%%%%%%%%%%%%%%%%%%%%%%%%%%%%%%%%%%%%%%%
%1. Concrete
Mat.fcksi=6;
```



```

Mat.fcrksi=7.5*sqrt(Mat.fcksi*1000)/1000;

Mat.v=0.0;
Mat.iEc1=4000;
Mat.iEc2=4000;
%ksi
eCrack=Mat.fcrksi/Mat.iEc1;

%2. Steel
Mat.iEs1=30000;
Mat.rhos1=0.02;
Mat.fys=60;
Mat.Esh=0.02*Mat.iEs1;

Mat.iEs2=30000;
Mat.rhos2=0.005;
Mat.eys=Mat.fys/Mat.iEs1;

%%%%%%%%%%%%%%%%%%%%%%%%%%%%%%%%%%%%%%%%%%%%%%%%%%%%%%%%%%%%%%%%%%%%%%%%
%ANALYSIS
%%%%%%%%%%%%%%%%%%%%%%%%%%%%%%%%%%%%%%%%%%%%%%%%%%%%%%%%%%%%%%%%%%%%%%%%
P=105; %NUMBER OF INCRIMENTS
N=P+1;
dui=.001; %Applied Displacement (in)
%Initialize Individual Components
ex=zeros(N,1); Sx=zeros(N,1); Scx=zeros(N,1); Ssx=zeros(N,1);
ey=zeros(N,1); Sy=zeros(N,1); Scy=zeros(N,1); Ssy=zeros(N,1);
exy=zeros(N,1); Sxy=zeros(N,1); Scxy=zeros(N,1); Ssxy=zeros(N,1);
q5=zeros(N,1); A5=zeros(N,1); q6=zeros(N,1); A6=zeros(N,1);
q7=zeros(N,1); A7=zeros(N,1); q8=zeros(N,1); A8=zeros(N,1);
q3=zeros(N,1); A3=zeros(N,1);

Sc121=zeros(N,1); Sc122=zeros(N,1); Sc123=zeros(N,1);
e121=zeros(N,1); e122=zeros(N,1); e123=zeros(N,1);

eleffectiv=zeros(N,1); e2effectiv=zeros(N,1);

q=zeros(I.NGDF,1);

gamma12prev=0;
tau12prev=0;
deltagamma=0;

aaa=zeros(N,1); increment=zeros(N,1);

%initialize values for test, strains and stresses all values at zero
%initialize cracked material properties of concrete
%initialize cracked concrete in both directions

e=[0;0;0];
Sc=[0;0;0];
Ss=[0;0;0];

```

```

e12=[0;0;0];
Sc12=[0;0;0];

E.e1MaxExcr=0.0002768; %Assumed max excursion strains
E.e2MaxExcr=0.0004205;
E.E1extr=2042.8; %Assumed max excursion Secant Moduli
E.E2extr=1326.79;
E.ec1effprev=0;
E.ec2effprev=0;

e1MaxExcr=E.e1MaxExcr;
e2MaxExcr=E.e2MaxExcr;
E1extr=E.E1extr;
E2extr=E.E2extr;

E.exmax=0;
E.eymax=0;
E.exprev=0;
E.eyprev=0;

es.exmax=0;
es.eymax=0;
es.exprev=0;
es.eyprev=0;
fs.fsxprev=0;
fs.fsyprev=0;

ec12.ec123prev=0;
fc12.fc123prev=0;

E.cracktwo=1; %Establishes the active crack

%Make first Guess as Dsmear, the Secant Stiffness Matrix as well as
%set the crack angle and rotation matrix
%first guess of material stiffness properties will be "SLIP UP"
theta=45; %crack angle
[T]=GetTMatrix(theta); %rotation matrix

Ds=zeros(3,3); %Steel stiffness matrix
Ds(1,1)=Mat.iEs1*Mat.rhos1;
Ds(2,2)=Mat.iEs2*Mat.rhos2;

DcCrack=zeros(3,3); %Cracked concrete stiffness matrix
DcCrack(1,1)=4000;
DcCrack(1,2)=0;
DcCrack(1,3)=2000;
DcCrack(2,1)=0;
DcCrack(2,2)=4000;
DcCrack(2,3)=0;
DcCrack(3,1)=4705.88;
DcCrack(3,2)=0;
DcCrack(3,3)=2392.16;

```

```

%rotate concrete Dc12 to Dcxy
DcCrackGlobal=inv(T)*DcCrack*(inv(T))';

%Smear the DconcreteCrack and the Dsteel in the Global Direction
Dsmear=Ds+DcCrackGlobal;

Tau_B=0; %initialize shear stress

aprev=0; %initialize convergence values
aold=0;

%Initialize Displacement Increment
du=0;

%CONTROL VALUES
limit1=.06; %displacement at which displacement direction reverses
limit=limit1;
V=2; %Vertical Load for proportional load vector

%%
%%%%%%%%%%%%%%%%%%%%%%%%%%%%%%%%%%%%%%%%%%%%%%%%%%%%%%%%%%%%%%%%%%%%%%%%
for i=1:P %incremental displacement loop
%%%%%%%%%%%%%%%%%%%%%%%%%%%%%%%%%%%%%%%%%%%%%%%%%%%%%%%%%%%%%%%%%%%%%%%%

%%
if abs(q(5))>=limit(1) %criteria for direction of loading
    dui=-dui;
end

du=du+dui; %iterate displacement at specified increment

    converge=0; %initializes convergence values for
                %each increment
    count=0;

%%
    while converge==0 %convergence loop
        count=count+1;

%%
        %solve for the actions, strains and displacements
        [A,e,q,a,aold] =
SolveCompressiontest3(I,Geo,Dsmear,du,V,aold,dui);

        %rotate strains to the crack(1-2) direction
        [e12]=straintransformation(e,theta);

```

```

        %solve for concrete stresses in 1-2 direction
        [DcCrack, Sc12, E] =
getConcreteStress(e, e12, Mat, E, Tau_B);

        %Solve for Stresses in steel
        [Ds, Ss] = getSteelStress(e, es, fs, Mat, dui);

        %Rotate concrete stresses to global direction (x-y)
        [Sc]=stresstransformation(Sc12, -theta);

        %Compute total stress
        St=Ss+Sc;

        %rotate concrete Dc12 to Dcxy
        DcCrackGlobal=inv(T)*DcCrack*(inv(T))';

        %Smear the DconcreteCrack and the Dsteel in the
%Global Direction
        Dsmear=Ds+DcCrackGlobal;

        % Converge on load factor "a"
        delta_a=abs(a-aprev);
        aprev=a;

        if delta_a < .0001 %convergence tolerance
            converge=1;
        else
            converge=0;
        end
        if count == 50 %convergence iteration limit
            converge=1;
        end

        %solve for Tau_B
        deltagamma=e12(3)-e123(i);
        Tau_B=tau12prev+Mat.iGc*(deltagamma);

        if i==1
            tau12prev=Sc12(3);
        else
            tau12prev=Sc123(i);
        end

%%
        end %end of convergence loop
%%

        %Track of Strain and Stress Components (Global)
        ex(i+1)=e(1);
        ey(i+1)=e(2);      %Total Strain and Total Stress
        exy(i+1)=e(3);
        Sx(i+1)=St(1);
        Sy(i+1)=St(2);
        Sxy(i+1)=St(3);

```

```

%Track of Individual Stresses (Global)
Scx(i+1)=Sc(1);
Scy(i+1)=Sc(2); %Concrete stresses
Scxy(i+1)=Sc(3);
Ssx(i+1)=Ss(1);
Ssy(i+1)=Ss(2); %Steel Stresses
Ssxy(i+1)=Ss(3);
%Forces & Displacements for the DOF's
q3(i+1)=q(3); %q is displacement, A is force
A3(i+1)=A(3);
q5(i+1)=q(5);
A5(i+1)=A(5);
q6(i+1)=q(6);
A6(i+1)=A(6);
q7(i+1)=q(7);
A7(i+1)=A(7);
q8(i+1)=q(8);
A8(i+1)=A(8);
%Track of 1-2 Direction Concrete Stresses
Sc121(i+1)=Sc12(1);
Sc122(i+1)=Sc12(2);
Sc123(i+1)=Sc12(3);
%Track of 1-2 direction strains
e121(i+1)=e12(1);
e122(i+1)=e12(2);
e123(i+1)=e12(3);
%track of epsilon effective
eleffectiv(i+1)=E.ec1eff;
e2effectiv(i+1)=E.ec2eff;
%max strains
es.exmax=max(ex);
es.eymax=max(ey);
%load vector factor "a"
aaa(i+1)=a;
increment(i+1)=du;

%keep track of last converged strain and stress values
es.exprev=ex(i+1); %strains
es.eyprev=ey(i+1);
fs.fsxprev=Ssx(i+1); %steel stresses
fs.fsyprev=Ssy(i+1);

ec12.ec123prev=e123(i+1);
fc12.fc123prev=Sc123(i+1);

E.ec1effprev=E.ec1eff; %effective strains
E.ec2effprev=E.ec2eff;

%max excursion effective tensile strain and
%concrete tension stiffening curve
eff1test=max(eleffectiv,E.e1MaxExcr);
E.e1MaxExcr=max(eff1test);
eff2test=max(e2effectiv,E.e2MaxExcr);

```

```

E.e2MaxExcr=max(eff2test);

E.E1extr=(Mat.fcrksi/(sqrt(1+200*E.e1MaxExcr)))/E.e1MaxExcr;
E.E2extr=(Mat.fcrksi/(sqrt(1+200*E.e2MaxExcr)))/E.e2MaxExcr;

end %end of incremental displacement loop

%%%%%%%%%%%%%%%%%%%%%%%%%%%%%%%%%%%%%%%%%%%%%%%%%%%%%%%%%%%%%%%%%%%%%%%%
%PLOTS
%%%%%%%%%%%%%%%%%%%%%%%%%%%%%%%%%%%%%%%%%%%%%%%%%%%%%%%%%%%%%%%%%%%%%%%%

subplot(4,3,1)
plot(e121,Sc121,'.-')
xlabel('\epsilon_1')
ylabel('\sigma_c_1(ksi)')
grid on;
hold on;

subplot(4,3,2)
plot(e122,Sc122,'.-')
xlabel('\epsilon_2')
ylabel('\sigma_c_2 (ksi)')
grid on;
hold on;

subplot(4,3,3)
plot(q7,A7,'.-',q5,A5,'.-')
xlabel('Displ q7 & q5')
ylabel('F A7 & A5')
grid On;
hold on;

subplot(4,3,4)
plot(q6,A6,'.-',q8,A8,'.-')
xlabel('Displ q6 & q8')
ylabel('F A6 & A8')
grid on;
hold on;

subplot(4,3,5)
plot(ey,Scy,'.-')
hold on
grid on
xlabel('\epsilon_y')
ylabel('\sigma_c_y')

subplot(4,3,6)
plot(exy,Scxy,'.-')
hold on
grid on
xlabel('\gamma_x_y')
ylabel('\tau_c_x_y')

```

```

subplot(4,3,7)
plot(e123,Sc123,'.-')
xlabel('\gamma_1_2')
ylabel('\tau_c_1_2')
grid on;
hold on;

%%%%%%%%%%%%%%%%%%%%%%%%%%%%%%%%%%%%%%%%%%%%%%%%%%%%%%%%%%%%%%%%%%%%%%%%
%PLOT STEEL
%%%%%%%%%%%%%%%%%%%%%%%%%%%%%%%%%%%%%%%%%%%%%%%%%%%%%%%%%%%%%%%%%%%%%%%%

% figure
subplot(4,3,8)
plot(ex,Ssx,'.-')
hold on
grid on
xlabel('\epsilon_x')
ylabel('\sigma_s_t_x')

%%%%%%%%%%%%%%%%%%%%%%%%%%%%%%%%%%%%%%%%%%%%%%%%%%%%%%%%%%%%%%%%%%%%%%%%

subplot(4,3,10)
plot(incriment,aaa,'.-');
grid on;
hold on;
xlabel('du')
ylabel('a')

subplot(4,3,11)
plot(ey,Sy,'.-');
grid on;
hold on;
xlabel('\epsilon_x')
ylabel('\sigma_c_x')

subplot(4,3,12)
plot(q3,A3,'.-');
grid on;
hold on;
xlabel('q3')
ylabel('A3')

subplot(4,3,9)
plot(ey,Ssy,'.-');
grid on;
hold on;
xlabel('\epsilon_y')
ylabel('\sigma_s_y')

%%%%%%%%%%%%%%%%%%%%%%%%%%%%%%%%%%%%%%%%%%%%%%%%%%%%%%%%%%%%%%%%%%%%%%%%
%Various Plots

```

```

%%%%%%%%%%%%%%%%%%%%%%%%%%%%%%%%%%%%%%%%%%%%%%%%%%%%%%%%%%%%%%%%%%%%%%%%

% figure
% plot(e123,e121,'.-')
% grid on;
% xlabel('Shear Strain, \gamma_1_2')
% ylabel('Normal Strain, \epsilon_1')

% plot(e123,Sc123,'.-')
% xlabel('Shear Strain, \gamma_1_2')
% ylabel('Shear Stress, \tau_c_1_2')
% grid on;

% plot(ex,Ssx,'.-')
% grid on
% xlabel('\epsilon_x')
% ylabel('\sigma_s_t_x')

% plot(e121,Sc121,'.-')
% xlabel('\epsilon_1')
% ylabel('\sigma_c_1(ksi)')
% grid on;

% plot(e1effectiv,Sc121,'.-')
% xlabel('Effective Strain, \epsilon_1')
% ylabel('Concrete Normal Stress, \sigma_c_1 (ksi)')
% grid on;

% plot(e123,Sc121,'.-')
% xlabel('\epsilon_1')
% ylabel('\sigma_c_1(ksi)')
% grid on;

% plot(incriment,aaa,'.-');
% grid on;
% xlabel('du')
% ylabel('a')

%%%%%%%%%%%%%%%%%%%%%%%%%%%%%%%%%%%%%%%%%%%%%%%%%%%%%%%%%%%%%%%%%%%%%%%%
%PLOT FACTORED DEFORMED SHAPE
%%%%%%%%%%%%%%%%%%%%%%%%%%%%%%%%%%%%%%%%%%%%%%%%%%%%%%%%%%%%%%%%%%%%%%%%
% %factor displacements for plotting
% factor=100;
% d3=q3(i+1)*factor;d5=q5(i+1)*factor;d6=q6(i+1)*factor;
% d7=q7(i+1)*factor;d8=q8(i+1)*factor;
%
% x1=0;y1=0;x2=10;y2=0;x3=10; y3=10;x4=0;y4=10;
% x_1=x1+0;y_1=y1+0; x_2=x2+d3;y_2=y2+0;
% x_3=x3+d5;y_3=y3+d6; x_4=x4+d7;y_4=y4+d8;
%
% posx=[x_1; x_2; x_3; x_4 ;0];posy=[y_1; y_2; y_3; y_4;0];

```



```

% recx=[x1;x2;x3;x4;0];recy=[y1;y2;y3;y4;0];
%
% subplot(4,3,9)
% plot(posx,posy,'-ro',recx,recy,'-o');
% xlim([-3,20]);
% ylim([-3,15]);

```

## B.2 Constant Vertical Load (CVL) Master File

```

%%%%%%%%%%%%%%%%%%%%%%%%%%%%%%%%%%%%%%%%%%%%%%%%%%%%%%%%%%%%%%%%%%%%%%%%
%%%%%%%%
%%CONSTANT VERTICAL LOAD (CVL) MASTER FILE
%%DISPLACEMENT-CONTROLLED ANALYSIS
%%RECTANGULAR MEMBRANE USING 4-NODED BI-LINEAR RECTANGULAR ELEMENT
    %BY JEFFREY MITCHELL % JULY 2010 %MATLAB 7.4.0 (R2007a)
%%%%%%%%%%%%%%%%%%%%%%%%%%%%%%%%%%%%%%%%%%%%%%%%%%%%%%%%%%%%%%%%%%%%%%%%
%%%%%%%%
clear all;

%INITIALIZE
MATRICES%%%%%%%%%%%%%%%%%%%%%%%%%%%%%%%%%%%%%%%%%%%%%%%%%%%%%%%%%%%%%%%%%%%%%%%%
I.NE=1; % Number of elements
I.NGDF=8; % Number of Global Degrees of Freedom
I.NLDF=8; % Number of Local Degrees of Freedom
%I.NC = 4; % Number of constraints
I.ESM=zeros(I.NLDF,I.NLDF); %Initialize element stiffness matrix
I.GSM=zeros(I.NGDF,I.NGDF); %Initialize global stiffness matrix
I.GSMs=zeros(I.NGDF,I.NGDF); %Initialize global stiffness matrix for
%steel
I.GSMc=zeros(I.NGDF,I.NGDF); %Initialize global stiffness matrix for
%concr.
I.IG=zeros(I.NE,I.NLDF); %Initialize connectivity matrix
%I.IBC = zeros(NC); %Initialize boundary conditions matrix
I.q = zeros(I.NGDF,1); %Initialize displacement vector
I.IG = [1 2 3 4 5 6 7 8]; %Connectivity Matrix

% ELEMENT
GEOMETRY%%%%%%%%%%%%%%%%%%%%%%%%%%%%%%%%%%%%%%%%%%%%%%%%%%%%%%%%%%%%%%%%%%%%%%%%
%Unit: kip-in
Geo.a=10; Geo.b=10; Geo.t=2; %in

% MATERIAL PROPERTIES
%%%%%%%%%%%%%%%%%%%%%%%%%%%%%%%%%%%%%%%%%%%%%%%%%%%%%%%%%%%%%%%%%%%%%%%%
%1. Concrete
Mat.fcksi=6;
Mat.fcrksi=7.5*sqrt(Mat.fcksi*1000)/1000;

Mat.v=0.0;
Mat.iEc1=4000;
Mat.eo=2*-Mat.fcksi/Mat.iEc1;

```

```

Mat.iEc2=4000;                               Mat.iGc=Mat.iEc1/2/(1+Mat.v);
%ksi
eCrack=Mat.fcrksi/Mat.iEc1;

%2. Steel
Mat.iEs1=30000;                               Mat.iEs2=30000;
Mat.rhos1=0.02;                               Mat.rhos2=0.002;
Mat.fys=60;                                   Mat.eyes=Mat.fys/Mat.iEs1;
Mat.Esh=0.02*Mat.iEs1;

%%%%%%%%%%%%%%%%%%%%%%%%%%%%%%%%%%%%%%%%%%%%%%%%%%%%%%%%%%%%%%%%%%%%%%%%
%ANALYSIS
%%%%%%%%%%%%%%%%%%%%%%%%%%%%%%%%%%%%%%%%%%%%%%%%%%%%%%%%%%%%%%%%%%%%%%%%
P=60; %NUMBER OF INCRIMENTS
N=P+1;
dui=.001; %Applied Displacement (in)
%Initialize Individual Components
ex=zeros(N,1); Sx=zeros(N,1); Scx=zeros(N,1); Ssx=zeros(N,1);
ey=zeros(N,1); Sy=zeros(N,1); Scy=zeros(N,1); Ssy=zeros(N,1);
exy=zeros(N,1); Sxy=zeros(N,1); Scxy=zeros(N,1); Ssxy=zeros(N,1);
q5=zeros(N,1); A5=zeros(N,1); q6=zeros(N,1); A6=zeros(N,1);
q7=zeros(N,1); A7=zeros(N,1); q8=zeros(N,1); A8=zeros(N,1);
q3=zeros(N,1); A3=zeros(N,1);

Sc121=zeros(N,1); Sc122=zeros(N,1); Sc123=zeros(N,1);
e121=zeros(N,1); e122=zeros(N,1); e123=zeros(N,1);

eleffectiv=zeros(N,1); e2effectiv=zeros(N,1);

Ss121=zeros(N,1); Ss122=zeros(N,1); Ss123=zeros(N,1);
TausTauc=zeros(N,1);

q=zeros(I.NGDF,1);

gamma12prev=0;
tau12prev=0;
deltagamma=0;

aaa=zeros(N,1); increment=zeros(N,1);

%initialize values for test, strains and stresses all values at zero
%initialize cracked material properties of concrete
%initialize cracked concrete in both directions

e=[0;0;0];
Sc=[0;0;0];
Ss=[0;0;0];
e12=[0;0;0];

```

```

Sc12= [0;0;0];

E.e1MaxExcr=0.0002768; %Assumed max excursion strains
E.e2MaxExcr=0.0004205;
E.E1extr=2042.8; %Assumed max excursion Secant Moduli
E.E2extr=1326.79;
E.ec1effprev=0;
E.ec2effprev=0;

e1MaxExcr=E.e1MaxExcr;
e2MaxExcr=E.e2MaxExcr;
E1extr=E.E1extr;
E2extr=E.E2extr;

E.exmax=0;
E.eymax=0;
E.exprev=0;
E.eyprev=0;

es.exmax=0;
es.eymax=0;
es.exprev=0;
es.eyprev=0;
fs.fsxprev=0;
fs.fsyprev=0;

ec12.ec123prev=0;
fc12.fc123prev=0;

E.cracktwo=0; %Establishes the active crack

%Make first Guess as Dsmear, the Secant Stiffness Matrix as well as
set the
%crack angle and rotation matrix
%first guess of material stiffness properties will be "SLIP UP"
theta=45; %crack angle
[T]=GetTMatrix(theta); %rotation matrix

Ds=zeros(3,3); %steel stiffness matrix
Ds(1,1)=Mat.iEs1*Mat.rhos1;
Ds(2,2)=Mat.iEs2*Mat.rhos2;

DcCrack=zeros(3,3); %cracked concrete stiffness matrix
DcCrack(1,1)=4000;
DcCrack(1,2)=0;
DcCrack(1,3)=2000;
DcCrack(2,1)=0;
DcCrack(2,2)=4000;
DcCrack(2,3)=0;
DcCrack(3,1)=4705.88;
DcCrack(3,2)=0;
DcCrack(3,3)=2392.16;

```

```

%rotate concrete Dc12 to Dcxy
DcCrackGlobal=inv(T)*DcCrack*(inv(T))';

%Smear the DconcreteCrack and the Dsteel in the Global Direction
Dsmear=Ds+DcCrackGlobal;

Tau_B=0; %initialize shear stress

aprev=0; %initialize convergence values
aold=0;

%Initialize Displacement Increment
du=0;

%%%%%%%%%%%%%%%%%%%%%%%%%%%%%%%%%%%%%%%%%%%%%%%%%%%%%%%%%%%%%%%%%%%%%%%%
%CONTROL VALUES
%%%%%%%%%%%%%%%%%%%%%%%%%%%%%%%%%%%%%%%%%%%%%%%%%%%%%%%%%%%%%%%%%%%%%%%%
limit1=.06; %displacement at which displacement direction reverses
limit=limit1;
V=18; %Constant vertical Load for proportional load vector
cond33=0;

%%

%%%%%%%%%%%%%%%%%%%%%%%%%%%%%%%%%%%%%%%%%%%%%%%%%%%%%%%%%%%%%%%%%%%%%%%%
%%
for i=1:P %incremental displacement loop
%%%%%%%%%%%%%%%%%%%%%%%%%%%%%%%%%%%%%%%%%%%%%%%%%%%%%%%%%%%%%%%%%%%%%%%%
%%
%%
if abs(q(5))>=limit(1) %criteria for direction of loading
    dui=-dui;
end

du=du+dui; %iterate displacement at specified increment

    converge=0; %initializes convergence values for
                %each increment
    count=0;

%%
    while converge==0 %convergence loop
        count=count+1;

%%
        %solve for the actions, strains and displacements
        [A,e,q,a,aold] =
SolveCompressiontestBload(I,Geo,Dsmear,du,V,aold,dui);

```

```

%rotate strains to the crack(1-2) direction
[e12]=straintransformation(e,theta);

%calculate the shear stress Tau^b
deltagamma=e12(3)-ec12.ec123prev;
Tau_B=fc12.fc123prev+Mat.iGc*(deltagamma);

%solve for concrete stresses in 1-2 direction
[cond33,DcCrack,Sc12,E] =
getConcreteStress(e,e12,Mat,E,Tau_B,cond33);

%Solve for Stresses in steel
[Ds,Ss] = getSteelStress(e,es,fs,Mat,dui);

%Rotate concrete stresses to global x-y
[Sc]=stresstransformation(Sc12,-theta);

%Compute total shear stress
Sxsmear=Ss(1)*Mat.rhos1;
Sysmear=Ss(2)*Mat.rhos2;
Sssmear=zeros(3,1);
Sssmear(1)=Sxsmear;
Sssmear(2)=Sysmear;
St=Sssmear+Sc;
[Ss12]=stresstransformation(Sssmear,theta); %steel
%to 1-2 dir
addTau=Ss12(3)+Sc12(3); %steel plus concrete shear
%stress

%rotate concrete Dc12 to Dcxy
DcCrackGlobal=inv(T)*DcCrack*(inv(T))';

%Smear the DconcreteCrack and the Dsteel in the
%Global Direction
Dsmear=Ds+DcCrackGlobal;

% Converge load factor "a"
delta_a=abs(a-aprev);
aprev=a;

if delta_a < .0001 %convergence tolerance
    converge=1;
else
    converge=0;
end
if count == 50 %convergence iteration limit
    converge=1;
end

%%
end %end of convergence loop

```

```

%%
%Track of Strain and Stress Components (Global)
ex(i+1)=e(1);
ey(i+1)=e(2);          %Total Strain and Total Stress
exy(i+1)=e(3);
Sx(i+1)=St(1);
Sy(i+1)=St(2);
Sxy(i+1)=St(3);
%Track of Individual Stresses (Global)
Scx(i+1)=Sc(1);
Scy(i+1)=Sc(2);      %Concrete stresses
Scxy(i+1)=Sc(3);
Ssx(i+1)=Ss(1);
Ssy(i+1)=Ss(2);     %Steel Stresses
Ssxy(i+1)=Ss(3);
%Force Displacement for DOF 5
q3(i+1)=q(3);  %q is displacement, A is force
A3(i+1)=A(3);
q5(i+1)=q(5);
A5(i+1)=A(5);
q6(i+1)=q(6);
A6(i+1)=A(6);
q7(i+1)=q(7);
A7(i+1)=A(7);
q8(i+1)=q(8);
A8(i+1)=A(8);
%Track of 1-2 Direction Concrete Stresses
Sc121(i+1)=Sc12(1);
Sc122(i+1)=Sc12(2);
Sc123(i+1)=Sc12(3);
%Track of 1-2 direction strains
e121(i+1)=e12(1);
e122(i+1)=e12(2);
e123(i+1)=e12(3);
%track of epsilon effective
eleffectiv(i+1)=E.ec1eff;
e2effectiv(i+1)=E.ec2eff;
%max strains
es.exmax=max(ex);
es.eymax=max(ey);
%load vector factor "a"
aaa(i+1)=a;
incriment(i+1)=du;
%rotated steel
Ss121(i+1)=Ss12(1);
Ss122(i+1)=Ss12(2);
Ss123(i+1)=Ss12(3);
TausTauc(i+1)=addTau;
%keep track of last converged strain and stress values
es.exprev=ex(i+1);
es.eyprev=ey(i+1);
fs.fsxprev=Ssx(i+1);

```

```

fs.fsyprev=Ssy(i+1);

ec12.ec123prev=e123(i+1);
fc12.fc123prev=Sc123(i+1);

E.ec1effprev=E.ec1eff;
E.ec2effprev=E.ec2eff;

%max excursion effective tensile strain
%concrete tension stiffening curve
eff1test=max(e1effectiv,E.e1MaxExcr);
E.e1MaxExcr=max(eff1test);
eff2test=max(e2effectiv,E.e2MaxExcr);
E.e2MaxExcr=max(eff2test);

E.E1extr=(Mat.fcrksi/(sqrt(1+200*E.e1MaxExcr)))/E.e1MaxExcr;
E.E2extr=(Mat.fcrksi/(sqrt(1+200*E.e2MaxExcr)))/E.e2MaxExcr;

% %%%%%%%%%%%
% %%PLOT SHAPE
% %%%%%%%%%%%
% %factor displacements for plotting
%
% factor=100;
% d3=q3(i+1)*factor;d5=q5(i+1)*factor;d6=q6(i+1)*factor;
% d7=q7(i+1)*factor;d8=q8(i+1)*factor;
%
% x1=0;y1=0;x2=10;y2=0;x3=10; y3=10;x4=0;y4=10;
% x_1=x1+0;y_1=y1+0; x_2=x2+d3;y_2=y2+0;
% x_3=x3+d5;y_3=y3+d6; x_4=x4+d7;y_4=y4+d8;
%
% posx=[x_1; x_2; x_3; x_4 ;0];posy=[y_1; y_2; y_3; y_4;0];
% recx=[x1;x2;x3;x4;0];recy=[y1;y2;y3;y4;0];
%
% subplot(4,3,9)
% plot(posx,posy,'-ro',recx,recy,'-o');
% xlim([-3,20]);
% ylim([-3,15]);

end %end of incremental displacement loop

%%%%%%%%%%
%PLOTS
%%%%%%%%%%
subplot(4,3,1)
plot(e121,Sc121,'.-')
xlabel('\epsilon_1')
ylabel('\sigma_c_1(ksi)')
grid on;
hold on;

subplot(4,3,2)

```

```

plot (e122,Sc122, '-.-')
xlabel ('\epsilon_2')
ylabel ('\sigma_c_2 (ksi)')
grid on;
hold on;

subplot(4,3,3)
plot (q7,A7, '-.-',q5,A5, '-.-')
xlabel ('Displ q7 & q5')
ylabel ('F A7 & A5')
grid On;
hold on;

subplot(4,3,4)
plot (q6,A6, '-.-',q8,A8, '-.-')
xlabel ('Displ q6 & q8')
ylabel ('F A6 & A8')
grid on;
hold on;

subplot(4,3,5)
plot (ey,Scy, '-.-')
hold on
grid on
xlabel ('\epsilon_y')
ylabel ('\sigma_c_y')

subplot(4,3,6)
plot (exy,Scxy, '-.-')
hold on
grid on
xlabel ('\gamma_x_y')
ylabel ('\tau_c_x_y')

subplot(4,3,7)
plot (e123,Sc123, '-.-')
xlabel ('\gamma_1_2')
ylabel ('\tau_c_1_2')
grid on;
hold on;

%%%%%%%%%%%%%%%%%%%%%%%%%%%%%%%%%%%%%%%%%%%%%%%%%%%%%%%%%%%%%%%%%%%%%%%%
%PLOT STEEL
%%%%%%%%%%%%%%%%%%%%%%%%%%%%%%%%%%%%%%%%%%%%%%%%%%%%%%%%%%%%%%%%%%%%%%%%

% figure
subplot(4,3,8)
plot (ex,Ssx, '-.-')
hold on
grid on
xlabel ('\epsilon_x')
ylabel ('\sigma_s_t_x')

```



```

%%%%%%%%%%%%%%%%%%%%%%%%%%%%%%%%%%%%%%%%%%%%%%%%%%%%%%%%%%%%%%%%%%%%%%%%
subplot(4,3,10)
plot(incriment,aaa,'.-');
grid on;
hold on;
xlabel('du')
ylabel('a')

subplot(4,3,11)
plot(ex,Scx,'.-');
grid on;
hold on;
xlabel('\epsilon_x')
ylabel('\sigma_c_x')

subplot(4,3,12)
plot(q3,A3,'.-');
grid on;
hold on;
xlabel('q3')
ylabel('A3')

subplot(4,3,9)
plot(ey,Ssy,'.-');
grid on;
hold on;
xlabel('\epsilon_y')
ylabel('\sigma_s_y')

%%%%%%%%%%%%%%%%%%%%%%%%%%%%%%%%%%%%%%%%%%%%%%%%%%%%%%%%%%%%%%%%%%%%%%%%
%PLOT FACTORED DEFORMED SHAPE
%%%%%%%%%%%%%%%%%%%%%%%%%%%%%%%%%%%%%%%%%%%%%%%%%%%%%%%%%%%%%%%%%%%%%%%%
% figure
% for j=1:P
%
%   factor=100;
%   d3=q3(j+1)*factor;d5=q5(j+1)*factor;d6=q6(j+1)*factor;
%   d7=q7(j+1)*factor;d8=q8(j+1)*factor;
%
%   x1=0;y1=0;x2=10;y2=0;x3=10; y3=10;x4=0;y4=10;
%   x_1=x1+0;y_1=y1+0; x_2=x2+d3;y_2=y2+0;
%   x_3=x3+d5;y_3=y3+d6; x_4=x4+d7;y_4=y4+d8;
%
%   posx=[x_1; x_2; x_3; x_4 ;0];posy=[y_1; y_2; y_3; y_4;0];
%   recx=[x1;x2;x3;x4;0];recy=[y1;y2;y3;y4;0];
%
%
%   plot(posx,posy,'-ro',recx,recy,'-o');
%   hold on;
%   xlim([-3,20]);

```

```

%      ylim([-3,15]);
% end

%%%%%%%%%%%%%%%%%%%%%%%%%%%%%%%%%%%%%%%%%%%%%%%%%%%%%%%%%%%%%%%%%%%%%%%%
%Various Plots
%%%%%%%%%%%%%%%%%%%%%%%%%%%%%%%%%%%%%%%%%%%%%%%%%%%%%%%%%%%%%%%%%%%%%%%%
% figure
% plot(e123,e1effectiv,'.-')
% grid on;
% xlabel('Shear Strain, \gamma_1_2')
% ylabel('Normal Strain, \epsilon_1')

% plot(e123,Sc123,'.-')
% xlabel('Shear Strain, \gamma_1_2')
% ylabel('Shear Stress, \tau_c_1_2')
% grid on;

% plot(e1effectiv,Sc121,'.-')
% xlabel('Effective Strain, \epsilon_1')
% ylabel('Concrete Normal Stress, \sigma_c_1 (ksi)')
% grid on;

% plot(ex,Ssx,'.-')
% grid on
% xlabel('\epsilon_x')
% ylabel('\sigma_s_t_x')

% plot(e121,Sc121,'.-')
% xlabel('\epsilon_1')
% ylabel('\sigma_c_1(ksi)')
% grid on;
%
% plot(incriment,e1effectiv,'.-');
% grid on;
% xlabel('du')
% ylabel('^e\epsilon_1')

% plot(e123,Ss123,'.-',e123,Sc123,'s-',e123,TausTauc,'*-')
% grid on;
% xlabel('Shear Strain, \gamma_1_2')
% ylabel('Shear Stress, \tau_1_2')
% legend('\tau_s (1-2 dir)', '\tau_c (1-2 dir)', '\tau_s + \tau_c (1-2
dir)')

```

## B.3 Modified Newton Raphson Method (MNRM)

### Master File

```

%%%%%%%%%%%%%%%%%%%%%%%%%%%%%%%%%%%%%%%%%%%%%%%%%%%%%%%%%%%%%%%%%%%%%%%%
%%%%%%%%
%%%MODIFIED NEWTON RAPHSON METHOD (MNRM) MASTER FILE
%%%DISPLACEMENT-CONTROLLED ANALYSIS
%%%RECTANGULAR MEMBRANE USING 4-NODED BI-LINEAR RECTANGULAR ELEMENT
      %BY JEFFREY MITCHELL % JULY 2010 %MATLAB 7.4.0 (R2007a)
%%%%%%%%%%%%%%%%%%%%%%%%%%%%%%%%%%%%%%%%%%%%%%%%%%%%%%%%%%%%%%%%%%%%%%%%
%%%%%%%%
clear all;

%INITIALIZE
MATRICES%%%%%%%%%%%%%%%%%%%%%%%%%%%%%%%%%%%%%%%%%%%%%%%%%%%%%%%%%%%%%%%%%%%%%%%%
I.NE=1; % Number of elements
I.NGDF=8; % Number of Global Degrees of Freedom
I.NLDF=8; % Number of Local Degrees of Freedom
%I.NC = 4; % Number of constraints
I.ESM=zeros(I.NLDF,I.NLDF); %Initialize element stiffness matrix
I.GSM=zeros(I.NGDF,I.NGDF); %Initialize global stiffness matrix
I.GSMs=zeros(I.NGDF,I.NGDF); %Initialize global stiffness matrix for
%steel
I.GSMc=zeros(I.NGDF,I.NGDF); %Initialize global stiffness matrix for
%concr.
I.IG=zeros(I.NE,I.NLDF); %Initialize connectivity matrix
%I.IBC = zeros(NC); %Initialize boundary conditions matrix
I.q = zeros(I.NGDF,1); %Initialize displacement vector
I.IG = [1 2 3 4 5 6 7 8]; %Connectivity Matrix

% ELEMENT
GEOMETRY%%%%%%%%%%%%%%%%%%%%%%%%%%%%%%%%%%%%%%%%%%%%%%%%%%%%%%%%%%%%%%%%%%%%%%%%
%Unit: kip-in
Geo.a=10; Geo.b=10; Geo.t=2; %in

% MATERIAL PROPERTIES
%%%%%%%%%%%%%%%%%%%%%%%%%%%%%%%%%%%%%%%%%%%%%%%%%%%%%%%%%%%%%%%%%%%%%%%%
%1. Concrete
Mat.fcksi=6;
Mat.fcrksi=7.5*sqrt(Mat.fcksi*1000)/1000;

Mat.v=0.0;
Mat.iEc1=4000; Mat.eo=2*-Mat.fcksi/Mat.iEc1;
Mat.iEc2=4000; Mat.iGc=Mat.iEc1/2/(1+Mat.v);
%ksi
eCrack=Mat.fcrksi/Mat.iEc1;

%2. Steel
Mat.iEs1=30000; Mat.iEs2=30000;
Mat.rhos1=0.02; Mat.rhos2=0.002;

```

```

Mat.fys=60;                               Mat.eyes=Mat.fys/Mat.iEs1;
Mat.Esh=0.02*Mat.iEs1;

%%%%%%%%%%%%%%%%%%%%%%%%%%%%%%%%%%%%%%%%%%%%%%%%%%%%%%%%%%%%%%%%%%%%%%%%
%%%%%%%%
%ANALYSIS
%%%%%%%%%%%%%%%%%%%%%%%%%%%%%%%%%%%%%%%%%%%%%%%%%%%%%%%%%%%%%%%%%%%%%%%%
%%%%%%%%%%%%%%%%%%%%%%%%%%%%%%%%%%%%%%%%%%%%%%%%%%%%%%%%%%%%%%%%%%%%%%%%
%%%%%%%%
P=60;   %number of increments
N=P+1;
dui=.001; %Applied Displacement (in)
%Initialize Individual Components
ex=zeros(N,1);  Sx=zeros(N,1); Scx=zeros(N,1); Ssx=zeros(N,1);
ey=zeros(N,1);  Sy=zeros(N,1); Scy=zeros(N,1); Ssy=zeros(N,1);
exy=zeros(N,1); Sxy=zeros(N,1); Scxy=zeros(N,1); Ssxy=zeros(N,1);
q5=zeros(N,1);  A5=zeros(N,1); q6=zeros(N,1); A6=zeros(N,1);
q7=zeros(N,1);  A7=zeros(N,1); q8=zeros(N,1); A8=zeros(N,1);
q3=zeros(N,1);  A3=zeros(N,1);

Sc121=zeros(N,1); Sc122=zeros(N,1); Sc123=zeros(N,1);
e121=zeros(N,1); e122=zeros(N,1); e123=zeros(N,1);

eleffectiv=zeros(N,1); e2effectiv=zeros(N,1);

Ss121=zeros(N,1); Ss122=zeros(N,1); Ss123=zeros(N,1);
TausTauc=zeros(N,1);

q=zeros(I.NGDF,1);

gamma12prev=0;
tau12prev=0;
deltagamma=0;

aaa=zeros(N,1); increment=zeros(N,1);

%initialize values for test, strains and stresses all values at zero
%initialize cracked material properties of concrete
%initialize cracked concrete in both directions

e=[0;0;0];
Sc=[0;0;0];
Ss=[0;0;0];
e12=[0;0;0];
Sc12=[0;0;0];

E.e1MaxExcr=0.0002768; %Assumed max excursion strains
E.e2MaxExcr=0.0004205;
E.E1extr=2042.8;      %Assumed max excursion Secant Moduli
E.E2extr=1326.79;
E.ecleffprev=0;

```

```

E.ec2effprev=0;

e1MaxExcr=E.e1MaxExcr;
e2MaxExcr=E.e2MaxExcr;
E1extr=E.E1extr;
E2extr=E.E2extr;

E.exmax=0;
E.eymax=0;
E.exprev=0;
E.eyprev=0;

es.exmax=0;
es.eymax=0;
es.exprev=0;
es.eyprev=0;
fs.fsxprev=0;
fs.fsyprev=0;

ec12.ec123prev=0;
fc12.fc123prev=0;

E.cracktwo=0; %establishes the active crack

%Make first Guess as Dsmear, the Secant Stiffness Matrix as well as
%set the
%crack angle and rotation matrix
%first guess of material stiffness properties will be "NO SLIP"
theta=45; %crack angle
[T]=GetTMatrix(theta); %rotation matrix

Ds=zeros(3,3); %steel stiffness matrix
Ds(1,1)=Mat.iEs1*Mat.rhos1;
Ds(2,2)=Mat.iEs2*Mat.rhos2;

DcCrack=zeros(3,3); %crack concrete stiffness matrix
DcCrack(1,1)=4000;
DcCrack(1,2)=0;
DcCrack(1,3)=2000;
DcCrack(2,1)=0;
DcCrack(2,2)=4000;
DcCrack(2,3)=0;
DcCrack(3,1)=0;
DcCrack(3,2)=0;
DcCrack(3,3)=2000;

%rotate concrete Dc12 to Dcxy
DcCrackGlobal=inv(T)*DcCrack*(inv(T))';

%Smear the DconcreteCrack and the Dsteel in the Global Direction
Dsmear=Ds+DcCrackGlobal;

```

```

Tau_B=0; %initialize shear stress

aprev=0; %initialize convergence values
aold=0;
%Initialize Displacement Increment
du=0;
%%%%%%%%%%%%%%%%%%%%%%%%%%%%%%%%%%%%%%%%%%%%%%%%%%%%%%%%%%%%%%%%%%%%%%%%
%CONTROL VALUES
%%%%%%%%%%%%%%%%%%%%%%%%%%%%%%%%%%%%%%%%%%%%%%%%%%%%%%%%%%%%%%%%%%%%%%%%
limit1=.06; %displacement at which displacement direction reverses
limit=limit1;
V=18; %Constant Vertical Load for proportional load vector
cond33=0;

%%
%%%%%%%%%%%%%%%%%%%%%%%%%%%%%%%%%%%%%%%%%%%%%%%%%%%%%%%%%%%%%%%%%%%%%%%%
%%
for i=1:P %incremental displacement loop
%%%%%%%%%%%%%%%%%%%%%%%%%%%%%%%%%%%%%%%%%%%%%%%%%%%%%%%%%%%%%%%%%%%%%%%%
%%
if abs(q(5))>=limit(1) %criteria for direction of loading
    dui=-dui;
end

du=du+dui; %iterate displacement at specified increment

    converge=0; %initialize convergence value for
                %each increment
    count=0;

%%
    a=0;
    %solve for the actions, strains and displacements
    [A,e,q,a] =
SolveCompressiontestBload(I,Geo,Dsmear,du,V,dui);
    atrack=a;

    %rotate strain to the 1-2(crack) direction
    [e12]=straintransformation(e,theta);

    %calculate the shear stress Tau^b
    deltagamma=e12(3)-ec12.ec123prev;
    Tau_B=fc12.fc123prev+Mat.iGc*(deltagamma);

    %solve for concrete stresses in 1-2 direction
    [Dc,Sc12,E] = getCStressTest(e,e12,Mat,E,Tau_B);

    %Solve for Stresses in steel
    [Ds,ss] = getSStressTest(e,es,fs,Mat,dui);

```

```

%rotate concrete stresses to global x-y
[Sc]=stresstransformation(Sc12,-theta);

%Compute total shear stress
Sxsmeared=Ss(1)*Mat.rhos1;
Sysmeared=Ss(2)*Mat.rhos2;
Sssmeared=zeros(3,1);
Sssmeared(1)=Sxsmeared;
Sssmeared(2)=Sysmeared;
St=Sssmeared+Sc;
[Ss12]=stresstransformation(Sssmeared,theta); %steel
%to 1-2 dir
addTau=Ss12(3)+Sc12(3); %steel plus concrete shear
%stress

%rotate concrete Dc12 to Dcxy
DcCrackGlobal=inv(T)*DcCrack*(inv(T))';

%Smear the DconcreteCrack and the Dsteel in the
%Global Direction
Dsmear=Ds+DcCrackGlobal;

Q=q; %point 1, initial estimate of displacements

%solve for forces based on state of stress
[A0] = SolveStressEquil(St,Geo);

[KK,BMAT] = getKmatrix(Geo,I,Dsmear);

%solve for deltaA
Fs=[-1;-1;-1;1;1;1;1;-1];
Bbar=[0;0;0;0;0;-V;0;-V];
DeltaA=(A0-Bbar)-A0(5)*Fs;
DeltaAprev=DeltaA;

%%
while converge == 0 %start of convergence loop
%%

    %solve for deltaD Point 2
    [DeltaD,DeltaDp] = getDeltaD (KK,DeltaA);

    %compute new total displ
    QA=Q-DeltaD;

    %enforce PDOF and compute change in displacement
    [A,e,q,a] =
SolveCompressiontestBload(I,Geo,Dsmear,DeltaDp,0,dui);

```

```

%compute new set of displ with correct PDOF
QB=QA+q;

%compute new strains
e=BMAT*QB;

%reset value for initial estimate of
%displacement
Q=QB;

%rotate strain to the 1-2(crack) direction
[e12]=straintransformation(e,theta);

%calculate shear stress
deltagamma=e12(3)-ec12.ec123prev;
Tau_B=fc12.fc123prev+Mat.iGc*(deltagamma);

%solve for concrete stresses in 1-2 direction
[DcCrack,Sc12,E] =
getCStressTest(e,e12,Mat,E,Tau_B);

%curves
%Solve for Stresses in steel using basic yield
[Ds,ss] = getSStressTest(e,es,fs,Mat,dui);

%rotate concrete stresses to global x-y
[Sc]=stresstransformation(Sc12,-theta);

%Compute total shear stress
Sxsmeared=Ss(1)*Mat.rhos1;
Sysmeared=Ss(2)*Mat.rhos2;
Sssmeared=zeros(3,1);
Sssmeared(1)=Sxsmeared;
Sssmeared(2)=Sysmeared;
St=Sssmeared+Sc;
[ss12]=stresstransformation(Sssmeared,theta);
addTau=ss12(3)+Sc12(3);

%rotate concrete Dc12 to Dcxy
DcCrackGlobal=inv(T)*DcCrack*(inv(T))';

%Smear the DconcreteCrack and the Dsteel in the
%Global Direction
Dsmear=Ds+DcCrackGlobal;

%calculate forces from state of stress
[A0] = SolveStressEquil(St,Geo);

%get new global stiffness matrix
[KK,BMAT] = getKmatrix(Geo,I,Dsmear);

```



```

        %solve for deltaA
        Bbar=[0;0;0;0;0;-V;0;-V];
        DeltaA=(A0-Bbar)-A0(5)*Fs;
        DeltaA(2)=0;
        DeltaA(4)=0;

        convTest=norm(DeltaA);
        if convTest < .00001 %convergence tolerance
            converge=1;
        end

        %Converged Displacements and Forces
        q=Q;
        A=KK*q;

        count=count+1;

        if count > 30 %convergence iteration limit
            converge=1;
        end
        %
%%
        end %end of convergence loop
%%

        %Track of Strain and Stress Components (Global)
        ex(i+1)=e(1);
        ey(i+1)=e(2); %Total Strain and Total Stress
        exy(i+1)=e(3);
        Sx(i+1)=St(1);
        Sy(i+1)=St(2);
        Sxy(i+1)=St(3);
        %Track of Individual Stresses (Global)
        Scx(i+1)=Sc(1);
        Scy(i+1)=Sc(2); %Concrete stresses
        Scxy(i+1)=Sc(3);
        Ssx(i+1)=Ss(1);
        Ssy(i+1)=Ss(2); %Steel Stresses
        Ssxy(i+1)=Ss(3);
        %Force Displacement for DOF 5
        q3(i+1)=q(3); %q is displacement, A is force
        A3(i+1)=A(3);
        q5(i+1)=q(5);
        A5(i+1)=A(5);
        q6(i+1)=q(6);
        A6(i+1)=A(6);
        q7(i+1)=q(7);
        A7(i+1)=A(7);
        q8(i+1)=q(8);
        A8(i+1)=A(8);
        %Track of 1-2 Direction Concrete Stresses
        Sc121(i+1)=Sc12(1);

```

```

Sc122(i+1)=Sc12(2);
Sc123(i+1)=Sc12(3);
%Track of 1-2 direction strains
e121(i+1)=e12(1);
e122(i+1)=e12(2);
e123(i+1)=e12(3);
%track of epsilon effective
eleffectiv(i+1)=E.ec1eff;
e2effectiv(i+1)=E.ec2eff;
%max strains
es.exmax=max(ex);
es.eymax=max(ey);
%load vector factor "a"
aaa(i+1)=atrack;
incriment(i+1)=du;
%rotated steel stresses
Ss121(i+1)=Ss12(1);
Ss122(i+1)=Ss12(2);
Ss123(i+1)=Ss12(3);
TausTauc(i+1)=addTau; %total shear stress (1-2 dir)

%keep track of last converged strain and stress values
es.exprev=ex(i+1);
es.eyprev=ey(i+1);
fs.fsxprev=Ssx(i+1);
fs.fsyprev=Ssy(i+1);

ec12.ec123prev=e123(i+1);
fc12.fc123prev=Sc123(i+1);

E.ec1effprev=E.ec1eff;
E.ec2effprev=E.ec2eff;

%max excursion effective tensile strain
%concrete tension stiffening curve
eff1test=max(eleffectiv,E.e1MaxExcr);
E.e1MaxExcr=max(eff1test);
eff2test=max(e2effectiv,E.e2MaxExcr);
E.e2MaxExcr=max(eff2test);

E.E1extr=(Mat.fcrksi/(sqrt(1+200*E.e1MaxExcr)))/E.e1MaxExcr;
E.E2extr=(Mat.fcrksi/(sqrt(1+200*E.e2MaxExcr)))/E.e2MaxExcr;

% %%%%%%%%%%%
% %%%PLOT SHAPE
% %%%%%%%%%%%
% %factor displacements for plotting
%
% factor=100;
% d3=q3(i+1)*factor;d5=q5(i+1)*factor;d6=q6(i+1)*factor;
% d7=q7(i+1)*factor;d8=q8(i+1)*factor;
%

```

```

% x1=0;y1=0;x2=10;y2=0;x3=10; y3=10;x4=0;y4=10;
% x_1=x1+0;y_1=y1+0; x_2=x2+d3;y_2=y2+0;
% x_3=x3+d5;y_3=y3+d6; x_4=x4+d7;y_4=y4+d8;
%
% posx=[x_1; x_2; x_3; x_4 ;0];posy=[y_1; y_2; y_3; y_4;0];
% recx=[x1;x2;x3;x4;0];recy=[y1;y2;y3;y4;0];
%
% subplot(4,3,9)
% plot(posx,posy,'-ro',recx,recy,'-o');
% xlim([-3,20]);
% ylim([-3,15]);

end %end of incremental displacement loop

%%%%%%%%%%%%%%%%%%%%%%%%%%%%%%%%%%%%%%%%%%%%%%%%%%%%%%%%%%%%%%%%%%%%%%%%
%PLOTS
%%%%%%%%%%%%%%%%%%%%%%%%%%%%%%%%%%%%%%%%%%%%%%%%%%%%%%%%%%%%%%%%%%%%%%%%
figure
subplot(4,3,1)
plot(e121,Sc121,'.-')
xlabel('\epsilon_1')
ylabel('\sigma_c_1(ksi)')
grid on;
hold on;

subplot(4,3,2)
plot(e122,Sc122,'.-')
xlabel('\epsilon_2')
ylabel('\sigma_c_2 (ksi)')
grid on;
hold on;

subplot(4,3,3)
plot(q7,A7,'.-',q5,A5,'.-')
xlabel('Displ q7 & q5')
ylabel('F A7 & A5')
grid On;
hold on;

subplot(4,3,4)
plot(q6,A6,'.-',q8,A8,'.-')
xlabel('Displ q6 & q8')
ylabel('F A6 & A8')
grid on;
hold on;

subplot(4,3,5)
plot(ey,Scy,'.-')
hold on
grid on
xlabel('\epsilon_y')
ylabel('\sigma_c_y')

```

```

subplot(4,3,6)
plot(exy,Scxy,'.-')
hold on
grid on
xlabel('\gamma_x_y')
ylabel('\tau_c_x_y')

subplot(4,3,7)
plot(e123,Sc123,'.-')
xlabel('\gamma_1_2')
ylabel('\tau_c_1_2')
grid on;
hold on;

%%%%%%%%%%%%%%%%%%%%%%%%%%%%%%%%%%%%%%%%%%%%%%%%%%%%%%%%%%%%%%%%%%%%%%%%
%PLOT STEEL
%%%%%%%%%%%%%%%%%%%%%%%%%%%%%%%%%%%%%%%%%%%%%%%%%%%%%%%%%%%%%%%%%%%%%%%%

% figure
subplot(4,3,8)
plot(ex,Ssx,'.-')
hold on
grid on
xlabel('\epsilon_x')
ylabel('\sigma_s_t_x')

subplot(4,3,10)
plot(incriment,aaa,'.-');
grid on;
hold on;
xlabel('du')
ylabel('a')

subplot(4,3,11)
plot(ex,Scx,'.-');
grid on;
hold on;
xlabel('\epsilon_x')
ylabel('\sigma_c_x')

subplot(4,3,12)
plot(q3,A3,'.-');
grid on;
hold on;
xlabel('q3')
ylabel('A3')

subplot(4,3,9)
plot(ey,Ssy,'.-');
grid on;
hold on;

```

```

xlabel('\epsilon_y')
ylabel('\sigma_s_y')

%%%%%%%%%%%%%%%%%%%%%%%%%%%%%%%%%%%%%%%%%%%%%%%%%%%%%%%%%%%%%%%%%%%%%%%%
%PLOT FACTORED DEFORMED SHAPE
%%%%%%%%%%%%%%%%%%%%%%%%%%%%%%%%%%%%%%%%%%%%%%%%%%%%%%%%%%%%%%%%%%%%%%%%
%figure
% for j=1:P
%
%     factor=100;
%     d3=q3(j+1)*factor;d5=q5(j+1)*factor;d6=q6(j+1)*factor;
%     d7=q7(j+1)*factor;d8=q8(j+1)*factor;
%
%     x1=0;y1=0;x2=10;y2=0;x3=10; y3=10;x4=0;y4=10;
%     x_1=x1+0;y_1=y1+0; x_2=x2+d3;y_2=y2+0;
%     x_3=x3+d5;y_3=y3+d6; x_4=x4+d7;y_4=y4+d8;
%
%     posx=[x_1; x_2; x_3; x_4 ;0];posy=[y_1; y_2; y_3; y_4;0];
%     recx=[x1;x2;x3;x4;0];recy=[y1;y2;y3;y4;0];
%
%
%     plot(posx,posy,'-ro',recx,recy,'-o');
%     hold on;
%     xlim([-3,20]);
%     ylim([-3,15]);
% end

%%%%%%%%%%%%%%%%%%%%%%%%%%%%%%%%%%%%%%%%%%%%%%%%%%%%%%%%%%%%%%%%%%%%%%%%
%Various Plots
%%%%%%%%%%%%%%%%%%%%%%%%%%%%%%%%%%%%%%%%%%%%%%%%%%%%%%%%%%%%%%%%%%%%%%%%
%figure
% plot(e123,e121,'.-')
% grid on;
% xlabel('Shear Strain, \gamma_1_2')
% ylabel('Normal Strain, \epsilon_1')

% hold on;
% plot(e123,Sc123,'r.-')
% xlabel('Shear Strain, \gamma_1_2')
% ylabel('Shear Stress, \tau_c_1_2')
% grid on;

% plot(ex,Ssx,'.-')
% grid on
% xlabel('\epsilon_x')
% ylabel('\sigma_s_t_x')

% plot(e121,Sc121,'.-')
% xlabel('\epsilon_1')
% ylabel('\sigma_c_1(ksi)')
% grid on;

```

```

% plot(e1effectiv,Sc121,'.-')
% xlabel('Effective Strain, \epsilon_1')
% ylabel('Concrete Normal Stress, \sigma_c_1 (ksi)')
% grid on;

% plot(e123,Sc121,'.-')
% xlabel('\epsilon_1')
% ylabel('\sigma_c_1(ksi)')
% grid on;

% plot(incriment,aaa,'.-');
% grid on;
% xlabel('du')
% ylabel('a')

% plot(e123,Ss123,'.-',e123,Sc123,'s-',e123,TausTauc,'*-')
% grid on;
% xlabel('Shear Strain, \gamma_1_2')
% ylabel('Shear Stress, \tau_1_2')
% legend('\tau_s (1-2 dir)', '\tau_c (1-2 dir)', '\tau_s + \tau_c (1-2
dir)')

```

## B.4 Crack Strain Separated (CSS) Master File

```

%%%%%%%%%%%%%%%%%%%%%%%%%%%%%%%%%%%%%%%%%%%%%%%%%%%%%%%%%%%%%%%%%%%%%%%%
%%%%%%%%
%%CRACK STRAIN SEPARATED (CSS)MASTER FILE
%%DISPLACEMENT-CONTROLLED ANALYSIS
%%RECTANGULAR MEMBRANE USING 4-NODED BI-LINEAR RECTANGULAR ELEMENT
    %BY JEFFREY MITCHELL % JULY 2010 %MATLAB 7.4.0 (R2007a)
%%%%%%%%%%%%%%%%%%%%%%%%%%%%%%%%%%%%%%%%%%%%%%%%%%%%%%%%%%%%%%%%%%%%%%%%
%%%%%%%%
clear all;

%INITIALIZE
MATRICES%%%%%%%%%%%%%%%%%%%%%%%%%%%%%%%%%%%%%%%%%%%%%%%%%%%%%%%%%%%%%%%%%%%%%%%%
I.NE=1; % Number of elements
I.NGDF=8; % Number of Global Degrees of Freedom
I.NLDF=8; % Number of Local Degrees of Freedom
%I.NC = 4; % Number of constraints
I.ESM=zeros(I.NLDF,I.NLDF); %Initialize element stiffness matrix
I.GSM=zeros(I.NGDF,I.NGDF); %Initialize global stiffness matrix
I.GSMs=zeros(I.NGDF,I.NGDF); %Initialize global stiffness matrix for
%steel
I.GSMc=zeros(I.NGDF,I.NGDF); %Initialize global stiffness matrix for
%concr.
I.IG=zeros(I.NE,I.NLDF); %Initialize connectivity matrix

```

```

%I.IBC = zeros(NC); %Initialize boundary conditions matrix
I.q = zeros(I.NGDF,1); %Initialize displacement vector
I.IG = [1 2 3 4 5 6 7 8]; %Connectivity Matrix

% ELEMENT
GEOMETRY%%%%%%%%%%%%%%%%%%%%%%%%%%%%%%%%%%%%%%%%%%%%%%%%%%%%%%%%%%%%%%%%%%%%%%%%%%
%Unit: kip-in
Geo.a=10; Geo.b=10; Geo.t=2; %in

% MATERIAL PROPERTIES
%%%%%%%%%%%%%%%%%%%%%%%%%%%%%%%%%%%%%%%%%%%%%%%%%%%%%%%%%%%%%%%%%%%%%%%%%%
%1. Concrete
Mat.fcksi=6;
Mat.fcrksi=7.5*sqrt(Mat.fcksi*1000)/1000;

Mat.v=0.0;
Mat.iEc1=4000;
Mat.iEc2=4000;
%ksi
eCrack=Mat.fcrksi/Mat.iEc1;

Mat.eo=2*-Mat.fcksi/Mat.iEc1;
Mat.iGc=Mat.iEc1/2/(1+Mat.v);

%2. Steel
Mat.iEs1=30000;
Mat.rhos1=0.02;
Mat.fys=60;
Mat.Esh=0.02*Mat.iEs1;

Mat.iEs2=30000;
Mat.rhos2=0.002;
Mat.eyS=Mat.fys/Mat.iEs1;

%%%%%%%%%%%%%%%%%%%%%%%%%%%%%%%%%%%%%%%%%%%%%%%%%%%%%%%%%%%%%%%%%%%%%%%%%%
%ANALYSIS
%%%%%%%%%%%%%%%%%%%%%%%%%%%%%%%%%%%%%%%%%%%%%%%%%%%%%%%%%%%%%%%%%%%%%%%%%%
%NUMBER OF INCRIMENTS
P=60;
N=P+1;
dui=.001; %Applied Displacement (in)
%Initialize Individual Components
ex=zeros(N,1); Sx=zeros(N,1); Scx=zeros(N,1); Ssx=zeros(N,1);
ey=zeros(N,1); Sy=zeros(N,1); Scy=zeros(N,1); Ssy=zeros(N,1);
exy=zeros(N,1); Sxy=zeros(N,1); Scxy=zeros(N,1); Ssxy=zeros(N,1);
q5=zeros(N,1); A5=zeros(N,1); q6=zeros(N,1); A6=zeros(N,1);
q7=zeros(N,1); A7=zeros(N,1); q8=zeros(N,1); A8=zeros(N,1);
q3=zeros(N,1); A3=zeros(N,1);

Sc121=zeros(N,1); Sc122=zeros(N,1); Sc123=zeros(N,1);
e121=zeros(N,1); e122=zeros(N,1); e123=zeros(N,1);

eleffectiv=zeros(N,1); e2effectiv=zeros(N,1);

Ss121=zeros(N,1); Ss122=zeros(N,1); Ss123=zeros(N,1);
TausTauc=zeros(N,1);

```

```

e123cr1=zeros(N,1); e123cr2=zeros(N,1);
crackstrain=zeros(N,1); concstrain=zeros(N,1);
cshearstress=zeros(N,1);
crackshearstress=zeros(N,1);

q=zeros(I.NGDF,1);

gamma12prev=0;
tau12prev=0;
deltagamma=0;

aaa=zeros(N,1); increment=zeros(N,1);

%initialize values for test, strains and stresses all values at zero
%initialize cracked material properties of concrete
%initialize cracked concrete in both directions

e=[0;0;0];
Sc=[0;0;0];
Ss=[0;0;0];
e12=[0;0;0];
Sc12=[0;0;0];

E.e1MaxExcr=0.0002768; %Assumed max excursion strains
E.e2MaxExcr=0.0004205;
E.E1extr=2042.8; %Assumed max excursion Secant Moduli
E.E2extr=1326.79;
E.ec1effprev=0;
E.ec2effprev=0;

e1MaxExcr=E.e1MaxExcr;
e2MaxExcr=E.e2MaxExcr;
E1extr=E.E1extr;
E2extr=E.E2extr;

E.exmax=0;
E.eymax=0;
E.exprev=0;
E.eyprev=0;

es.exmax=0;
es.eymax=0;
es.exprev=0;
es.eyprev=0;
fs.fsxprev=0;
fs.fsyprev=0;

ec12.ec123prev=0;
fc12.fc123prev=0;

net.e123cr1old=0; %net cracking strains

```



```

net.e123cr2old=0;
net.e123net1=0;
net.e123net2=0;
net.e123cr1=0;
net.e123cr2=0;

E.cracktwo=1; %establishes active crack number

%Make first Guess as Dsmear, the Secant Stiffness Matrix as well as
%set the crack angle and rotation matrix
%first guess of material stiffness properties will be "NO SLIP"
theta=45; %crack angle
[T]=GetTMatrix(theta); %rotation matrix

Dsi=zeros(3,3); % initial steel stiffness matrix
Dsi(1,1)=Mat.iEs1*Mat.rhos1;
Dsi(2,2)=Mat.iEs2*Mat.rhos2;

Dci=zeros(3,3); %initial concrete stiffness matrix
Dci(1,1)=4000;
Dci(1,2)=0;
Dci(1,3)=2000;
Dci(2,1)=0;
Dci(2,2)=4000;
Dci(2,3)=0;
Dci(3,1)=0;
Dci(3,2)=0;
Dci(3,3)=2000;

Tau_B=0; %initialize shear stress

%Initialize Displacement Increment
du=0;
%%%%%%%%%%%%%%%%%%%%%%%%%%%%%%%%%%%%%%%%%%%%%%%%%%%%%%%%%%%%%%%%%%%%%%%%
%CONTROL VALUES
%%%%%%%%%%%%%%%%%%%%%%%%%%%%%%%%%%%%%%%%%%%%%%%%%%%%%%%%%%%%%%%%%%%%%%%%
limit1=.06; %displacement at which displacement direction reverses
limit=limit1;
V=18; %Constant Vertical Load for proportional load vector

%%
for i=1:P %incremental displacement loop

%%
if abs(q(5))>=limit(1) %criteria for direction of loading
    dui=-dui;
end

du=du+dui ; %iterate displacement at specified increment

%%POINT 0%%

```

```

        converge=0;
        count=0;

        %Establishes the active crack for the current
%iteration
        [CrackNum,TorC]=getState(E,Mat,net,e12,Tau_B);

        if i==1 %estimates stiffness matrices for
                %the first displacement increment
                DcCrack=Dci;
                Ds=Dsi;
        end

        %rotate the concrete stiffness matrix to global
%direction
        DcCrackGlobal=inv(T)*DcCrack*(inv(T))';

        %smears the steel and concrete D matrices
        Dsmear=Ds+DcCrackGlobal;

        %Estimate displacements and strains from previously
        %converged stiffness matrix
        [A,e,q,a] =
SolveCompressiontestBload(I,Geo,Dsmear,du,V,dui);
        atrack=a;
        %%POINT 1%%
        %Represents the first set of estimated displacements
%D^0
        Qold=q;

        %%
        while converge == 0 %convergence loop

        %%
                %rotate strains to crack direction (1-2)
                [e12]=straintransformation(e,theta);

                %calculate the net shearing strain
                net.e123net1=e12(3)-net.e123cr2old;
                net.e123net2=e12(3)-net.e123cr1old;

                %calcuclate the shear stress tau^b
                deltagamma=e12(3)-ec12.ec123prev;
                Tau_B=fc12.fc123prev+Mat.iGc*(deltagamma);

                %Calculate the concrete stresses and update
%concrete stiffness matrix
                [DcCrack,Sc12,gammacr,E] =
getCStressCSS(E,Mat,e12,net,Tau_B,CrackNum,TorC);

```

```

%stiffness matrix      %Calculate the steel stress and update steel
                      [Ds,Ss] = getSStressCSS(e,es,fs,Mat,dui);

%direction            %rotate concrete stiffness matrix to global
                      DcCrackGlobal=inv(T)*DcCrack*(inv(T))';

                      %smear steel and concrete stiffness matrices
                      Dsmear=Ds+DcCrackGlobal;

%direction            %rotate concrete stresses to the global
                      [Sc]=stresstransformation(Sc12,-theta);

                      %calculate the total global shear stress
                      Sxsmeared=Ss(1)*Mat.rhos1;
                      Sysmeared=Ss(2)*Mat.rhos2;
                      Sssmeared=zeros(3,1);
                      Sssmeared(1)=Sxsmeared;
                      Sssmeared(2)=Sysmeared;
                      St=Sssmeared+Sc;
                      [Ss12]=stresstransformation(Sssmeared,theta);
                      addTau=Ss12(3)+Sc12(3);

                      %compute forces from the state of stress
                      [A0] = SolveStressEquil(St,Geo);

                      %update global stiffness matrix
                      [KK,BMAT] = getKmatrix(Geo,I,Dsmear);

                      %compute the change in force
                      %%%POINT 2%%
                      Fs=[-1;-1;-1;1;1;1;1;-1];
                      Bbar=[0;0;0;0;0;-V;0;-V];
                      DeltaA=(A0-Bbar)-A0(5)*Fs;
                      DeltaA(2)=0;
                      DeltaA(4)=0;
                      DeltaA;
                      convTest=norm(DeltaA); %value for convergence

                      %compute change in displ due to change in force
                      [DeltaD,DeltaDp] = getDeltaD (KK,DeltaA);

                      %%%POINT 3%%
                      %calculate new total displ with released PDOF
                      QA=Qold-DeltaD;

                      %enforce PDOF and compute change in displ from
%the previous change in PDOF "DeltaDp"

```

```

[A,e,deltaq,a] =
SolveCompressiontestBlood(I,Geo,Dsmear,DeltaDp,0,dui);

%%%POINT 4%%%
%compute new set of displ with correct PDOF
QB=QA+deltaq;

%compute new strains
e=BMAT*QB;

%set new displ equal to new "POINT 1"
Qold=QB;

%rotate strains to the crack direction
[e12]=straintransformation(e,theta);

%convergence criteria
if convTest < .00001 %convergence tolerance
    converge=1;
end

count=count+1;

if count > 30 %convergence iteration limit
    converge=1;
end

%update new displacements and forces to be
%stored once converged
q=Qold;
A=KK*q;

%%
end %end of convergence loop
%%

%Converged Displacements and Forces
q=Qold;
A=KK*q;
%strains in terms of the 1-2(crack) direction
[e12]=straintransformation(e,theta);

%calculate the shear stress
deltagamma=e12(3)-ec12.ec123prev;
Tau_B=fc12.fc123prev+Mat.iGc*(deltagamma);

%calcualte the updated concrete stresses and
%stiffness matrix with converged displacements and strains
[DcCrack,Sc12,gammacr,E] =
getCStressCSS(E,Mat,e12,net,Tau_B,CrackNum,TorC);

```

```

%update steel stresses and stiffness matrix with
%converged displacements and strains
[Ds, Ss] = getSStressCSS(e, es, fs, Mat, dui);

%Solve for concrete stresses in global x-y
[Sc] = stresstransformation(Sc12, -theta);

%Compute total shear stress
Sxsmeared = Ss(1) * Mat.rhos1;
Sysmeared = Ss(2) * Mat.rhos2;
Sssmeared = zeros(3, 1);
Sssmeared(1) = Sxsmeared;
Sssmeared(2) = Sysmeared;
St = Sssmeared + Sc;
[Ss12] = stresstransformation(Sssmeared, theta);
addTau = Ss12(3) + Sc12(3);

%update net shearing strain
net.e123net1 = e12(3) - net.e123cr2old;
net.e123net2 = e12(3) - net.e123cr1old;

%store crack shearing strains
if CrackNum == 1
    net.e123cr1old = gammacr;
elseif CrackNum == 2
    net.e123cr2old = gammacr;
end

%track of individual crack stresses and strains for
%concrete and steel
gammacon = e12(3) - gammacr;
gammaG = Mat.iGc * gammacon;
crackstress = Sc12(3) - gammaG;
eleff = e12(1) - abs(gammacr/2.0);

%Track of Strain and Stress Components (Global)
ex(i+1) = e(1);
ey(i+1) = e(2); %Total Strain and Total Stress
exy(i+1) = e(3);
Sx(i+1) = St(1);
Sy(i+1) = St(2);
Sxy(i+1) = St(3);
%Track of Individual Stresses (Global)
Scx(i+1) = Sc(1);
Scy(i+1) = Sc(2); %Concrete stresses
Scxy(i+1) = Sc(3);
Ssx(i+1) = Ss(1);
Ssy(i+1) = Ss(2); %Steel Stresses
Ssxy(i+1) = Ss(3);
%Force Displacement for DOF 5
q3(i+1) = q(3); %q is displacement, A is force
A3(i+1) = A(3);

```

```

q5(i+1)=q(5);
A5(i+1)=A(5);
q6(i+1)=q(6);
A6(i+1)=A(6);
q7(i+1)=q(7);
A7(i+1)=A(7);
q8(i+1)=q(8);
A8(i+1)=A(8);
%Track of 1-2 Direction Concrete Stresses
Sc121(i+1)=Sc12(1);
Sc122(i+1)=Sc12(2);
Sc123(i+1)=Sc12(3);
%Track of 1-2 direction strains
e121(i+1)=e12(1);
e122(i+1)=e12(2);
e123(i+1)=e12(3);
%track of epsilon effective
eleffectiv(i+1)=eleff;
e2effectiv(i+1)=E.ec2eff;
%max strains
es.exmax=max(ex);
es.eymax=max(ey);
%load vector factor "a"
aaa(i+1)=atrack;
incriment(i+1)=du;
%gamma crack
crackstrain(i+1)=gammaacr;
concstrain(i+1)=gammacon;
cshearstress(i+1)=gammaG;
crackshearstress(i+1)=crackstress;
%rotated steel stresses
Ss121(i+1)=Ss12(1);
Ss122(i+1)=Ss12(2);
Ss123(i+1)=Ss12(3);
TausTauc(i+1)=addTau;
%keep track of last converged strain and stress values
es.exprev=ex(i+1);
es.eyprev=ey(i+1);
fs.fsxprev=Ssx(i+1);
fs.fsyprev=Ssy(i+1);

ec12.ec123prev=e123(i+1);
fc12.fc123prev=Sc123(i+1);

E.ec1effprev=E.ec1eff;
E.ec2effprev=E.ec2eff;

%max excursion effective tensile strain
%cocrete tension stiffening curve
eff1test=max(eleffectiv,E.e1MaxExcr);
E.e1MaxExcr=max(eff1test);
eff2test=max(e2effectiv,E.e2MaxExcr);
E.e2MaxExcr=max(eff2test);

```

```

E.E1extr=(Mat.fcrksi/(sqrt(1+200*E.e1MaxExcr)))/E.e1MaxExcr;
E.E2extr=(Mat.fcrksi/(sqrt(1+200*E.e2MaxExcr)))/E.e2MaxExcr;

%%%%%%%%%%
%%%PLOT SHAPE
%%%%%%%%%%
%factor displacements for plotting

% factor=100;
% d3=q3(i+1)*factor;d5=q5(i+1)*factor;d6=q6(i+1)*factor;
% d7=q7(i+1)*factor;d8=q8(i+1)*factor;
%
% x1=0;y1=0;x2=10;y2=0;x3=10; y3=10;x4=0;y4=10;
% x_1=x1+0;y_1=y1+0; x_2=x2+d3;y_2=y2+0;
% x_3=x3+d5;y_3=y3+d6; x_4=x4+d7;y_4=y4+d8;
%
% posx=[x_1; x_2; x_3; x_4 ;0];posy=[y_1; y_2; y_3; y_4;0];
% recx=[x1;x2;x3;x4;0];recy=[y1;y2;y3;y4;0];
%
%
% plot(posx,posy,'-ro',recx,recy,'-o');
% xlim([-3,20]);
% ylim([-3,15]);

end %end of incremental displacement loop
%%%%%%%%%%
%PLOTS
%%%%%%%%%%

figure
subplot(4,3,1)
plot(e121,Sc121,'.-')
xlabel('\epsilon_1')
ylabel('\sigma_c_1(ksi)')
grid on;
hold on;

subplot(4,3,2)
plot(e122,Sc122,'.-')
xlabel('\epsilon_2')
ylabel('\sigma_c_2 (ksi)')
grid on;
hold on;

subplot(4,3,3)
plot(q7,A7,'.-',q5,A5,'.-')
xlabel('Displ q7 & q5')
ylabel('F A7 & A5')
grid On;
hold on;

```

```

subplot(4,3,4)
plot(q6,A6,'.-',q8,A8,'.-')
xlabel('Displ q6 & q8')
ylabel('F A6 & A8')
grid on;
hold on;

subplot(4,3,5)
plot(ey,Scy,'.-')
hold on
grid on
xlabel('\epsilon_y')
ylabel('\sigma_c_y')

subplot(4,3,6)
plot(exy,Scxy,'.-')
hold on
grid on
xlabel('\gamma_x_y')
ylabel('\tau_c_x_y')

subplot(4,3,7)
plot(e123,Sc123,'.-')
xlabel('\gamma_1_2')
ylabel('\tau_c_1_2')
grid on;
hold on;

%%%%%%%%%%%%%%%%%%%%%%%%%%%%%%%%%%%%%%%%%%%%%%%%%%%%%%%%%%%%%%%%%%%%%%%%
%PLOT STEEL
%%%%%%%%%%%%%%%%%%%%%%%%%%%%%%%%%%%%%%%%%%%%%%%%%%%%%%%%%%%%%%%%%%%%%%%%

% figure
subplot(4,3,8)
plot(ex,Ssx,'.-')
hold on
grid on
xlabel('\epsilon_x')
ylabel('\sigma_s_t_x')

%%%%%%%%%%%%%%%%%%%%%%%%%%%%%%%%%%%%%%%%%%%%%%%%%%%%%%%%%%%%%%%%%%%%%%%%

subplot(4,3,10)
plot(incriment,aaa,'.-');
grid on;
hold on;
xlabel('du')
ylabel('a')

subplot(4,3,11)
plot(ex,Scx,'.-');
grid on;

```



```

hold on;
xlabel('\epsilon_x')
ylabel('\sigma_c_x')

subplot(4,3,12)
plot(q3,A3,'.-');
grid on;
hold on;
xlabel('q3')
ylabel('A3')

subplot(4,3,9)
plot(ey,Ssy,'.-');
grid on;
hold on;
xlabel('\epsilon_y')
ylabel('\sigma_s_y')

%%%%%%%%%%%%%%%%%%%%%%%%%%%%%%%%%%%%%%%%%%%%%%%%%%%%%%%%%%%%%%%%%%%%%%%%
%PLOT FACTORED DEFORMED SHAPE
%%%%%%%%%%%%%%%%%%%%%%%%%%%%%%%%%%%%%%%%%%%%%%%%%%%%%%%%%%%%%%%%%%%%%%%%
% figure(1)
% for j=1:P
%
%     factor=100;
%     d3=q3(j+1)*factor;d5=q5(j+1)*factor;d6=q6(j+1)*factor;
%     d7=q7(j+1)*factor;d8=q8(j+1)*factor;
%
%     x1=0;y1=0;x2=10;y2=0;x3=10; y3=10;x4=0;y4=10;
%     x_1=x1+0;y_1=y1+0; x_2=x2+d3;y_2=y2+0;
%     x_3=x3+d5;y_3=y3+d6; x_4=x4+d7;y_4=y4+d8;
%
%     posx=[x_1; x_2; x_3; x_4 ;0];posy=[y_1; y_2; y_3; y_4;0];
%     recx=[x1;x2;x3;x4;0];recy=[y1;y2;y3;y4;0];
%
%
%     plot(posx,posy,'-ro',recx,recy,'-o');
%     hold on;
%     xlim([-3,20]);
%     ylim([-3,15]);
% end

%%%%%%%%%%%%%%%%%%%%%%%%%%%%%%%%%%%%%%%%%%%%%%%%%%%%%%%%%%%%%%%%%%%%%%%%
%Various Plots
%%%%%%%%%%%%%%%%%%%%%%%%%%%%%%%%%%%%%%%%%%%%%%%%%%%%%%%%%%%%%%%%%%%%%%%%
% plot(e123,e121,'.-',crackstrain,e121,'.-')
% grid on;
% xlabel('Shear Strain, \gamma_1_2')
% ylabel('Normal Strain, \epsilon_1')

% plot(e123,concstrain,'.-',e123,crackstrain,'.-',e123,e123,'.-')
% xlabel('Shear Strain, \gamma_1_2')

```

```

% ylabel('\gamma_c_r, and \gamma_c_o_n_c_r_e_t_e')
% grid on;

% plot(e123,Sc123,'.-',concstrain,Sc123,'.-',crackstrain,Sc123,'.-')
% xlabel('Shear Strain, \gamma_1_2')
% ylabel('\gamma_c_r, and \gamma_c_o_n_c_r_e_t_e')
% grid on;

% hold on;
% plot(incriment,Sxy,'g.-')
% grid on;
% xlabel('Prescribed Displacement, d_u')
% ylabel('Total Global Shear Stress, \tau_x_y')

% plot(e123,Sc123,'.-',e123,ss123,'.-',e123,Sc123+ss123,'.-')
% xlabel('Shear Strain, \gamma_1_2')
% ylabel('Shear Stress, \tau_c_1_2')
% grid on;

% plot(e123,Sc123,'.-')
% xlabel('Shear Strain, \gamma_1_2')
% ylabel('Shear Stress, \tau_c_1_2')
% grid on;

% plot(ex,ssx,'.-')
% grid on
% xlabel('\epsilon_x')
% ylabel('\sigma_s_t_x')

% plot(e121,Sc121,'.-')
% xlabel('\epsilon_1')
% ylabel('\sigma_c_1(ksi)')
% grid on;

% plot(e1effectiv,Sc121,'.-')
% xlabel('Effective Strain, ^e\epsilon_1')
% ylabel('Concrete Normal Stress, \sigma_c_1 (ksi)')
% grid on;

% plot(e123,Sc121,'.-')
% xlabel('\epsilon_1')
% ylabel('\sigma_c_1(ksi)')
% grid on;

% plot(incriment,aaa,'.-');
% grid on;
% xlabel('du')
% ylabel('a')

% plot(e123,ss123,'.-',e123,Sc123,'s-',e123,TausTauc,'*-')

```

```
% grid on;
% xlabel('Shear Strain, \gamma_{1_2}')
% ylabel('Shear Stress, \tau_{1_2}')
% legend('\tau_s (1-2 dir)', '\tau_c (1-2 dir)', '\tau_s + \tau_c (1-2
dir)')
```

# References

- [1] ACI Committee 318, “Building Code Requirements for Structural Concrete (ACI 318-08) and Commentary (318R-08).” American Concrete Institute, Farmington Hills, MI, 2005, pp. 167-170.
- [2] Belmouden, Y., and Pierino, L., “Analytical Model for Predicting Nonlinear Reversed Cyclic Behavior of Reinforced Concrete Structural Walls,” *Engineering Structures*, V. 29, 2007, pp. 1263-1276.
- [3] Birkeland, P. W., and Birkeland H. W., “Connections in Precast Concrete Construction,” *Journal of the American Concrete Institute, Proceedings*, V. 63, No. 3, March 1966, pp. 345-367.
- [4] Cervenka, V, “Constitutive Model for Cracked Reinforced Concrete,” *ACI Journal*, V. 82, No. 6, November-December 1985, pp. 877-882.
- [5] Dagher, H. J., and Kulendran, S., “Finite Element Modeling of Corrosion Damage in Concrete Structures,” *ACI Structural Journal*, V. 89, No. 6, November-December 1992, pp. 699-708.
- [6] Gebreyouhannes, E., Kishi, T., and Maekawa, K., “Shear Fatigue Response of Cracked Concrete Interface,” *Journal of Advanced Concrete Technology*, V. 6, No. 2, June 2008, pp. 365-376.
- [7] Gérin, M., P.E., M. ASCE, and Adebar P., “Simple Rational Model for Reinforced Concrete Subjected to Seismic Shear,” *ASCE Journal of Structural Engineering*, V. 135, No. 7, July 2009, pp. 753-761.
- [8] Hu, H. T. and Schnobrich, W. C., “Nonlinear Analysis of Cracked Reinforced Concrete,” *ACI Structural Journal*, V. 87, No. 2, 1990, pp. 199-207.
- [9] Jones, Robert M. (1998). *Mechanics of Composite Materials, Second Edition*. CRC Press. pp. 72-78.
- [10] Mansour, M., and Hsu, T. T. C., “Behavior of Reinforced Concrete Elements under Cyclical Shear. I: Experiments,” *ASCE Journal of Structural Engineering*, V. 131, No. 1, January 2005, pp. 44-53.
- [11] Mansour, M., and Hsu, T. T. C., “Behavior of Reinforced Concrete Elements under Cyclical Shear. II: Theoretical Model,” *ASCE Journal of Structural Engineering*, V. 131, No. 1, January 2005, pp. 54-65.

- [12] Mattock, A. H., and Hawkins, N. M., "Shear Transfer in Reinforced Concrete—Recent Research," *Journal of the Prestressed Concrete Institute*, V. 17, No. 1, March-April 1972, pp. 55-75.
- [13] Palermo, D., and Vecchio F. J., "Simulation of Cyclically Loaded Concrete Structures Based on the Finite-Element Method," *ASCE Journal of Structural Engineering*, V. 133, No. 5, May 2007, pp. 728-738.
- [14] Pang, X. B, and Hsu, T. T. C, "Behavior of Reinforced Concrete Membrane Elements in Shear," *ACI Structural Journal*, V. 92, No. 6, November-December 1995, pp. 665-677.
- [15] So, Migeum, "Total-Strain Based Bond/Slip and Shear/Friction Membrane Model for Finite Element Analysis of Reinforced Concrete," Ph.D. dissertation, Washington University in St. Louis, St. Louis, MO, 2008, 240 pp.
- [16] Stevens, N. J., Uzumeri, S. M., Collins, M. P., and Will, G. T., "Constitutive Model for Reinforced Concrete finite Element Analysis," *ACI Structural Journal*, V. 88, No. 1, January- February 1991, pp. 49-59.
- [17] Umeki, K., Kitada, Y., Nishikawa, T., Maekawa, K., and Yamada, M., "Shear Transfer Constitutive Model for Pre-Cracked RC Plate Subjected to Combined Axial and Shear Stress," *Nuclear Engineering and Design*, V. 220, No. 2, 2003, pp.105-118.
- [18] Valluvan, R., Kreger, M. E., and Jirsa, J. O., "Evaluation of ACI 318-95 Shear-Friction Provisions," *ACI Structural Journal*, V. 96, No. 4, July-August 1999, pp. 473-482.
- [19] Vecchio, F. J., "Disturbed Stress Field Model for Reinforced Concrete: Formulation," *ASCE Journal of Structural Engineering*, V. 126, No. 9, September 2000, pp. 1070-1077.
- [20] Vecchio, F. J., Lai, D., Shim, W., and Ng J., "Disturbed Stress Field Model for Reinforced Concrete: Validation," *ASCE Journal of Structural Engineering*, V. 127, No. 4, April 2001, pp. 350-358.
- [21] Vecchio, F. J., "Nonlinear Finite Element Analysis of Reinforced Concrete Membranes," *ACI Structural Journal*, V. 86, No. 1, January-February 1989, pp. 26-35.
- [22] Vecchio, F. J., "Reinforced Concrete Membrane Element Formulations," *ASCE Journal of Structural Engineering*, V. 116, No.3, March 1990, pp. 730-750.
- [23] Vecchio, F. J., and Collins, M. P., "The Modified Compression-Field Theory for Reinforced Concrete Elements Subjected to Shear," *ACI Journal*, V. 83, No. 2, March-April 1986, pp. 219-231.

- [24] Walraven, J. C., “Rough Cracks Subjected to Earthquake Loading,” *ASCE Journal of Structural Engineering*, V. 120, No. 5, May 1994, pp. 1510-1524.
- [25] Wang, E. H., “Composite Confined Concrete,” Ph.D. dissertation, Washington University in St. Louis, St. Louis, MO, 1997, 260 pp.
- [26] Zhu, R. R. H., Hsu, T. T. C., and Lee, J. Y., “Rational Shear Modulus for Smeared-Crack Analysis for Reinforced Concrete,” *ACI Structural Journal*, V. 98, No. 4, July-August 2001, pp. 443-450.

NOTE: Reference [15] in conjunction with other work led to the publishing of the following papers:

- (1) Migeum So, Thomas G. Harmon, Gun Jin Yun, and Shirley Dyke, “Inclusion of Bond-Slip Behavior in 2D Membrane Model,” *ACI Structural Journal*, July-August, 2009.
- (2) Migeum So, Thomas G. Harmon, and Shirley Dyke, “FEA Implementation of Smeared Cyclic Bond-Slip Based 2D Membrane Model,” *ACI Structural Journal*, Jan-Feb, 2010.

In addition, the shear friction theory presented in So’s dissertation [15] has been accepted for publication as a paper in the *ACI Structural Journal*.

# Vita

## Jeffrey P. Mitchell

<b>Date of Birth</b>	November 9, 1985
<b>Place of Birth</b>	Hinsdale, Illinois
<b>Degrees</b>	M.S. Civil Engineering (Structures), August 2010 B.S. Civil Engineering, May 2008 Special Minor in Architecture, May 2008
<b>Professional Societies</b>	American Concrete Institute
<b>Honors</b>	NSF GK-12 Fellowship, 2008-2010

May 2010